1986

Pool boiling from GEWA surfaces in water and R-113

Zahid Hussain Ayub
Iowa State University

INFORMATION TO USERS

This reproduction was made from a copy of a manuscript sent to us for publication and microfilming. While the most advanced technology has been used to photograph and reproduce this manuscript, the quality of the reproduction is heavily dependent upon the quality of the material submitted. Pages in any manuscript may have indistinct print. In all cases the best available copy has been filmed.

The following explanation of techniques is provided to help clarify notations which may appear on this reproduction.

1. Manuscripts may not always be complete. When it is not possible to obtain missing pages, a note appears to indicate this.

2. When copyrighted materials are removed from the manuscript, a note appears to indicate this.

3. Oversize materials (maps, drawings, and charts) are photographed by sectioning the original, beginning at the upper left hand corner and continuing from left to right in equal sections with small overlaps. Each oversize page is also filmed as one exposure and is available, for an additional charge, as a standard 35mm slide or in black and white paper format.*

4. Most photographs reproduce acceptably on positive microfilm or microfiche but lack clarity on xerographic copies made from the microfilm. For an additional charge, all photographs are available in black and white standard 35mm slide format.*

***For more information about black and white slides or enlarged paper reproductions, please contact the Dissertations Customer Services Department.**

Ayub, Zahid Hussain

POOL BOILING FROM GEWA SURFACES IN WATER AND R-113

Iowa State University PH.D. 1986

PLEASE NOTE:

In all cases this material has been filmed in the best possible way from the available copy. Problems encountered with this document have been identified here with a check mark __✓__.

1. Glossy photographs or pages _____
2. Colored illustrations, paper or print _____
3. Photographs with dark background __✓__
4. Illustrations are poor copy _____
5. Pages with black marks, not original copy _____
6. Print shows through as there is text on both sides of page _____
7. Indistinct, broken or small print on several pages _____
8. Print exceeds margin requirements _____
9. Tightly bound copy with print lost in spine _____
10. Computer printout pages with indistinct print _____
11. Page(s) _____ lacking when material received, and not available from school or author.
12. Page(s) _____ seem to be missing in numbering only as text follows.
13. Two pages numbered _____. Text follows.
14. Curling and wrinkled pages _____
15. Dissertation contains pages with print at a slant, filmed as received _____
16. Other _____

_____

_____

University
Microfilms
International

Pool boiling from GEWA surfaces in water and R-113

by

Zahid Hussain Ayub

A Dissertation Submitted to the

Graduate Faculty in Partial Fulfillment of the

Requirements for the Degree of

DOCTOR OF PHILOSOPHY

Major: Mechanical Engineering

Approved:

Signature was redacted for privacy.

In Charge of Major Work

Signature was redacted for privacy.

For the Major Department

Signature was redacted for privacy.

For the Graduate College

Iowa State University
Ames, Iowa

1986

TABLE OF CONTENTS

LIST OF TABLES

LIST OF FIGURES

LIST OF SYMBOLS

a	gap opening for bent-fin surface
A	surface area
A_c	tunnel cross-sectional area
A_i	inside surface area
A_o	outside surface area
A_t	tunnel/channel wall area
A_δ	liquid film area
c_p	specific heat
C_b	departure diameter constant
C_0	orifice constant
C_q	constant in natural convection correlation
C_{t1}	constant in Hitachi Model for Phase I
C_{t2}	constant in Hitachi Model for Phase II + III
C_T	constant in GEWA-T Model
C_3	constant in Hitachi Model for liquid inflow
d_b	departure diameter
d_0	pore diameter
D	outside diameter
D_{avg}	average diameter
D_b	base diameter (fin root diameter)
D_i	inside diameter
D_l	liquid capillary diameter
D_{tc}	diameter at thermocouple location
D_v	vapor channel diameter

f_b	ebullition frequency
g	gravitational acceleration
h	heat transfer coefficient
H	liquid level above test section
h_{fg}	latent heat
h_t	heat transfer coefficient at the tunnel wall
k_c	thermal conductivity of copper
k_l	thermal conductivity of liquid
L	length of test section
m_{l1}	liquid evaporated in Phase I
m_{l2}	liquid evaporated in Phase II + III
m_v	vapor mass
N	total number of pores
N_A	number of active pores
N_i	number of inactive pores
P_a	atmospheric pressure
P_r	Prandtl number
P_s^*	non-dimensional system pressure
P_v^*	non-dimensional vapor pressure in the tunnel
P_{vb}^*	non-dimensional vapor bubble pressure
q	heat transfer rate
q_I	heat transfer rate in Phase I
q_l	latent heat transfer rate
q''	heat flux
q''_{ex}	natural convection heat flux

q''_l	latent heat flux
r_0	pore radius
R	gas constant
S_T	GEWA-T gap width
t	time
ΔT	superheat
T_s	saturation temperature
ΔT_{sub}	subcooling
T_v	vapor temperature
T_w	wall temperature
T_0	initial vapor temperature
T_l	vapor temperature at hemispherical condition
ΔT_{t1}	superheat in Phase I
ΔT_{t2}	superheat in Phase II + III
U	overall heat transfer coefficient
V	volume
V_b	bubble departure volume
V_{hem}	hemispherical volume
V_t	tunnel volume
V_{vm}	mean vapor volume
V_{vm1}	mean vapor volume at the end of Phase I
V_{v1}	vapor volume at Phase I
x	constant in natural convection correlation
X	dummy variable
X_d	X at departure

y	constant in natural convection correlation
Z	non-dimensional mass flow at active sites
Z_i	non-dimensional mass flow at inactive sites
Z_{max}	maximum mass flow
β	coefficient of thermal expansion
β	ratio of active to total sites
δ	liquid film thickness
η	non-dimensional bubble height
η_d	non-dimensional recession
η'	bubble height
θ	time
θ_1	time for Phase I
θ_2	time for Phase II + III
θ_2^*	non-dimensional time for Phase II + III
λ	non-dimensional bubble height
λ_0	pore pitch
μ	dynamic viscosity of liquid
ρ_l	liquid density
ρ_v	vapor density
ρ_{vm1}	mean vapor density in Phase I
ρ_{vm2}	mean vapor density in Phase II + III
ρ_{v0}	initial vapor density
σ	surface tension
Φ	vapor generation rate
Φ^*	non-dimensional vapor generation rate/number of pores

τ	non-dimensional time
τ_{zmax}	time at maximum mass flow
ξ	non-dimensional recession
ξ_3	interface recession in Phase III
ξ'	recession at inactive site

I. INTRODUCTION

Enhanced heat transfer technology has been evident for quite some time. In fact, the records show that, in 1861, J.P. Joule attempted to increase the water side heat transfer coefficient in his classic study of steam condensation [1]. Heat transfer enhancement has gained momentum recently because of the increasing price of energy. Thermal engineers have been giving second thoughts to equipment that is effective but energy inefficient. Industry now demands more efficient, compact, and cost-competitive heat exchange units. This has resulted in the development of new types of heat transfer surfaces, from internally fluted tubes to externally structured surfaces [2]. During the last decade, there has been a rise in the number of these enhanced surfaces. Over 3000 technical papers and/or reports have been written [3], nearly 500 U.S. patents related to enhanced technology have been issued [4], and hundreds of firms worldwide advertise this technology [5].

A. Methods of Heat Transfer Enhancement

There are basically two ways by which heat transfer can be enhanced: active methods and passive methods. With active methods the enhancement is obtained by employing some external force or field, e.g., inducing mechanical vibrations or an electrostatic field. In the passive case no external force is applied, other than that required to provide fluid motion; enhancement is a result of surface geometry, i.e., finning the inside or outside of a tube with a surface that has a higher

heat transfer coefficient than a plain surface. Passive techniques have generally been more popular.

B. Performance of an Enhanced Surface

The merits of any enhanced surface are evaluated on the basis of its overall performance. In forced flow, an enhanced tube might result in a high heat transfer coefficient; but at the same time there might be a large increase in the pressure drop, which means more pumping power and ultimately greater cost. For either forced flow or natural convection, an enhanced surface may be used to achieve any of the following design objectives.

a. For constant q and fixed approach temperature ΔT, reduced A due to larger U value. Thus reduced size and weight.

b. For constant A and fixed ΔT, increased heat duty due to larger U value.

c. For constant q and A, reduced ΔT due to larger U value. Thus better thermodynamic (second law) efficiency.

C. Enhancement in Nucleate Pool Boiling

It is known that pool boiling is a very efficient mode of heat transfer. It is becoming increasingly important to reduce ΔT's in process heat exchange equipment; hence, boiling at low superheat is highly desirable. In the heating, ventilating, and air-conditioning industry the wall superheats are usually below 10 K. With plain tubes,

boiling is usually not achieved within this range. But if the plain tubes are replaced by some special surface tubes, then it is possible to attain boiling with low wall superheats.

Early successes in enhancement have resulted in the emergence of a variety of special types of enhanced surfaces for nucleate pool boiling [6]. These special surfaces can be classified into two categories: low fin and modified structured surfaces. The first category, introduced in the 1940's, includes simple rolled low fin tubes. The second category includes porous coatings and modified low fin tubes. The latter tubes are commercially available under such names as High Flux [7, 8], ECR40 [9], Thermoexcel-E [10], and GEWA-T [11, 12]. This category has lately gained impetus because of superior performance to the low fin tubes. It has been possible to attain boiling with these surfaces at as low as 1 K wall superheat. This characteristic of these surfaces has prompted their use in petrochemical processing, liquefaction, refrigeration, ocean thermal energy conversion, and electronic equipment cooling [13 - 26].

One of these special surfaces, a product of Wieland-Werke AG, is called GEWA-T [12]. The T-shape is formed out of the wall of a plain tube in two stages. The first stage results in a plain low fin surface, and then in the second stage the tip of each helical fin is notched and pressed by a roller assembly, resulting in a final T-shaped fin, as shown in Fig. 1. In the process, the tube takes on a slightly undulated internal surface and the finned portions are hardened. The inside of

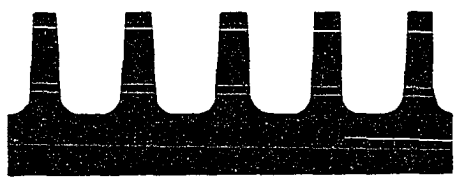

GEWA-K

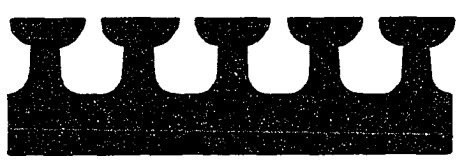

GEWA-T

FIGURE 1. GEWA surface profiles

the tube may be completely smooth or have a ridge-type enhancement. The unfinned ends, however, remain soft and are suitable for mechanical expansion into tube sheets. Besides better thermal performance, other advantages of GEWA-T tubes over plain fin tubes are

a. Due to the smooth outer surface, the tubes can be easily inserted and removed.
b. These tubes can be bent to U-shape or coiled to any shape.
c. Due to the smaller outside diameter, the tubes may be packed more closely.
d. No unfinned skips are needed, and the support plates may rest directly on the fins, resulting in an enlarged thermal exchange surface. A reduction of the tube length by about 10 to 15% is possible due to this factor alone, allowing a more compact shell-and-tube unit. As the unit becomes shorter, the water side pressure drop becomes smaller.

The increasing importance of this surface in process and power industry heat exchangers prompted the initiation of this study. The following chapters deal in detail with the experimental and theoretical aspects of pool boiling in water and R-113 on GEWA-T, pertinent plain fin tubes, and a smooth tube.

II. LITERATURE REVIEW

There are different ways of enhancing boiling heat transfer in process and power industry heat exchangers. As discussed in the previous chapter, different types of boiling surfaces have evolved during the past two decades [6]. The performances of these special surfaces have been evaluated by investigators in several countries and the information now available is quite large [3, 4, 27]. The two main streams of research in boiling concern flow boiling and natural convective or pool boiling. Because this study deals with the latter case, pool boiling enhancement will be taken up in detail.

The field of pool boiling has been of modern technological interest since the development of first steam driven devices in the 17th and 18th centuries. Since then extensive work has been done to develop efficient surfaces for use in heat exchangers. Some of these surfaces have produced very large improvements in pool boiling performance [28 - 32].

A. Definition of Basic Terms

It is important to clearly define in the beginning the relevant terms frequently encountered during the course of this study. In order to do so it was decided to plot typical boiling curves and then define various terms corresponding to the plot. Figure 2 shows standard boiling curves plotted on a log-log scale with heat flux on the ordinate and wall superheat on the abscissa. Curve 1 represents hypothetical smooth tube data and Curve 2 is for a hypothetical enhanced surface

tube. The heat flux in the plot is based on the outer diameter of the tubes. The terms are defined as follows.

1. Natural convection regime

This phenomenon is observed as a result of the fluid motion due to the density changes arising from heating. In a typical boiling curve this regime of heat transport is represented by the segment between points A1 - B1 (Curve 1) or A2 - B2 (Curve 2) as shown in Fig. 2.

2. Incipient and partial nucleate boiling

With wetting liquids of very low contact angle, large cavities are initially flooded and a rather high superheat is required for boiling inception (C1, C2). When boiling is first initiated and not all potential nucleation sites are active, the mode of heat transport is called partial nucleate boiling. This regime is represented by B1 - C1 or D1 and B2 - C2 or D2. The boiling spreads rapidly and the superheat decreases (D1, D2).

3. Developed nucleate boiling

With further increases in heat flux the number of nucleation sites and frequency of bubble generation increases and the curve assumes an approximately log-linear behavior. This mode is called developed or fully developed nucleate boiling, represented by D1 - E1 or D2 - E2.

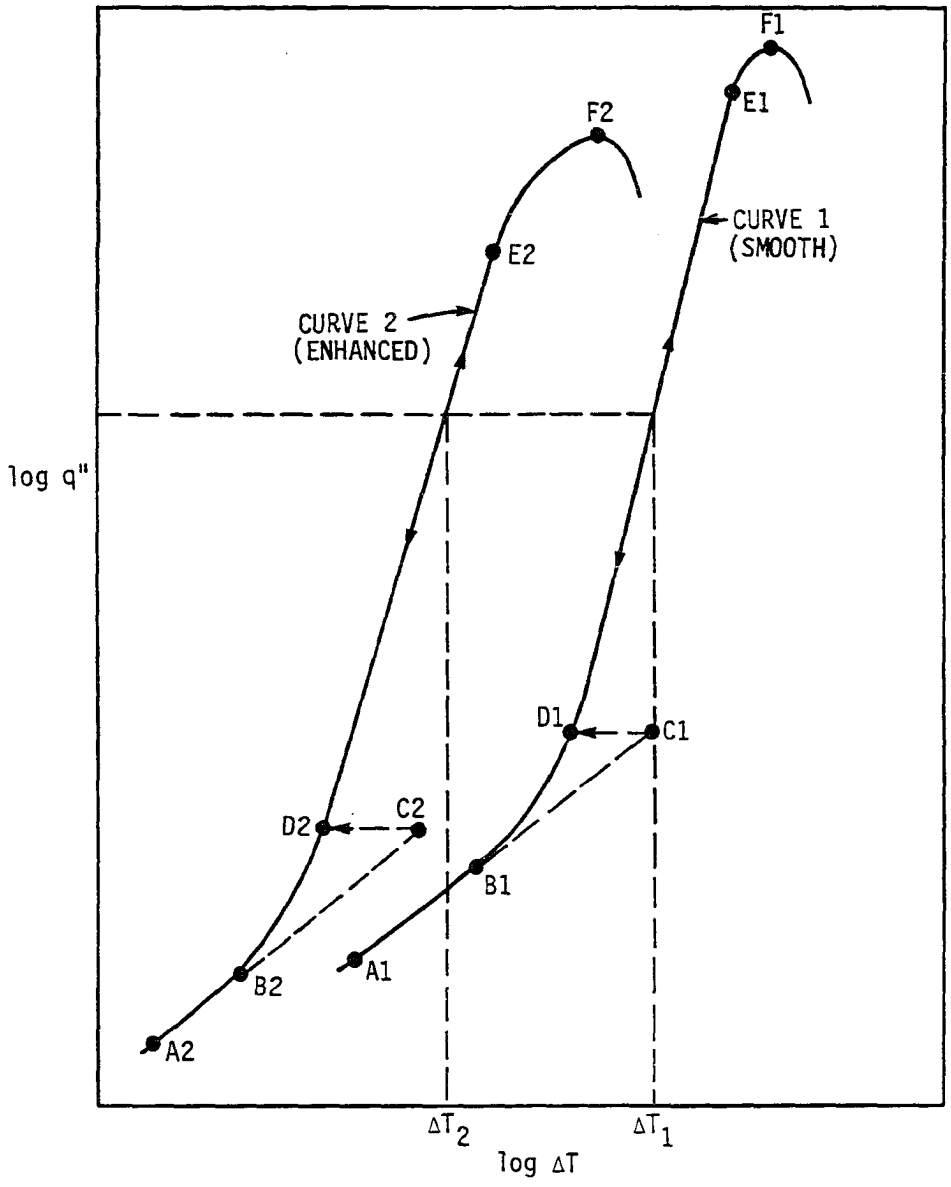

FIGURE 2. Typical boiling curves for smooth and enhanced surfaces

4. Departure from nucleate boiling (DNB)

The points E1 or E2 are called departure from nucleate boiling. The slope decreases due to bubble crowding. Enhanced surfaces usually have a more pronounced departure region.

5. Critical heat flux (CHF)

At point F1 or F2 the peak or critical heat flux is reached. With heat flux as the imposed variable, there is a large increase in wall superheat until film boiling is reached. In a temperature-controlled situation, the heat flux decreases when CHF is exceeded.

6. Hysteresis

If there is a substantial temperature overshoot, a different path is followed with decreasing heat flux, i.e., D1 - B1 or D2 - B2. This results in the so called boiling curve hysteresis.

7. Area basis for heat flux

In the entire text the heat flux is based on the outside diameter of the test section, unless mentioned specifically.

8. Enhancement

Enhancement is usually defined as the ratio of ΔT for the smooth tube (Curve 1) to ΔT for the enhanced tube (Curve 2) at a fixed heat flux, e.g., an enhancement of 2 denotes $\Delta T_1/\Delta T_2 = 2$, or a 50% reduction in the wall superheat. This method of enhancement representation is strictly correct for constant heat flux systems. The enhancement for

two-fluid heat exchangers cannot be evaluated directly as both heat flux and wall superheat change when the enhanced tube is introduced.

B. Plain Low Fin Surfaces

The first structured surface available in the market was plain low fin tubing. Due to their better performance over smooth tubes, these tubes were and are still used extensively in flooded evaporators. The parameters that influence the fin tube performance are the fin dimensions and material.

Katz et al. [33] tested low fin copper tubes of 740 fins/m in propane and dichlorodifluoromethane (R-12). Their data showed that for the same heat flux, the enhancement obtained was greater with R-12. At a heat flux of 80,000 W/m^2 and a system pressure of 5 bar, the enhancement in propane and R-12 was 1.6 and 1.8, respectively. Zieman and Katz [34] showed that at a system pressure of 17 bar and a heat flux of 150,000 W/m^2 the enhancement of a clean low fin copper tube was 2 when boiling isobutane.

Myers and Katz [35] tested 740 fins/m low fin copper tubes in R-12 at one atmosphere pressure. At a heat flux of 29,000 W/m^2, their results showed an enhancement of 1.2.

Bondurant and Westwater [36] tested horizontal copper tubes with transverse integral fins in R-113 at atmospheric pressure. One of the main objects of their study was to determine how close together fins could be placed before interference between adjacent fins caused

decreased performance. Their experimental results showed similar nucleate boiling performance for Tube D (C = 1.59 mm) and E (C = 3.18 mm), whereas the highest fin density Tube C (C = 0.79 mm) slightly outperformed the other two tubes. Here, C denotes the gap width between the adjacent fins. The observed peak nucleate heat fluxes showed the opposite trend. It was found that fins of height 6.35 mm could be put as close together as C = 1.58 mm with no effect, but at C = 0.79 mm the peak heat flux decreased by about 10%, and a change in vapor flow pattern occurred. Visually, it was observed that the tubes with relatively large clearances (C > 1.58 mm) allowed the vapor to flow circumferentially, while for C = 0.79 mm, the vapor ejection was altered and bubbles were forced out radially at different positions over the circumference.

Hesse [37] performed pool boiling experiments with grooved nickel tubes. The groove depth was 0.5 mm, fin thickness 0.4 mm, and fin pitch 1.0 mm (thus placing the tube in a low fin tube category). The working fluid was R-114. At a system pressure of 3 bar and a heat flux of 80,000 W/m^2, the enhancement obtained was 1.6, whereas at a same heat flux condition but a pressure of 6 bar the enhancement was 1.3. This result supports Gorenflo's [38] observation that, with a clearance between fins equal to twice the bubble departure diameter, heat transfer was lower than with tubes having either a smaller or a larger clearance between the fins. Gorenflo postulated that the improvement at low clearance was due to interaction between growing bubbles on the opposite

fins, and at large clearances it was due to the favorable flow conditions. Hesse's data indicate that for a fin clearance of 0.60 mm the bubble departure diameter (using the Fritz equation) was 0.58 mm at 6 bar and 0.65 mm at 3 bar. Consequently, at a lower pressure the bubbles grew to a size that interacted with the growing bubbles on the adjacent fin and resulted in a higher heat transfer coefficient.

Gorenflo's [38] results always suggested better performance for low fin tubes than the smooth tube. He attributed this to the pool convective currents around the finned tubes. But Hesse's [37] data showed no difference in heat transfer performance between smooth and finned tubes at a pressure of 6 bar, apparently because of the very small clearance between the fins. At these clearances the supply of liquid to the heated surface is restricted by the opposing vapor flow so that the additional convection is ineffective.

Zatell's [39] low fin tube data for 1020 fins/m and 740 fins/m in R-11 at one atmosphere showed no effect of fin density on the thermal performance. Gotoh et al. [40] tested 740 fins/m and 1020 fins/m copper low-finned tubes in R-11. Their results did not indicate appreciable effect on the heat transfer coefficient due to the change in fin density.

Yilmaz et al. [29, 30] tested Wieland's GEWA-K, low fin copper tube, 1200 fins/m and $A_o/A_i = 3.199$, in pure saturated isopropyl alcohol, p-xylene, and water at one atmosphere. At a heat flux of 200,000 W/m^2, the enhancement in isopropyl alcohol was 1.3, whereas the

enhancement in p-xylene was 2.8. However, with water, at a heat flux of 200,000 W/m^2, there was almost no enhancement, about 3%, suggesting the importance of fluid physical properties.

It has been observed by many investigators that the performance of tubes in bundles is different than that for single tubes alone. One of the early studies of the bundle effect was performed by Myers and Katz [35]. They studied boiling characteristics of low fin copper tubes in R-12, methyl chloride, sulfur dioxide, and propane. The four horizontal tubes were assembled in a vertical column designated by numbers 1 - 4 from bottom to top. For R-12 the bottom tube (No. 1) showed the lowest heat transfer coefficient, whereas an increase in the heat transfer coefficient was observed for Tubes 2, 3, and 4 at low heat flux levels. At heat fluxes higher than 16,100 W/m^2, data for Tubes 2 - 4 merged together. The top three tubes always showed better performance because of the agitation caused by vapor bubbles coming from the lower tubes.

The experiments of Danilova and Dyundin [41] involving boiling of R-12 and R-22 on 740 fins/m copper tube bundles also showed an increase in heat transfer coefficient from bottom to top, again indicating the strong influence of convective heat transfer of the vapor-liquid mixture moving upward.

Mueller and Hahne [42] tested 740 fins/m low fin copper tubes as a 2 tube vertical column bundle and an 18 tube, 3 column (6 tubes/column) bundle in R-11 at one bar system pressure. In the former arrangement the heat transfer coefficient for the bottom tube at low heat fluxes was

essentially the same as that for a single tube, whereas the heat transfer coefficient for the upper tube was strongly influenced by the convection currents from the lower tube. Similar behavior was observed with the second setup. The enhanced convection helped raise the heat transfer coefficient for all tubes above the first tube.

C. Structured Surfaces

Structured surfaces are the enhanced surfaces receiving most attention in industry today. Numerous patents have been filed [4]. As discussed in Chapter I these surfaces can be divided into two main categories: porous surfaces and modified fin surfaces.

1. Porous-coating surfaces

Extensive work has been performed on porous-coating surfaces; some recent work demonstrates the outstanding performance of this type of surface. Figure 3 shows a porous surface profile. At a heat flux of 40,000 W/m^2 and one atmosphere system pressure, Yilmaz et al. [29] observed an enhancement of 12.9 in p-xylene. At a heat flux of 60,000 W/m^2 and one atmosphere pressure, Yilmaz and Westwater [30] observed an enhancement of 5 in isopropyl alcohol. Marto and Lepere [28] also tested these tubes in R-113 and FC-72. They reported an enhancement of 5 at a heat flux of 40,000 W/m^2 and one atmosphere pressure. However, in the case of FC-72 an enhancement of only 3.5 was observed under similar conditions. The tests of Bergles and Chyu [43] with water and R-113 also demonstrated the large enhancement of High

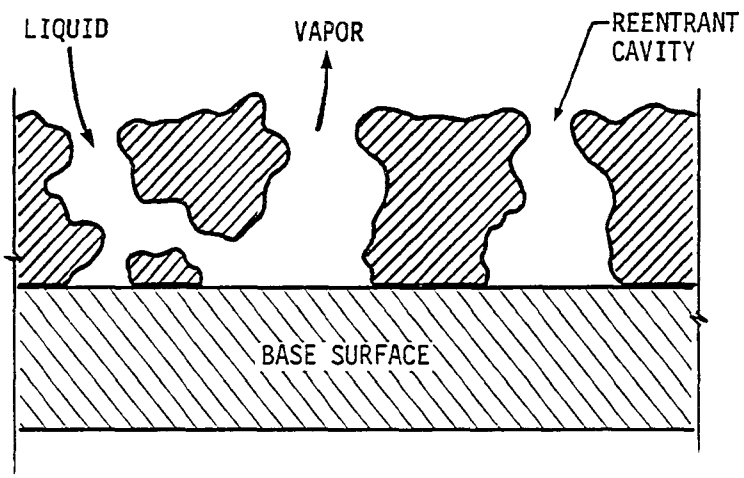

FIGURE 3. Porous surface cross section

Flux surface tubes over the plain tube at atmospheric conditions. At a heat flux of 40,000 W/m^2, they observed an enhancement of 4.5 and 7.4 in water and R-113, respectively. They also observed relatively large-scale boiling curve hysteresis in R-113, attributing it to the surface characteristics and liquid wettability. With water the temperature overshoots were trivial.

The thermal performance of porous surfaces is dependent on the pore size and the thickness of the porous layer [44]. Several mechanisms have been postulated for boiling from these surfaces. O'Neill et al. [15] postulated that a vapor bubble is formed in an interparticle space. Vapor is generated primarily by evaporation of the thin liquid film segments separating the bubbles from the particles. The bubble eventually grows and is squeezed out of a pore. Fresh liquid is supplied to the active sites via inactive pores, as the majority of the pores are interconnected via channels.

2. Modified fin surfaces

Webb [45] tested 740 fins/m, bent-over low fin copper tubes in saturated R-11. The bending resulted in a tight helical re-entrant type cavity all along the tube, as shown in Fig. 4. At a heat flux of 71,000 W/m^2 the enhancement obtained was 4. Webb suggested that it was important to control the groove opening. The optimum value of this gap was reported to be between 0.04 mm and 0.09 mm for R-11.

Webb [45] suggested that ordinarily saturated liquid rushes to nucleation sites which consequently requires higher flux to activate

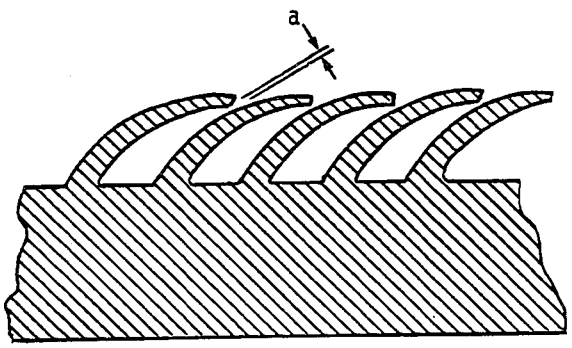

FIGURE 4. Bent-over fin cross section

them. But with this fin profile, superheated liquid flows onto the base surface and sides of the fins. This is due to the large hydraulic resistance imposed by a narrow fin gap "a" (Fig. 4) which tends to restrict the flow of liquid. Saturated liquid seeps into the groove along the length of gap "a" between rising columns, and then flows along the groove towards nucleation sites. As it seeps into the groove the liquid is heated so that it is brought to the superheated condition by the time it reaches the active sites. Thus only a small amount of heat need be added at each nucleation site to further raise the temperature of the liquid to the level required for nucleation. Hence, this channeling and directing of liquid onto the sites apparently decreases the heat flux required to form and release another bubble.

The second possible mechanism provided is that after the bubble departs some vapor is left behind. The liquid moves in, displacing the vapor residue to another location within the groove. This movement takes place apparently at high speed. As this liquid-vapor interface moves longitudinally within a groove, superheated liquid retained within the groove evaporates into it until detachment occurs at some new position. Ultimately a series of closely spaced bubble columns is generated along the entire length of each groove. Adjacent bubble columns indicated an out of phase departure frequency, thus confirming the existence of an oscillating liquid-vapor interface moving back and forth.

One of the structured surfaces in Zatell's [39] patent is similar to Webb's [45] bent-over fin surface, except for the fin density of 1020 fins/m. His tests in R-11 at one atmosphere established a clear superiority of the modified fin tube over a plain fin tube. The enhancement was 4 at a heat flux of 12,600 W/m^2. His results also showed that the thermal performance was closely related to the fin density. The tube with 1020 fins/m outperformed the tube with 740 fins/m.

Hitachi's Thermoexcel-E [10] is one of the recent developments in enhanced heat transfer technology. The surface has small parallel tunnels with discrete holes that communicate with the outside, as shown in Fig. 5. This peculiar geometry results in reentrant pores of uniform size, evenly distributed on the surface. The manufacturing operations include forming helical, interrupted fins and bending down the upper parts of the fins through high speed brushing to close the grooves between the neighboring fins.

Experimental results of Nakayama et al. [46] for boiling of R-11 on Thermoexcel-E showed clear enhancement of heat transfer. The enhancement obtained was 5 at the same heat flux. At a heat flux of 40,000 W/m^2 Yilmaz et al. [29] reported an enhancement of 9.4 and 2.4 for Thermoexcel-E while boiling saturated p-xylene and isopropyl alcohol at one atmosphere, respectively. Marto and Lepere [28] tested Thermoexcel-E in saturated R-113 and FC-72 at one atmosphere. They observed better performance of this surface in R-113 than in FC-72. The

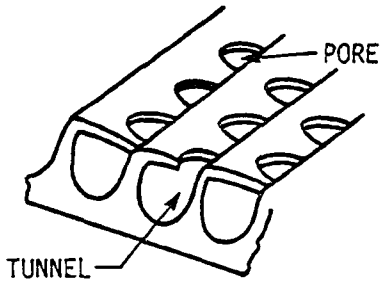

(a) IDEALIZED VIEW

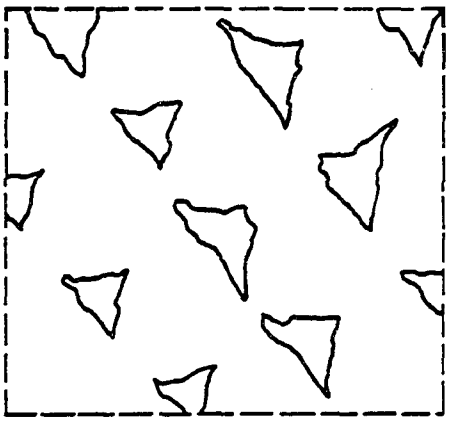

(b) TOP VIEW

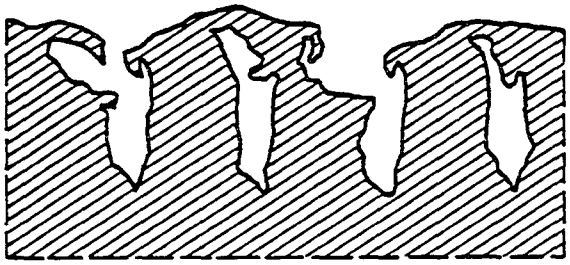

(c) ACTUAL CROSS SECTION VIEW

FIGURE 5. Geometry of the Thermoexcel-E surface

enhancement obtained at 40,000 W/m^2 was 3.3 and 2.3, respectively. With both fluids they observed a temperature overshoot problem that resulted in a boiling curve hysteresis. However, the overshoot was less pronounced with FC-72. The pool boiling data of Chyu and Bergles [47] with Thermoexcel-E in distilled water at one atmosphere showed better performance than a smooth tube, though the extent of the enhancement was lower than with the organic and cryogenic fluids studied in [28 - 30, 46, 48]. Thin film evaporation of the liquid inside the tunnels in Thermoexcel-E surface is believed to be the major source of heat transport [20, 21, 49 - 51].

One of the more recent development in modified fin enhanced surfaces is GEWA-T. This surface has already been tested by several investigators with boiling of various fluids. Stephan and Mitrovic [52] studied the performance of a GEWA-T tube within a bundle of such tubes in R-11. At constant heat flux, they observed an enhancement of 3. At a heat flux of 40,000 W/m^2, the pool boiling experiments of Yilmaz et al. [29, 30] with saturated p-xylene and isopropyl alcohol on GEWA-T tubes demonstrated an enhancement of 5.3 and 2.0, respectively. Their GEWA-T tubes showed somewhat lower performance as compared to High Flux and Thermoexcel-E tubes under similar conditions.

Pool boiling results of Marto and Lepere [28] indicated that the GEWA-T surface did not show as much of an enhancement at low heat fluxes as High Flux or Thermoexcel-E, whereas at high heat fluxes its performance improved. They attributed this to the large channels within

the GEWA-T surface giving it the characteristics of a plain low fin tube, rather than a surface with numerous pores. However, at high heat fluxes the large fin pitch delayed the coalescence of vapor columns. At 40,000 W/m^2 they measured an enhancement of 2.8 and 2.5 with R-113 and FC-72, respectively. They also observed that with GEWA-T, a few sites first became active at some incipient heat flux, and with the increase in heat flux, additional sites became active, subsequently activating a complete ring around the cylinder. With GEWA-T the temperature overshoot in R-113 was higher as compared to Thermoexcel-E or High Flux surfaces. They attributed this to the GEWA-T surface profile being so open that it allows R-113 to easily flood the channels.

Marvillet [53] tested a GEWA-T tube in R-12 at a system pressure of 4 bar. At a heat flux of 30,000 W/m^2 his data indicated an enhancement of 2.5.

In the original GEWA-T publication, Stephan and Mitrovic [52] postulated that the reason for the improvement in heat transfer coefficient with GEWA-T over GEWA-K was the fact that the T-shaped caps provide internal flow channels that promote two-phase flow within the channels, i.e., liquid entering at the bottom and vapor leaving at the top of the tube. In their view, the T-caps constrain the bubbles to move around the tube within the channel. During the process, the bubbles generated at the lower section move up the channel, sweeping other bubbles along their path and thereby increasing bubble frequency and local heat transfer.

Marto and Hernandez [54] tried to verify the qualitative liquid-vapor exchange mechanism of Stephan and Mitrovic. Contrary to the postulated mechanism, they observed low frequency, large diameter bubbles coming out of channels at the bottom of their test section. Their experiments with aluminum shrouds, having diametrically opposite windows of various aperture angles, indicated that these bubbles could be forced into the channels by the entering liquid. These shrouds resulted in increased boiling heat transfer coefficients at low heat fluxes due to favorable upward flow of the bubbles. At high heat fluxes the performance deteriorated because the shroud prevented some of the vapor from departing from the surface effectively.

Saier et al. [11] reported data on various gaps for GEWA-T; however, these data are difficult to interpret because of lack of constant conditions in the experiments, which utilized hot water heating. They concluded that with R-12 at 3.26 atmospheres, the optimum gap width was approximately S_T = 0.20 mm.

The experiments of Yilmaz et al. [48] with a GEWA-T tube bundle in p-xylene at one atmosphere indicated that there was a substantial degradation in heat transfer coefficient relative to single GEWA-T tubes at heat flux lower than 100,000 W/m^2. They attributed this to the disruption of the liquid feed mechanism. But on the other hand, at the same heat flux, the GEWA-T tube bundle out-performed an identical plain tube bundle. They also noticed that the performance improvement of the GEWA-T bundle relative to a single GEWA-T tube was less than the

performance improvement of plain tube bundle relative to single plain tube.

D. Fundamental Work Related to Structured Surfaces

One of the most important and common mechanism of heat transport in these enhanced surfaces is considered to be internal vaporization. The literature indicates that past theoretical studies have given due importance to this factor.

Macbeth [55] undertook a detailed study of porous surfaces and developed a static model. The analysis was performed on a matrix of vapor chimneys and liquid capillaries which simulates a porous boiler tube deposit or crud. He postulated that the liquid was fed through the surrounding capillaries connected at the base of the vapor chimney. A force balance was performed between the chimney base and outside liquid, employing the contributions due to gravity, surface tension, viscosity, and inertia. The model showed that the pressure within the vapor chimney oscillated with the varying resistance to vapor flow at the chimney mouth, thus producing a to-and-fro motion of the menisci in the liquid capillaries. This, in turn, led to continuous wetting and evaporation at the capillary wall. The model also indicated that in order to be valid, the liquid capillary diameter should always be smaller than the diameter of vapor chimney ($D_l < D_v$); the smaller the liquid capillaries, the better the liquid intake. Smirnov [56] also suggested vapor chimneys, but in a rather dense deposit matrix so that

the liquid feed occurred only in a reflux fashion on the chimney walls. These analyses can probably be applied to porous metallic matrices due to the general similarity of these structures.

Nakayama et al. [20, 21] developed a dynamic model for the Thermoexcel-E surface employing bubble initiation, development, and departure. A special scaled-up model was fabricated for a visual study. They observed a continuous vapor core and liquid at the corners of a single tunnel, proposing that this liquid was sucked in via inactive pores due to pressure reduction within the tunnel due to growth of bubbles at active pores. Their data showed a much larger contribution of latent heat transport than that observed for boiling from plain surfaces. This is because the vapor is generated internally and bubbles come out through the active pores.

Arshad and Thome [57] used a test piece similar to that of Nakayama et al. [50] except for different types of tunnels, i.e., square, triangular, and circular. The pores on the surface were discrete as in Thermoexcel-E. They observed bubble growth at different spots along the tunnel. Once boiling started, the liquid entered intermittently through the inactive pores, and a thin film between the wall and the vapor core was consistently observed until dryout. Bingshen et al. [58], using a visual apparatus similar to that of Nakayama et al. [20] with R-11, R-113, and water, observed that the tunnel was almost filled with vapor. Between the vapor and the wall of the tunnel a vibrating liquid film was observed. This pulsating

behavior of the liquid film indicated that there was a continuous flow of liquid into the tunnel through the inactive pores. They inferred that the total heat transfer was the sum of latent heat, convection within the tunnel, and bulk convection induced by departing bubbles at the outer surface. Liu and Ma [59] also observed the prominent role of thin film evaporation in a re-entrant type cavity. They prepared test pieces with triangular, rectangular, and a combination of triangular/rectangular shaped grooves. The maximum enhancement in water was 4. This enhancement strongly depended on the groove shape (maximum for the combination type groove).

Xin and Chao [60] performed pool boiling tests on a series of T-shaped fin surfaces in distilled water, ethyl alcohol, and R-113 at a system pressure of one atmosphere. The test surfaces were flat and oriented horizontally. At a heat flux of 80,000 W/m^2 the enhancement in R-113 for S_T = 0.14 mm was 2. At the same heat flux, the enhancement in water for S_T = 0.24 mm and S_T = 0.17 mm was 2.5 and 3.5, respectively. They proposed a counter-current two-phase flow model for this surface. They assumed the space formed by the T-fins as a vertical narrow gap with a closed bottom and top opening, that prevented the channel from being flooded by the liquid. It is assumed that the thin liquid film at the wall evaporates. This results in a vapor pressure development in the channel which eventually gets released via the narrow gap. This vapor release results in a pressure reduction that paves way for the liquid inflow which re-wets the groove wall, and the event is repeated

again. Because of the very short period of this cycle, it is assumed that there is almost a continuous stream of vapor instead of discrete vapor bubbles. Therefore, this phenomenon is considered as a counter-current two-phase flow, i.e., vapor continuously flowing out of the groove and liquid flowing into the groove. As they did not observe any bubble sites on the outside surface of the T-shaped fins, they assumed that the entire heat transfer contribution was by thin film evaporation within the groove.

E. Objectives of This Study

Due to the potential importance of GEWA surfaces in enhancing refrigeration and chemical process boilers, a study was undertaken to clarify pool boiling behavior and enhancement of these surfaces.

The preceding literature review indicate that there is a reasonable amount of literature available concerning the structured surfaces. But there are still unanswered questions regarding the mechanism/physics of boiling on these surfaces, and the effect of different geometries and fluids on the thermal performance. This is particularly true with the GEWA-T surface as it has been a recent development.

This study, therefore, will deal in detail with the developed nucleate boiling of R-113 and water on GEWA surfaces, with specific reference to the GEWA-T. The main reason for the use of R-113 is that it is convenient to handle at room temperature, and at the same time is a member of the flourocarbon family that is most widely used in

refrigeration and air-conditioning. Water was also used, again because of convenience and, above all, because of its wide use in the power and process industries.

Peak heat flux boiling will not be covered in this study due to the limitations on the test equipment. The study will deal particularly with the enhancement of different gap size GEWA-T tubes under atmospheric conditions in distilled water and R-113. A GEWA-K (low fin tube) will be included as the limiting case of a large gap size GEWA-T.

In order to understand the complex liquid-vapor exchange, attempts will be made to perform both experimental and visual studies. Based on these observations, a model will be developed for fully developed nucleate boiling.

III. EXPERIMENT

A. Test Facility and Test Section

The test facility included a 300 mm cubical Pyrex tank, an aluminum cover provided with ports for electrical wires and thermocouples, a liquid replenisher, a reflux condenser, auxiliary heaters, and a test section holder, as shown in Fig. 6.

In the case of water, though all metallic components were non-ferrous and the water used for the experiments was distilled, it was still decided to further deionize the water. In order to comply with this requirement, the distilled water in the tank was circulated in a closed loop by a pump (Oberdorfer 3000R, 600 rpm, driven by a Dayton capacitor ac motor, 0.5 hp, 1725 rpm) through a filter, and deionizer (Barnstead Ultrapure D8902), as shown in Fig. 7. The conductivity of water was measured by a purity meter (Barnstead Puromatic PM50). It was observed that the volume resistivity of the water increased from about 1 MΩ-cm to about 2 MΩ-cm after deionizing. Because the integrity of the deionizer cartridge was limited to 355 K, it was used under room temperature conditions. Ordinarily pure distilled water has a resistivity of about 18 MΩ-cm at 25 °C [61]. The reason for a comparatively low value was that the water used from the still was distilled once. Though the deionizing procedure was used for a period of two hours, the resistivity was still low. The reason for this low resistivity was the contamination from the fittings, piping, and test

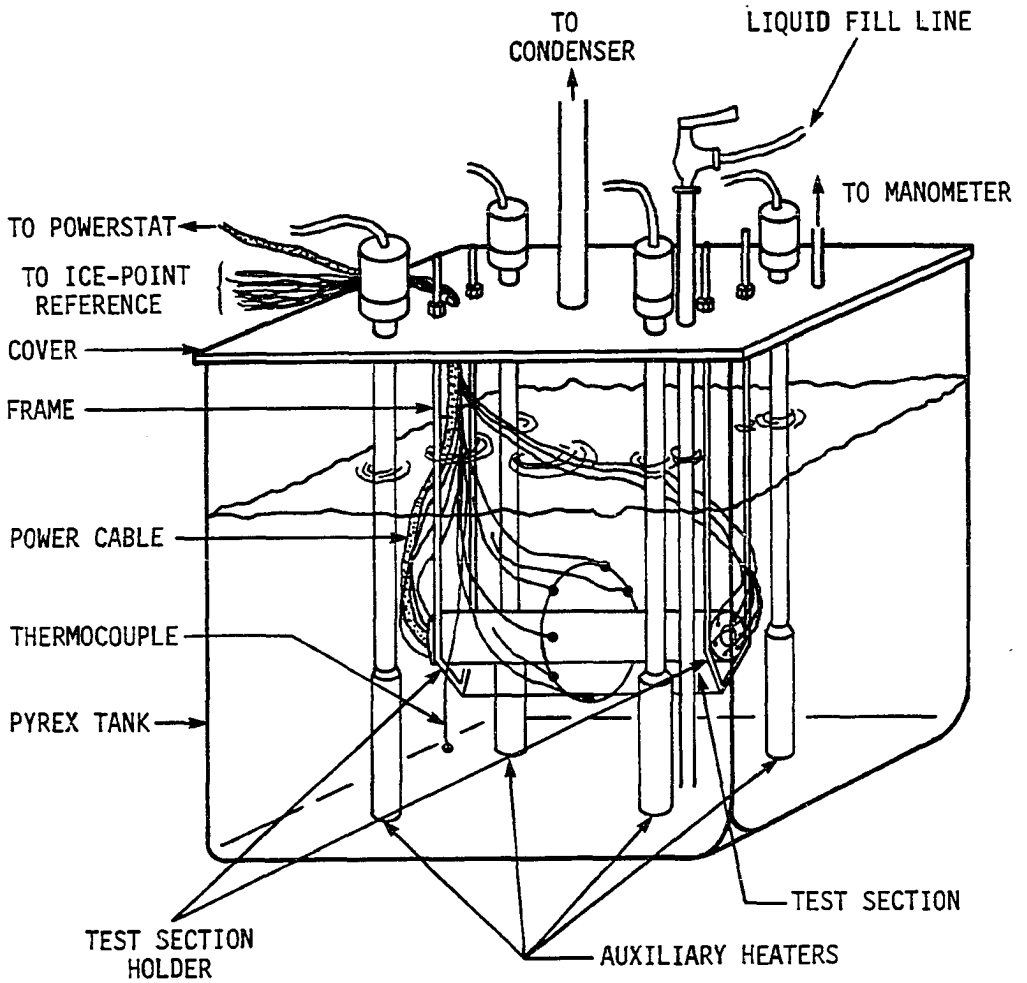

FIGURE 6. Pool boiling apparatus

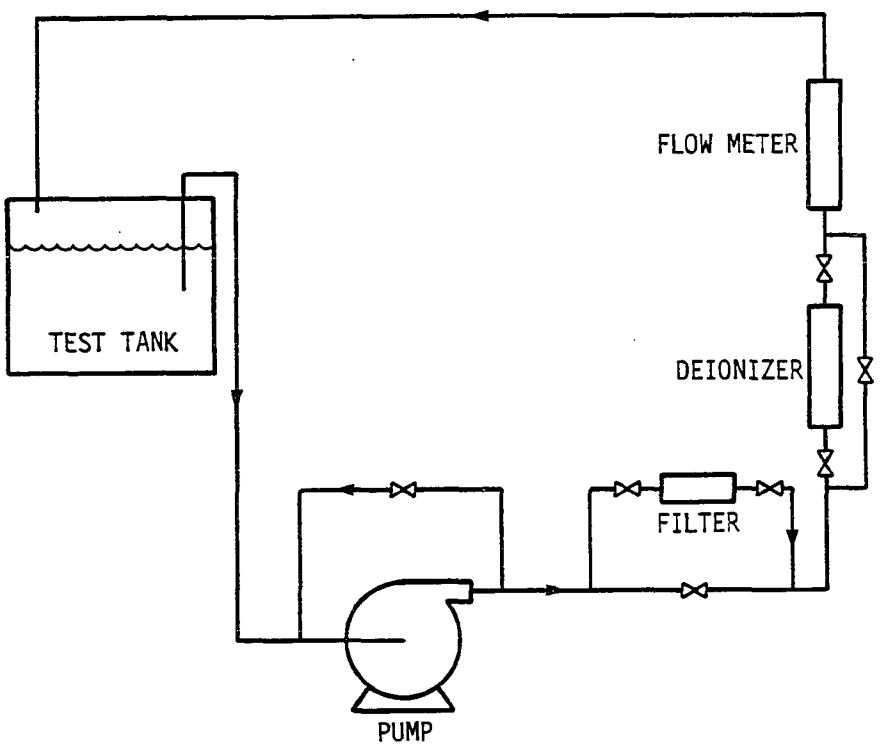

FIGURE 7. Distilled water deionizing loop

section. Insulation was provided on the bottom, sides, and top of the tank; one of the side panels was removable for visual observations. Buna-N served as a seal between the tank mouth and the aluminum cover plate.

An electrically heated cylindrical test section, consisting of a thick-walled copper tube with resistance heater on the inside, was mounted horizontally in the tank. GEWA-T and GEWA-K thick-walled tubes were tested. These tubes were specially prepared by Wieland-Werke AG of West Germany. A smooth (machined micro-roughness) thick-walled tube available from previous experiments [43] was also tested for reference. The dimensional specifics of these test sections are given in Table 1.

TABLE 1. Test section specifications

Test section	S_T,mm	fins/m	D,mm	D_b,mm	L,mm
GEWA-T19B	0.15	740	25.40	23.20	150.00
GEWA-T19C	0.25	740	25.40	23.20	150.00
GEWA-T19D	0.35	740	25.40	23.20	150.00
GEWA-T19E	0.55	740	26.04	23.42	150.00
GEWA-K19	0.99	740	26.40	23.42	150.00
GEWA-K26	0.73	1020	26.40	23.42	150.00
SM (plain)	-	-	25.40	25.40	150.00

The GEWA-T19E was fabricated in the Department of Mechanical Engineering. Since Wieland-Werke was unable to provide a thick walled cylinder that had a gap width in the 0.45 - 0.60 mm range, a GEWA-K19

tube was modified in a lathe using cylindrical steel rollers to flatten the tips. This result was surprisingly good, and the final product had a gap width of 0.55 ± 0.1 mm.

A detailed sketch of the GEWA-T test section is given in Fig. 8. Six thermocouples equally-spaced circumferentially at two axial locations, were installed. This was accomplished by drilling 1.4 mm diameter holes, 40 mm deep, from each end of the tubes. The bottoms of the thermocouple holes were located using the method devised by Chyu [62]. The radial position accuracy is estimated to be ± 0.04 mm. To minimize longitudinal conduction, silicone rubber and Devcon five-minute epoxy mixed with polystyrene foam were applied at the ends for use with water and R-113, respectively. The reason for using different types of insulation with both fluids was that silicone rubber is not compatible with R-113. Calibrated copper-constantan thermocouples of 30 gauge were employed to measure wall temperatures.

A Watlow Electric (J6A36; 240 V; 1000 W) cartridge heater was soft-soldered into each tube for better contact. It was found that the cartridge heaters had inactive zones at either end and in the middle of the heater. There were also weak circumferential gradients in power density, but those could be ignored. Analytically based corrections were applied to the overall power measurements to get the local heat fluxes [62].

Power supplied to the test section and auxiliary heaters was controlled via powerstats. Test section power was measured by a Feedback EW604 wattmeter.

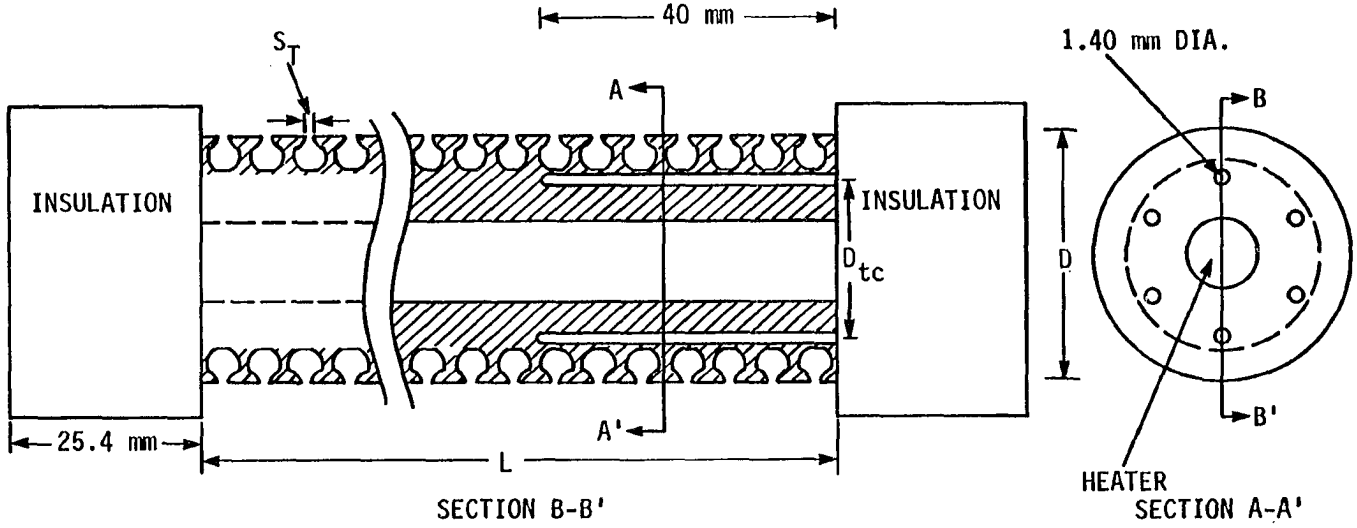

FIGURE 8. GEWA-T test section and thermocouple locations

The data were logged by the Heat Transfer Laboratory Data Acquisition System [63], basically composed of an electronic ice-point reference (Kaye Instruments K170-36C), an A/D converter (HP 3456A), a multichannel scanner (HP 3421A), a micro-computer (HP 9825), and a printer (HP 9871A).

The area used for the corrected heat flux was based on the length, L, and outside diameter, D. The wall thermocouple readings were adjusted for the small temperature gradient from the thermocouple beads to the fin base (D_b, root diameter) by employing the conduction equation in cylindrical coordinates:

$$\Delta T = \frac{q'' D_b}{2k_c} \ln(D_b/D_{tc}) \tag{3.1}$$

At high heat flux a temperature difference of 0.7 K was observed around the circumference of the test sections. Since no definite patterns were observed, it was decided to simply arithmetically average out the corrected wall temperatures. The pool temperature was measured by three thermocouples immersed in the tank around the test section at different locations. The saturation temperature corresponded to the pressure at the midplane of the test section, as obtained from the ambient pressure measured with a precision mercury barometer together with the hydrostatic head, as shown in Appendix 1. The chamber pressure was essentially atmospheric as no significant difference was observed by a mercury manometer installed between the chamber and the environment.

The pressure measured was within a range of 729 - 746 mm of mercury. The uncertainty in average wall superheat was estimated to be ± 0.1 K (Appendix 7).

B. Experimental Procedure

The regular test sections were first cleaned with chlorinol and water and, finally, with acetone. The tank, too, was cleaned with acetone before each run. Since the main purpose of the present studies was not incipient boiling, only one method of surface treatment was employed.

Water was allowed to run through the reflux condenser during the entire experiment. Power was given to the pool by four auxiliary heaters (Chromolox CSL 11600) and the test section. Degassing at a test section heat flux of 60,000 W/m^2 continued for three hours with water and 35,000 W/m^2 for one hour with R-113. The power to the test section was then slowly but continuously reduced to zero. The pool was maintained close to saturation temperature with the auxiliary heaters for the next 30 minutes. A slight sub-cooling of 0.1 - 0.3 K was unavoidable.

The power to the test section was raised in increments. Readings were taken five to ten minutes after each power change. This time was observed to be sufficient to attain steady-state conditions. Before recording the data, the auxiliary heaters were shut off to minimize convective effects. Most of the vapor was condensed back into the pool;

however, some loss of test fluid through the condenser and via minute leaks was unavoidable. Thus, the test fluid was replenished during the course of the run so that a nearly constant liquid level of 10 cm above the midplane of the test section was maintained.

Test-section power, atmospheric pressure, and pool level data were fed into the computer for each run. The data acquisition system, in turn, carried out the required thermocouple sampling and calculations. Due to some fluctuations, each channel was scanned ten times and the average corrected wall temperature was calculated. Finally, the wall superheat for each flux level was calculated.

The curves for experimental results of GEWA surfaces were coded as follows:

X-YnnZ/L

where,

- X = type of surface
- Y = code for structure
- nn = fins per inch
- Z = gap width designation
- L = type of liquid

For example, GEWA-T19D/W or F relates to

- GEWA = X

- T = Y
- 19 = nn
- D = Z
- W or F = L

C. Special Thermocouples

In order to gain insight into the vaporization processes occurring in the channels, it was decided to implant some thermocouples in one channel of the GEWA-T19D test section. The object was to suspend the thermocouples in the channel without touching either the side walls of the adjacent fins or the base of the tube, as shown in Fig. 9a. This was not an easy task in view of the dimensions involved. Very small diameter (40 gauge, copper-constantan) thermocouples were utilized. A first attempt to secure them with epoxy did not work as the epoxy drained into the channel by capillary action, eventually clogging the channel. It was then decided to drill holes through the fin at an angle to the horizontal as shown in Fig. 9. Before performing this operation, a 100X sketch was drawn in order to determine the proper location of the holes. Finally, four thermocouples were installed in the same channel 60 degrees apart at the same angular position as the main thermocouples in the test section, as depicted in Fig. 9b.

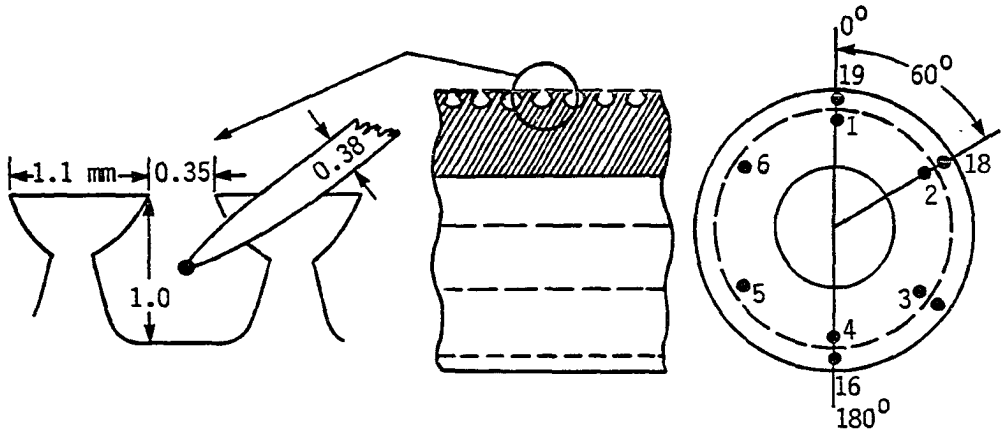

a. Details of in-groove thermocouples

b. Position of thermocouples in the test section and the channel

FIGURE 9. Special thermocouples

D. Scaled Up Models

For detailed visual tests, GEWA-T single groove simulators were fabricated as shown in Figs. 10 and 11.

For tests with water a scaled-up model was fabricated from a brass block, as shown in Fig. 10. First, a brass 30.48 mm cube was machined to a trapezoidal shape. A 12.7 mm hole was then bored to install a cartridge heater (120 V, 150 W). The top rectangular portion, 1 mm x 2 mm x 30.48 mm was milled to form two rectangular fins. Next, a thin brass strip 2 mm x 0.2 mm x 30.48 mm was carefully soldered to the outer fin ends. Finally, the strip was machined off at the center, along the 30.48 mm length. This resulted in a slit of 0.35 mm along the groove similar to that for the GEWA-T19D.

The side walls in the scaled-up model in Fig. 11 were fabricated from polycarbonate glass sheet. As polycarbonate glass cannot withstand temperatures above about 330 K, this simulator was only used with R-113. Two 38 mm x 42 mm rectangular pieces were cut from the sheet. Two very thin strips of transparent flexible plastic, each folded at 90 degrees, were glued by super glue to the lower sides of these rectangular pieces, as shown in Fig. 11b. The rectangular pieces were then glued vertically to a 54 mm x 25.4 mm x 12.7 mm brass block in such a way that the transparent pieces faced each other and resulted in a continuous slit with a gap width 0.35 mm, again similar to that for the GEWA-T19D. Then two other strips, 38 mm x 7 mm, were glued at the other opposite sides, resulting in a box with the top side open. No heater was installed in

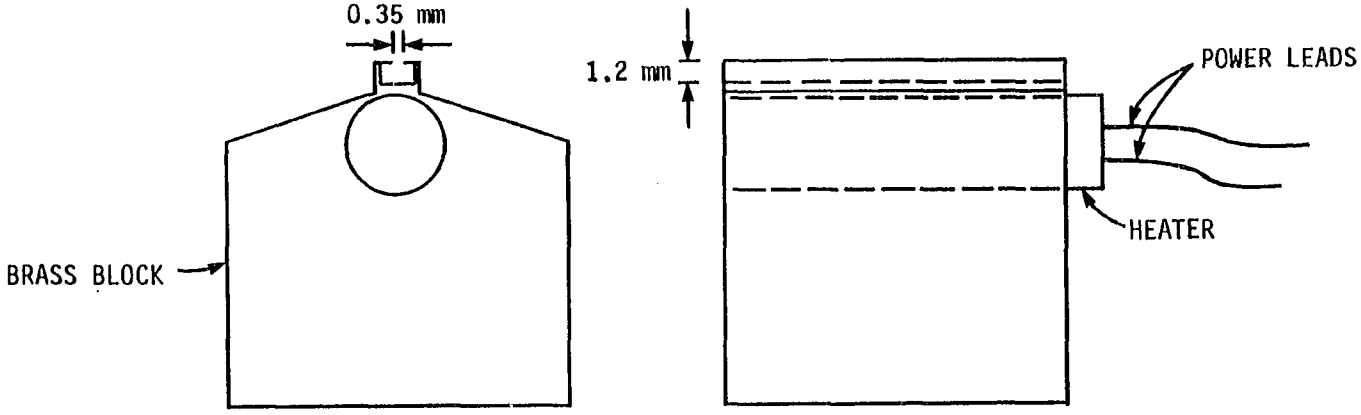

FIGURE 10. Single channel GEWA-T19D simulator for water

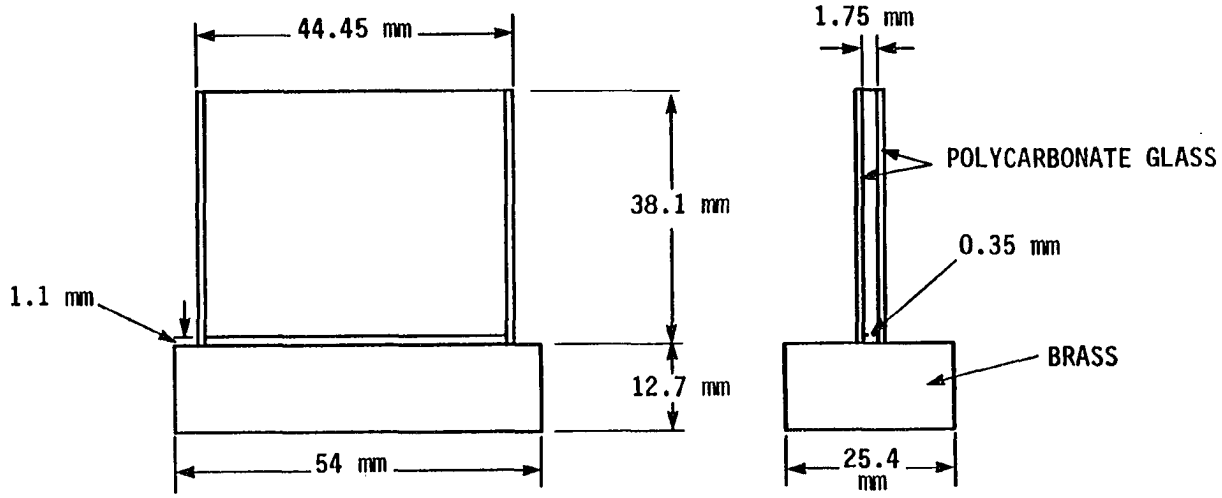

FIGURE 11. Single channel GEWA-T19D simulator for R-113

the base block, rather the entire test section was placed over a hot plate. In order to compensate for the rapid depletion of R-113, a constant supply of R-113 was maintained by injection with a needle syringe.

IV. RESULTS AND DISCUSSION

More than twenty-five test runs were performed on smooth, GEWA-T, and GEWA-K tubes in saturated distilled water and R-113. Some of these tests were repeated after several months to verify the reproducibility. The repeat runs were always in excellent agreement.

A. Smooth Tube/Water and R-113

Smooth tube data were used as a reference for GEWA-K and GEWA-T data. The low heat flux, non-boiling portion of the curves were higher than the predicted natural convection data [64]. This could be due to residual enhanced pool convection from the heaters and some sub-cooling. A small sub-cooling, ΔT_{sub}, could substantially elevate the boiling curve in the low superheat region since $q'' = h\ (\Delta T + \Delta T_{sub})$. The water data shown in Fig. 12 indicate no temperature overshoot, whereas a relatively mild overshoot was observed with R-113 as shown in Fig. 13. If the heat flux had been delicately controlled then an increasing flux path, as shown in Fig. 13 by the dashed line, would have been observed.

B. GEWA-K/Water and R-113

GEWA-K with 740 and 1020 fins/m were tested in water and R-113. At low heat flux, the mode of heat transfer was by natural convection. As the power to the test section was increased, bubble activity was observed from within the channels. The bubbles were ejected at the top, although some of them might have been formed at sites other than the

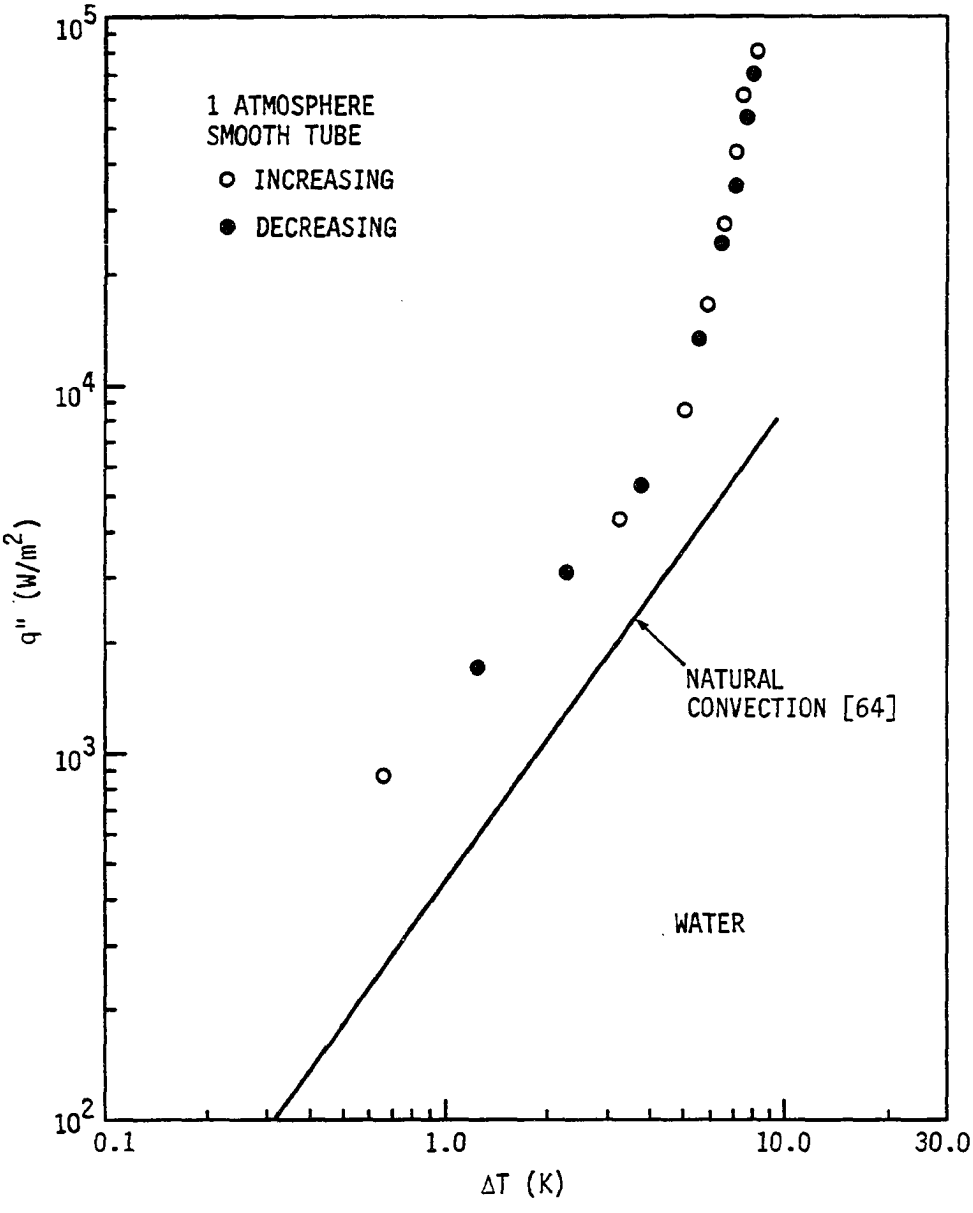

FIGURE 12. Smooth tube data with water

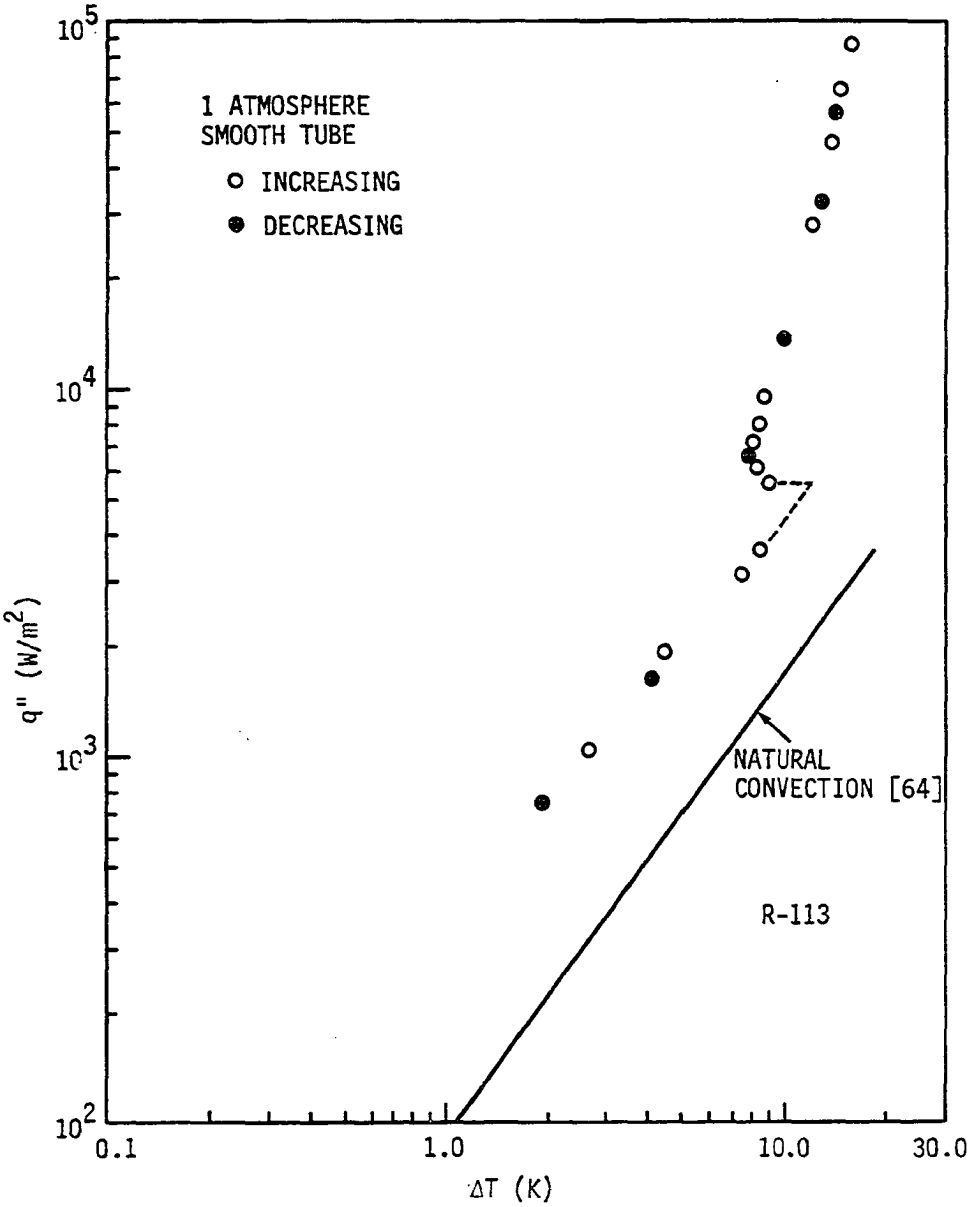

FIGURE 13. Smooth tube data with R-113

top, but because of favorable flow conditions they were swept upward along the channel. This is the point of incipient boiling, indicated by Point A in Figs. 14 and 15. Beyond Point A, the bubble activity became more vigorous with an increase in the heat flux. Bubbles of comparatively low frequency, but with large departure diameters, were observed at the bottom of the test-section. Between Points B and C, bubbles were observed not only at the top and bottom but also at the sides. At a heat flux of 80,000 W/m^2 the enhancement is 1.14 and 1.56 for water and R-113, respectively.

Fin density has very little effect on the thermal performance, and on the basis of total surface area ($\pi \times D_i \times L \times A_o/A_i$), the data are virtually identical, as shown in Fig. 16.

Since there was a limit on the heater power, very high heat flux data could not be recorded; however, the water data (based on total surface area) appear to conform with the results of Yilmaz and Westwater [30]. Higher flux data from this study, when extrapolated, merge with their lower heat flux data, as shown in Fig. 17.

C. GEWA-T/Water

Boiling tests for four different GEWA-T surfaces were performed. No temperature overshoots were observed with any of these tubes. Since no other water data are available in the literature, it was difficult to directly verify the results. However, it is felt that the boiling curves are reliable since they were found to be quite repeatable.

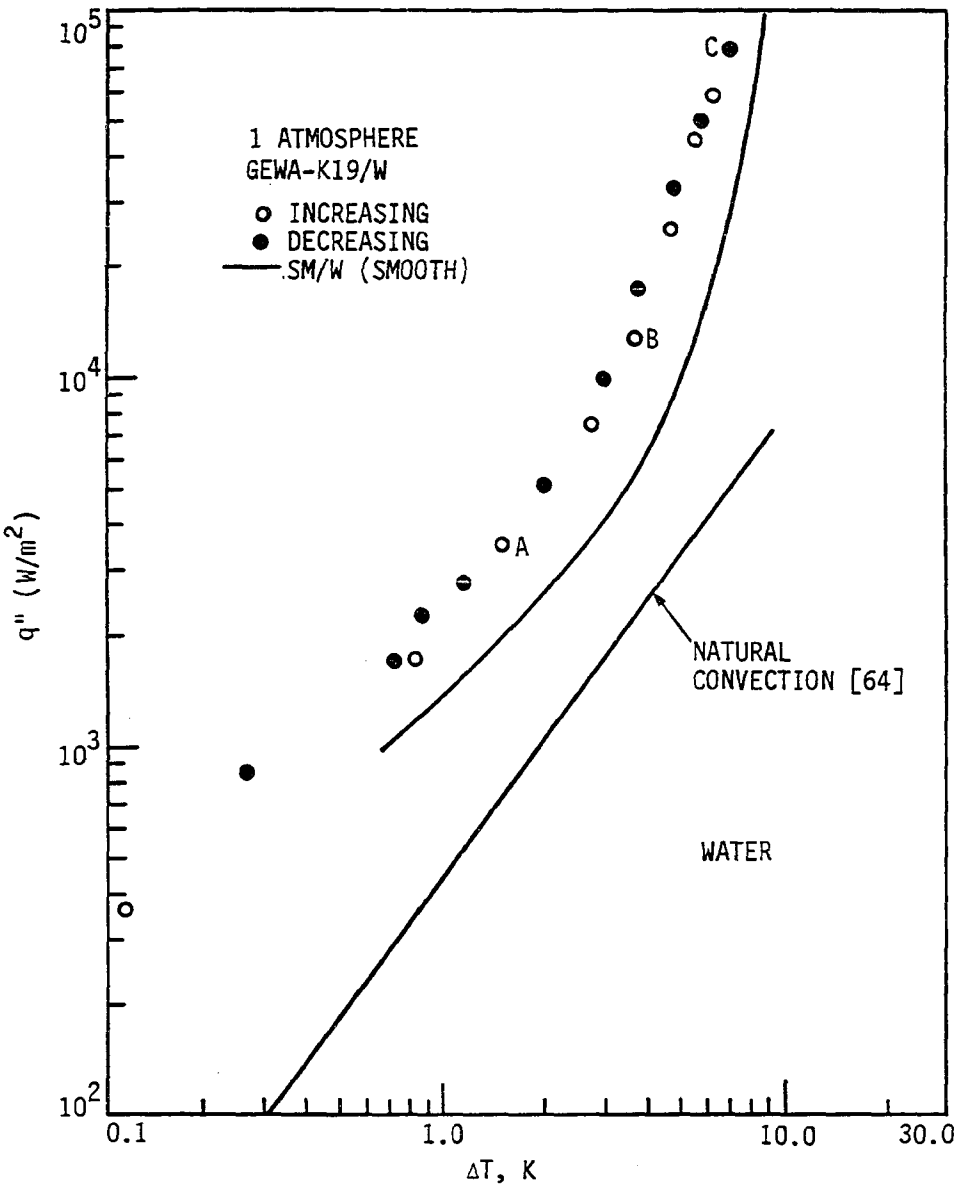

FIGURE 14. Plain fin GEWA-K19/W data

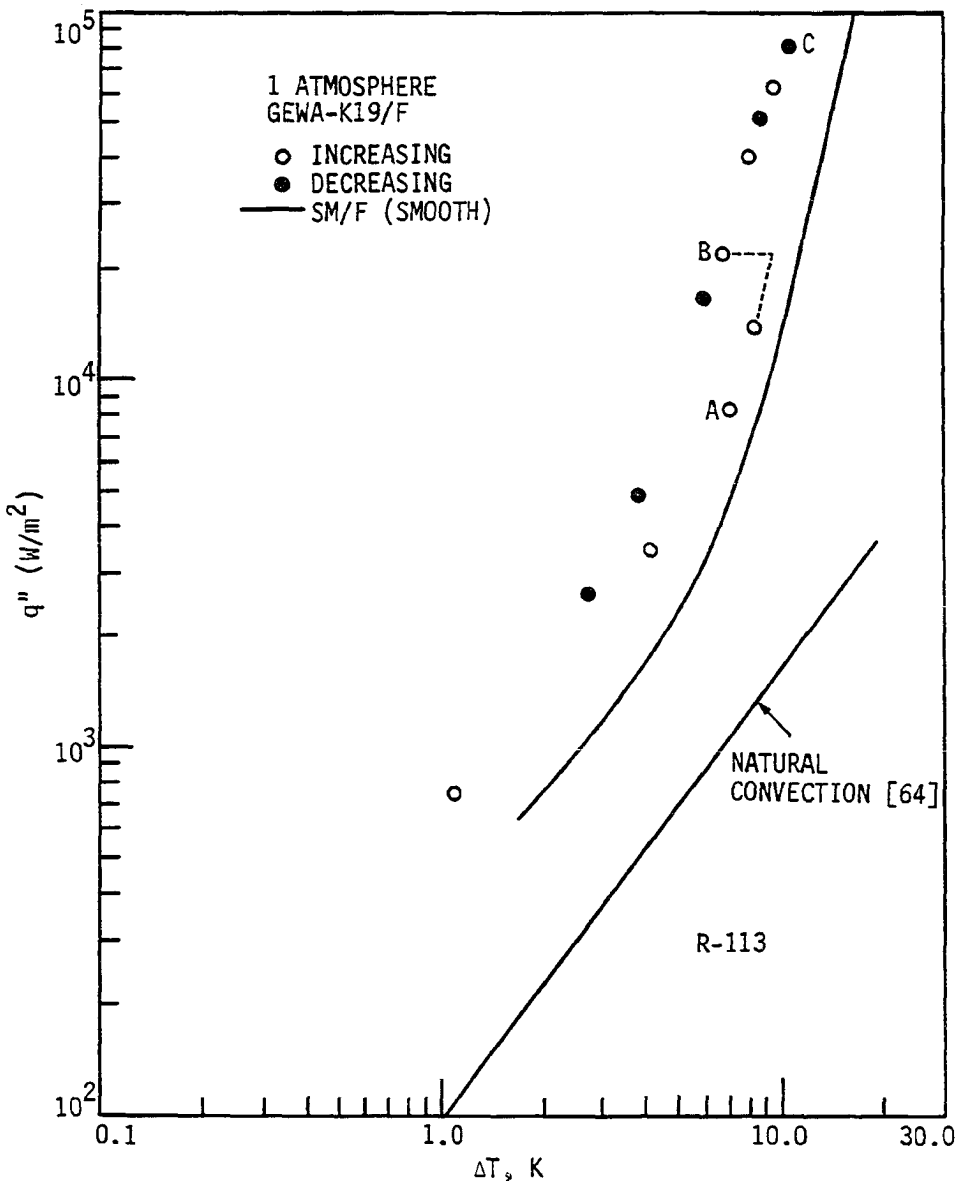

FIGURE 15. Plain fin GEWA-K19/F data

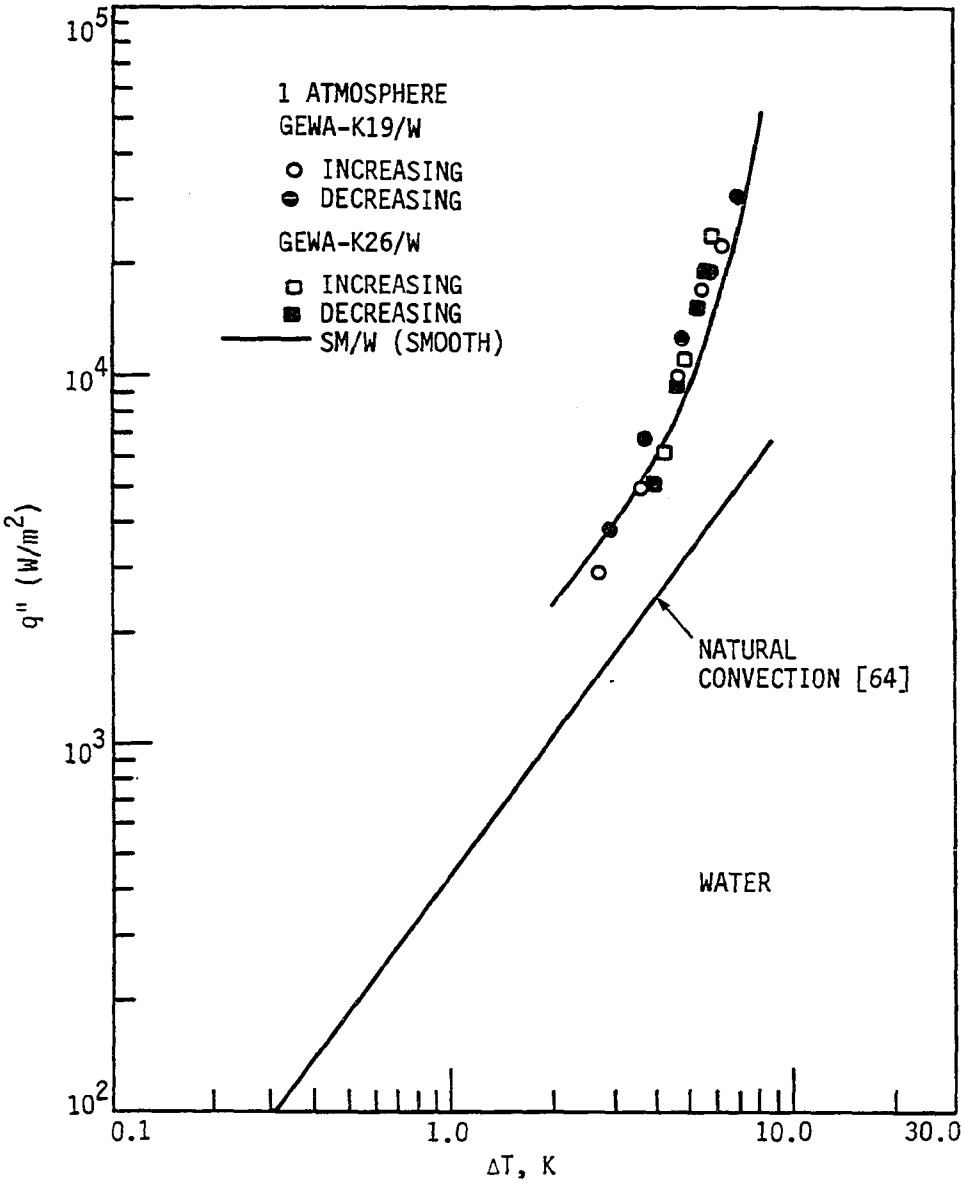

FIGURE 16. Boiling data for GEWA-K19/W and GEWA-K26/W

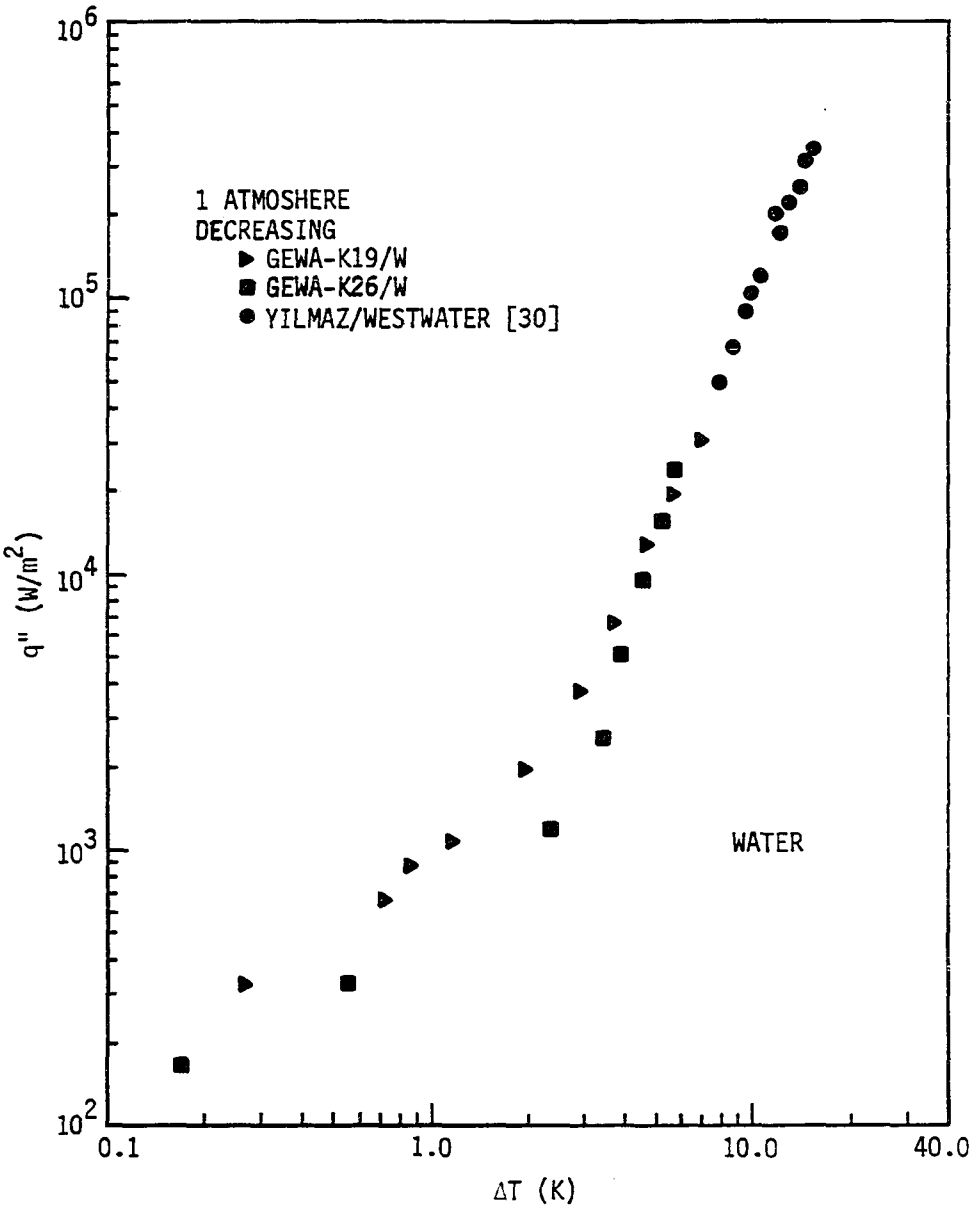

FIGURE 17. Comparison of GEWA-K data with [30]

1. GEWA-T19B/W

This test section had the smallest gap width, S_T = 0.15 mm. Low heat flux data were similar to the GEWA-K data. Natural convective currents, similar to GEWA-K were observed, indicating that in the natural convective zone it did not make any difference whether the fins were standard low fin or modified T-fin. This is due to the fact that for the same fin density the area ratio, A_o/A_i, remains the same for both types of surfaces. Bubbles started emerging from the top portion at a heat flux indicated by Point A in Fig. 18.

With a further increase in the heat flux, the bubble activity increased and at the same time started spreading all over the tube. Large ellipsoidal-shaped bubbles were observed at the bottom of the test section that swept upward along the circumference after detachment. They moved on either side of the tube depending upon the force imposed on them due to buoyancy and pool convective currents.

At a heat flux of 17,000 - 20,000 W/m^2 the vapor streams coalesced approximately 12.7 mm above the top of the test section. This distance decreased with an increase in the heat flux. But even at higher heat flux there was always some distance between the top of the tube and the point of coalescence. The GEWA-T surfaces have a substantial axial spacing between the bubble sites (channels); this allows for liquid inflow into the channels, and delays the departure from nucleate boiling. Hence this phenomenon gives this surface an advantage over the High Flux and Thermoexcel-E at high heat flux, as observed by Marto and

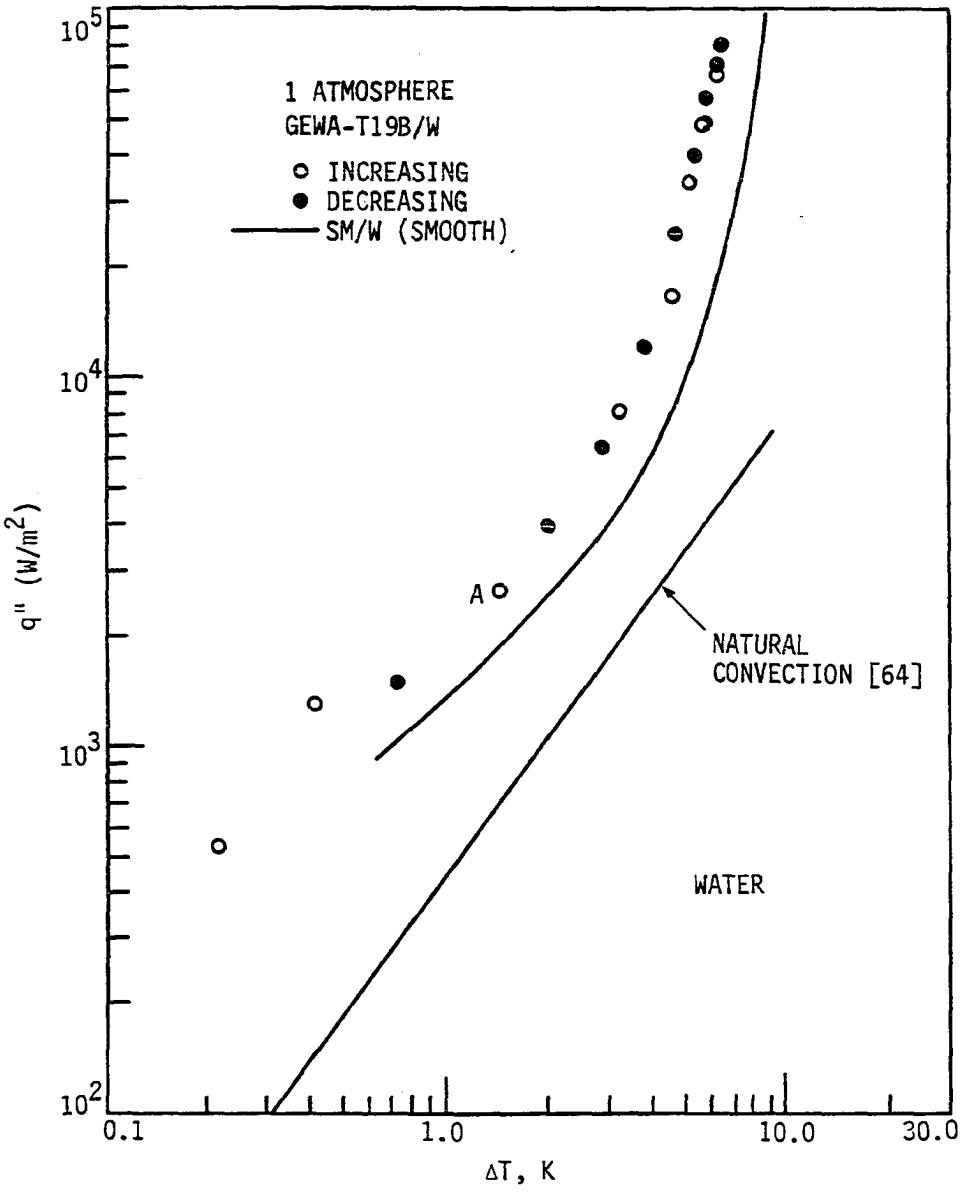

FIGURE 18. Boiling data for GEWA-T19B/W

Lepere [28]. The decreasing heat flux data followed the increasing heat flux data, indicating that the system was well degassed. Figure 19 shows data for a repeat run performed six months after the first test. The excellent reproducibility suggests lack of experimental error and stability of the liquid-surface condition.

The non-boiling portion is above the natural convection portion of a smooth tube. This is because of the larger surface area of the enhanced surface. The data approximately coincide when the enhanced tube data are multiplied by the area factor, A/A_o.

2. GEWA-T19C/W

The bubble activity was very similar to GEWA-T19B/W, and the boiling curve was again well-behaved as shown in Fig. 20. But at a heat flux less than 10,000 W/m^2, there was a larger shift of the boiling curve toward the left as compared to GEWA-T19B/W data. This shift was due to "rogue sites" at a low increasing heat flux. At a higher heat flux more sites became active, thus increasing the number of active channels. With decreasing heat flux, below a heat flux of 3,000 W/m^2, those 6 - 9 rogue sites were still active although at that point in time the total boiling period was well over 6 hours. These sites were probably the result of imperfections or indentations developed during the manufacturing process.

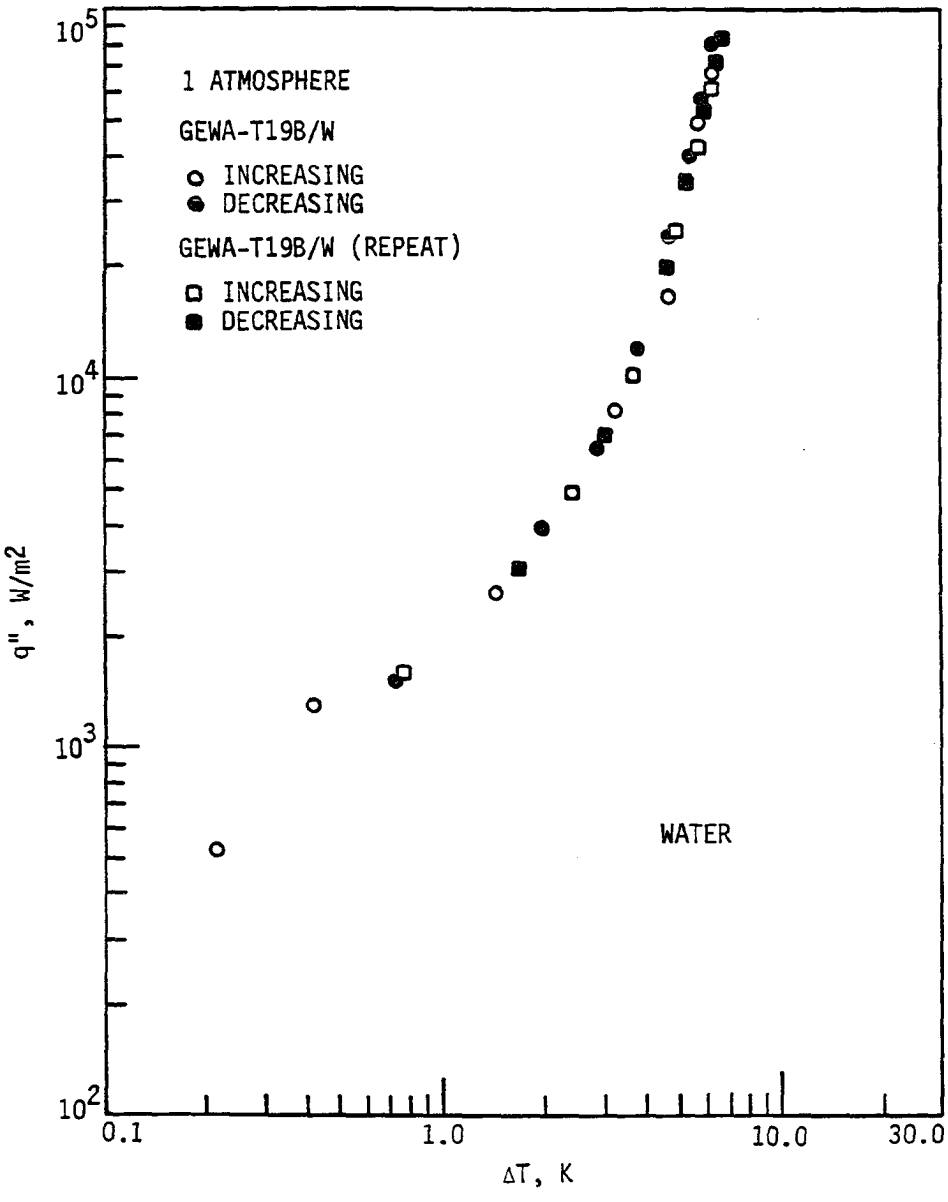

FIGURE 19. Boiling data for repeat run of GEWA-T19B/W

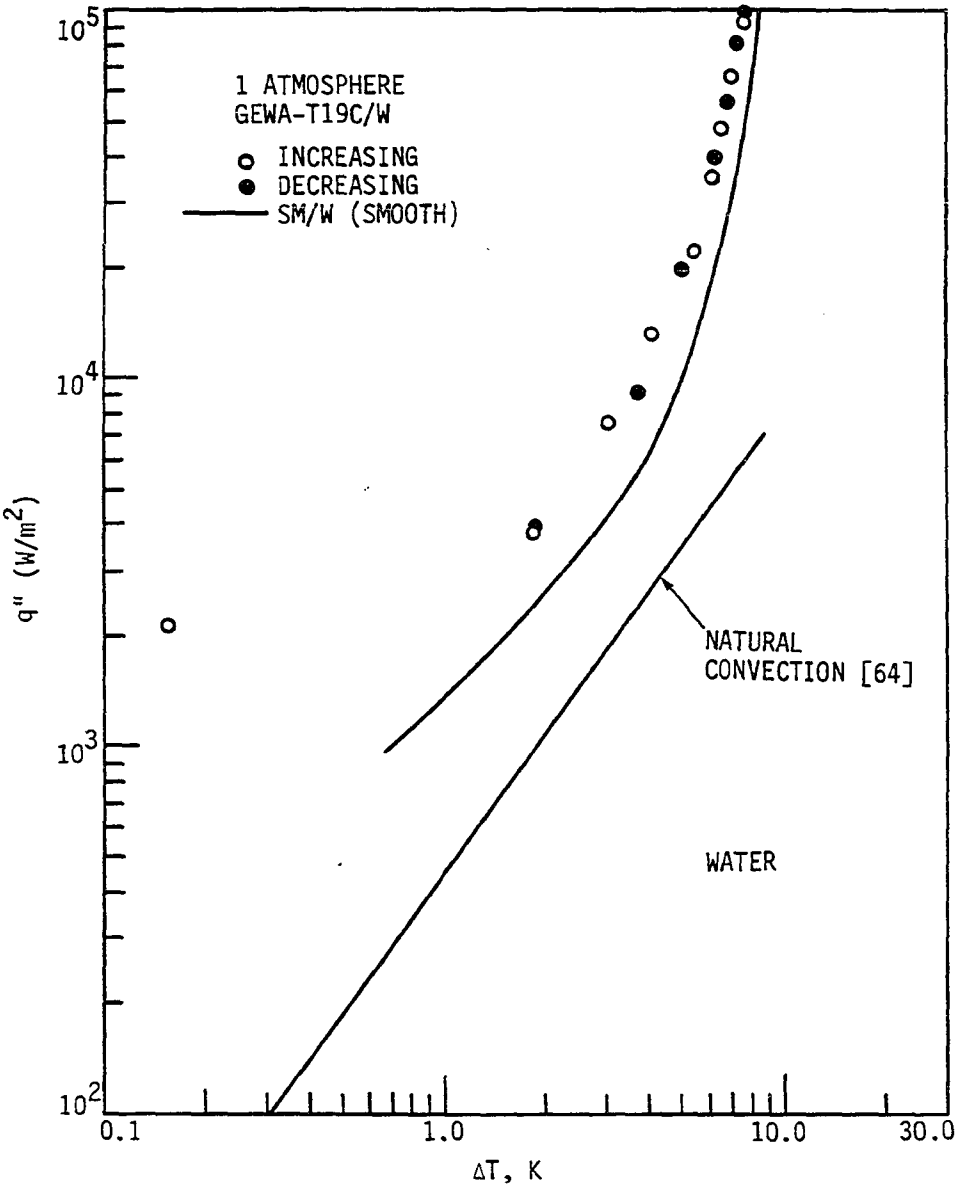

FIGURE 20. Boiling data for GEWA-T19C/W

3. GEWA-T19D/W

In the nucleate boiling zone, the overall bubble activity was similar to that for GEWA-T19B/W and GEWA-T19C/W. Beyond Point A in Fig. 21, individual bubbles appeared. As the heat flux was increased, the site density increased. The activity became more rapid above a heat flux of 35,000 W/m^2 (Point B). During the decreasing heat flux mode, the data followed almost the same path.

In order to further confirm the stability of the boiling surface and the integrity of the heating system, a new cartridge heater was installed in the same test section and the test section was rotated by 180 degrees. The data were similar in the partial and developed nucleate boiling zones, as shown in Fig. 22. The shift difference in the natural convection zone might have been due to incomplete degassing or the presence of a slight sub-cooling in the earlier experiment.

4. GEWA-T19E/W

The general boiling behavior with GEWA-T19E/W was similar to that of the other GEWA-T surfaces. For the data shown in Fig. 23, the bubble activity was also similar except that due to the large gap width, bubbling within the channel was much more observable. Especially at heat fluxes less than 10,000 W/m^2, it was easy to observe at the slit the pulsating interface caused by the bubble growth and departure. The bubbles developed at the slit, grew into a spherical shape and were anchored close to the rim of the slit.

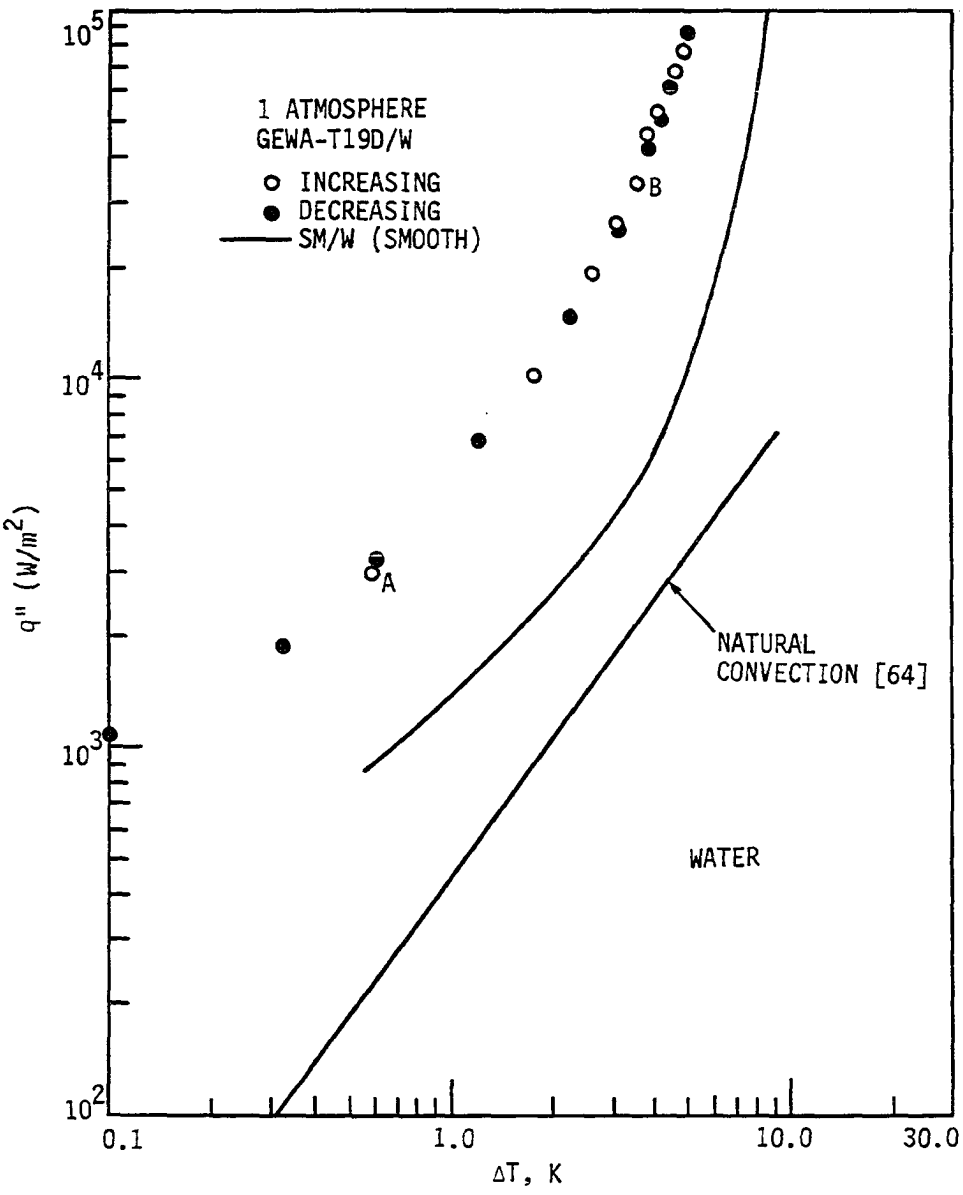

FIGURE 21. Boiling data for GEWA-T19D/W

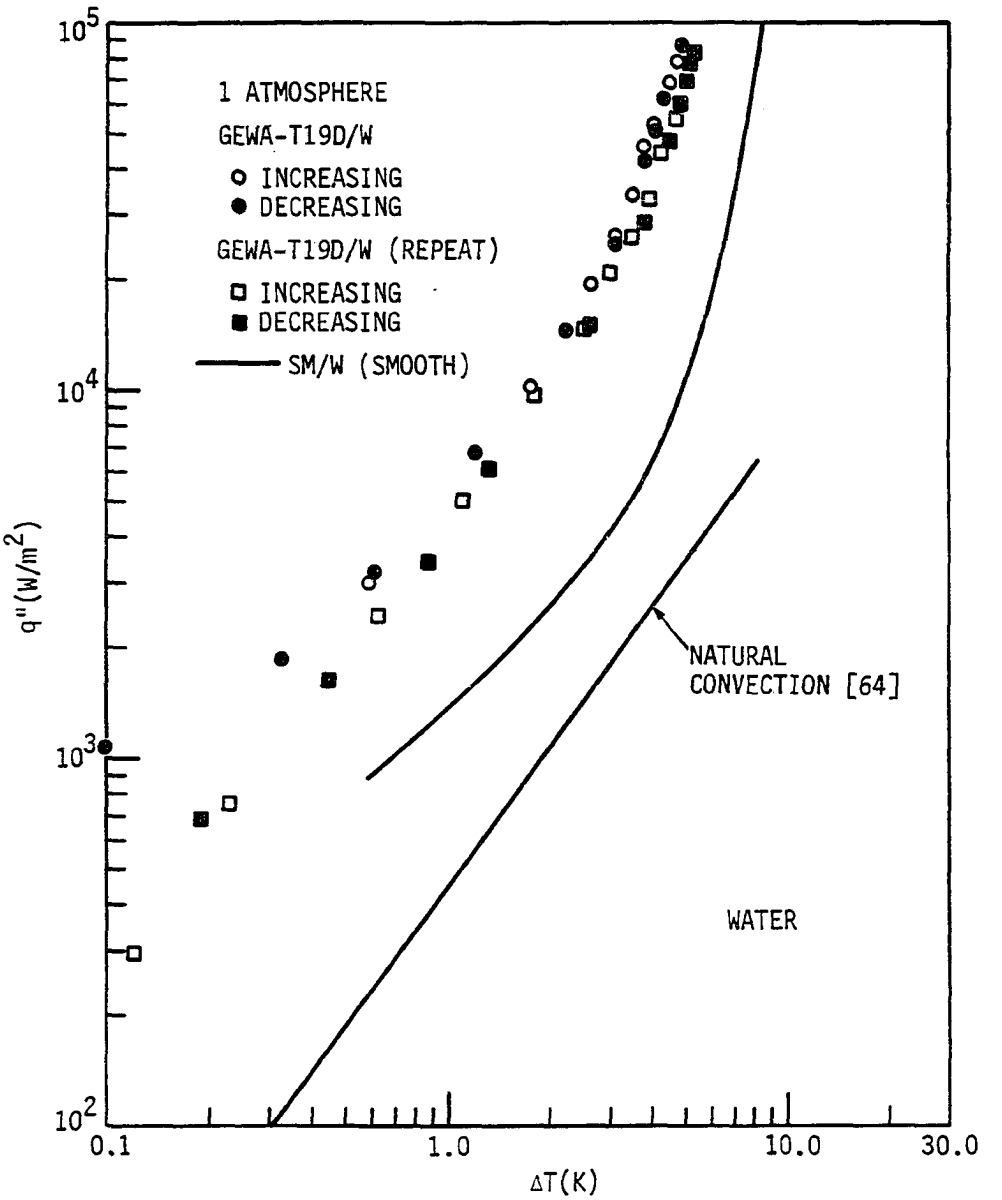

FIGURE 22. Boiling data for GEWA-T19D/W (rotated by 180°)

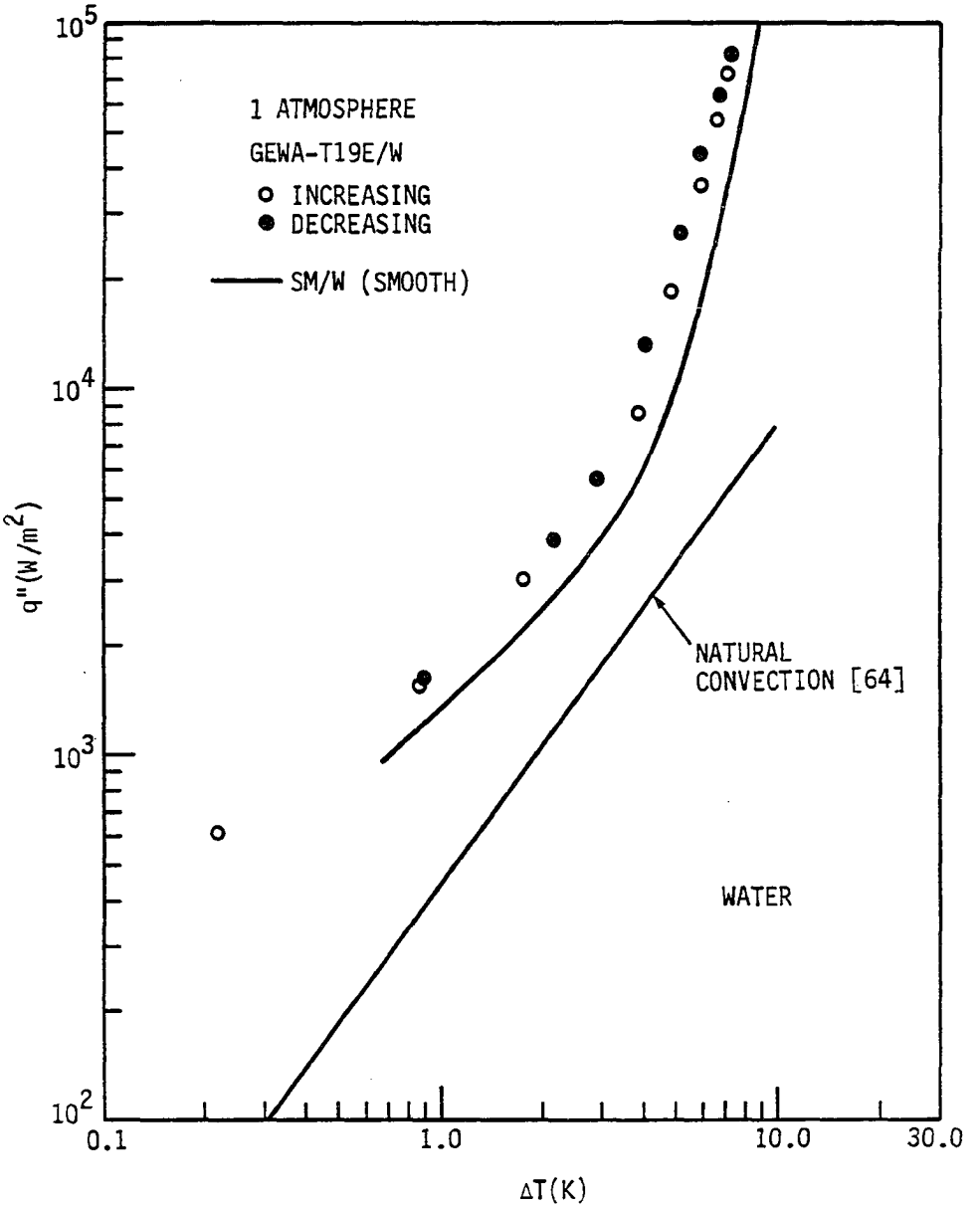

FIGURE 23. Boiling data for GEWA-T19E/W

D. Dependence of Enhancement on Gap Width with Water

A composite plot of the boiling curves for the four GEWA-T tubes is shown in Fig. 24. As judged by the degree of the shift of the boiling curves to the left, the enhancement is modest. The improvement in boiling performance is less than that reported for refrigerants [28, 52, 54]. At a heat flux of 80,000 W/m^2 the enhancement for GEWA-T19B, C, D, E is 1.3, 1.08, 1.6, and 1.1, respectively.

These results indicate that the gap size affected the thermal performance. No systematic data exist for this kind of study, except a partial study conducted by Saier et al. [11] for R-12 in which they concluded that there was an optimum gap width at S_T = 0.20 mm. At heat fluxes greater than 10,000 W/m^2, the present data show performance peaks at S_T = 0.35 mm and 0.15 mm rather than a single maximum, as shown in Fig. 25. This behavior is clearly different from that suggested by Saier et al.

E. Visual Tests in Water

Each test section demonstrated that at medium and high heat fluxes, ejection of vapor from the channels occurred around the circumference of the test sections rather than only near the top as proposed by Stephan and Mitrovic [52]. Some bubbles were ejected from the bottom as well, as observed by Marto and Hernandez [54]. Visual observations and photographs clearly showed bubble activity all around the tube though not necessarily at each channel as shown in Fig. 26. It was observed that the site activity was a function of heat flux.

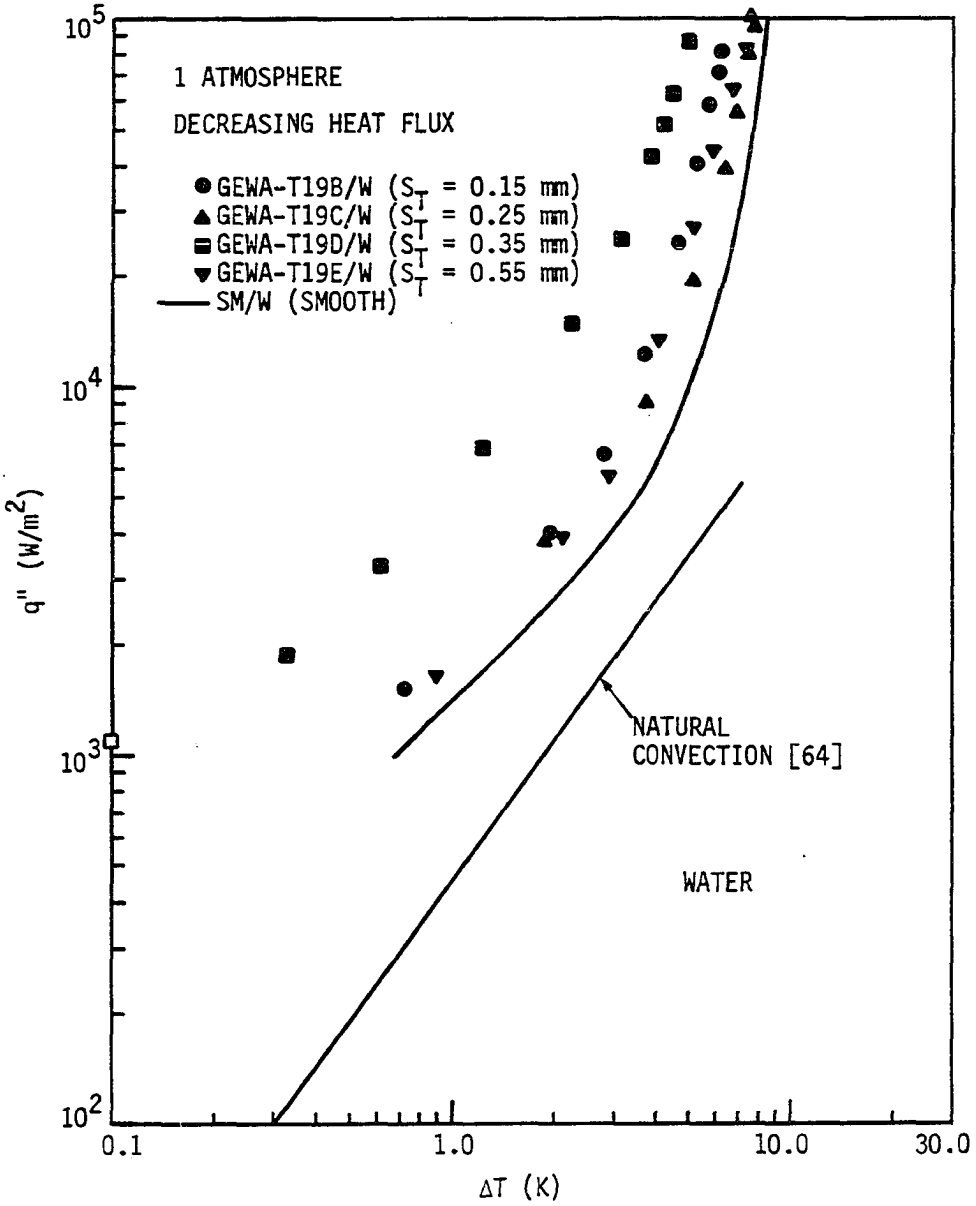

FIGURE 24. Composite plot for different GEWA-T surfaces in water

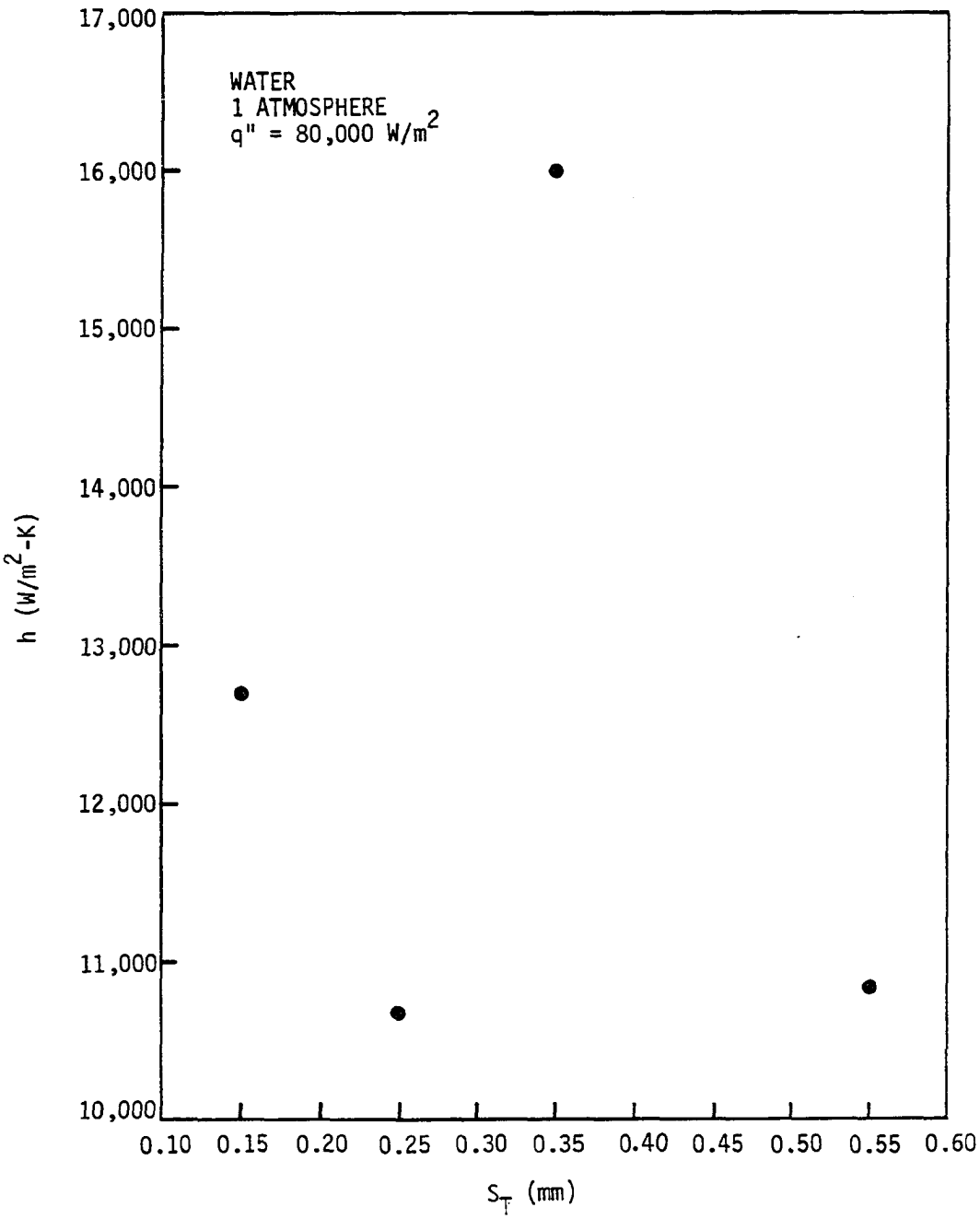

FIGURE 25. Heat transfer coefficient vs. gap width for water

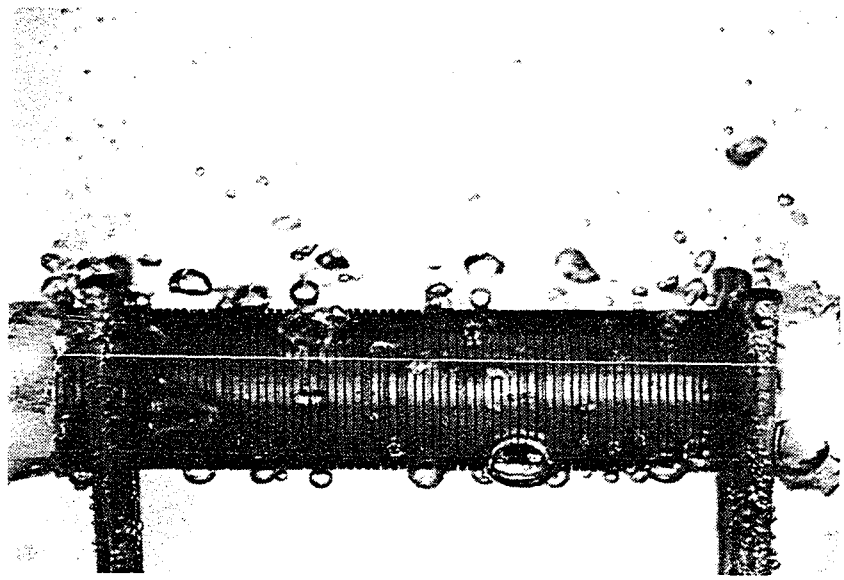

FIGURE 26. Boiling water on GEWA-T19C at 50,000 W/m^2

Another technique was employed to identify the liquid flow paths. This was accomplished by carefully introducing blue dye into the water at numerous locations around the circumference of the test section using a hypodermic needle and a syringe. It was found that within the developed nucleate boiling mode, there was a pattern of liquid inflow at different locations around the test section. At random channel locations along the axis of the test section, these liquid-feed spots were at either side, near the bottom, at either side above the horizontal plane, and at top dead center. This liquid was vaporized, and bubbles were ejected at adjacent locations directly at the bottom, at either side around the horizontal midplane, and at either side near the top.

This flow pattern was further confirmed by the small diameter special thermocouples installed in a single channel of GEWA-T19D, as shown in Fig. 9. Under boiling conditions, the recorded temperatures, as presented in Fig. 27, were always slightly above saturation. As the heat flux increased, the temperature fluctuations increased to as much as ± 0.95 K. The thermocouples were apparently responding to periodic flow of superheated liquid and saturated vapor in the channel. To assure that these results were not associated with thermocouple bias errors, the test section was rotated 180 degrees. Similar results were obtained.

The GEWA-T19D simulator shown in Fig. 10 was tested in a pool of distilled saturated water. Since it had an isolated channel, it was

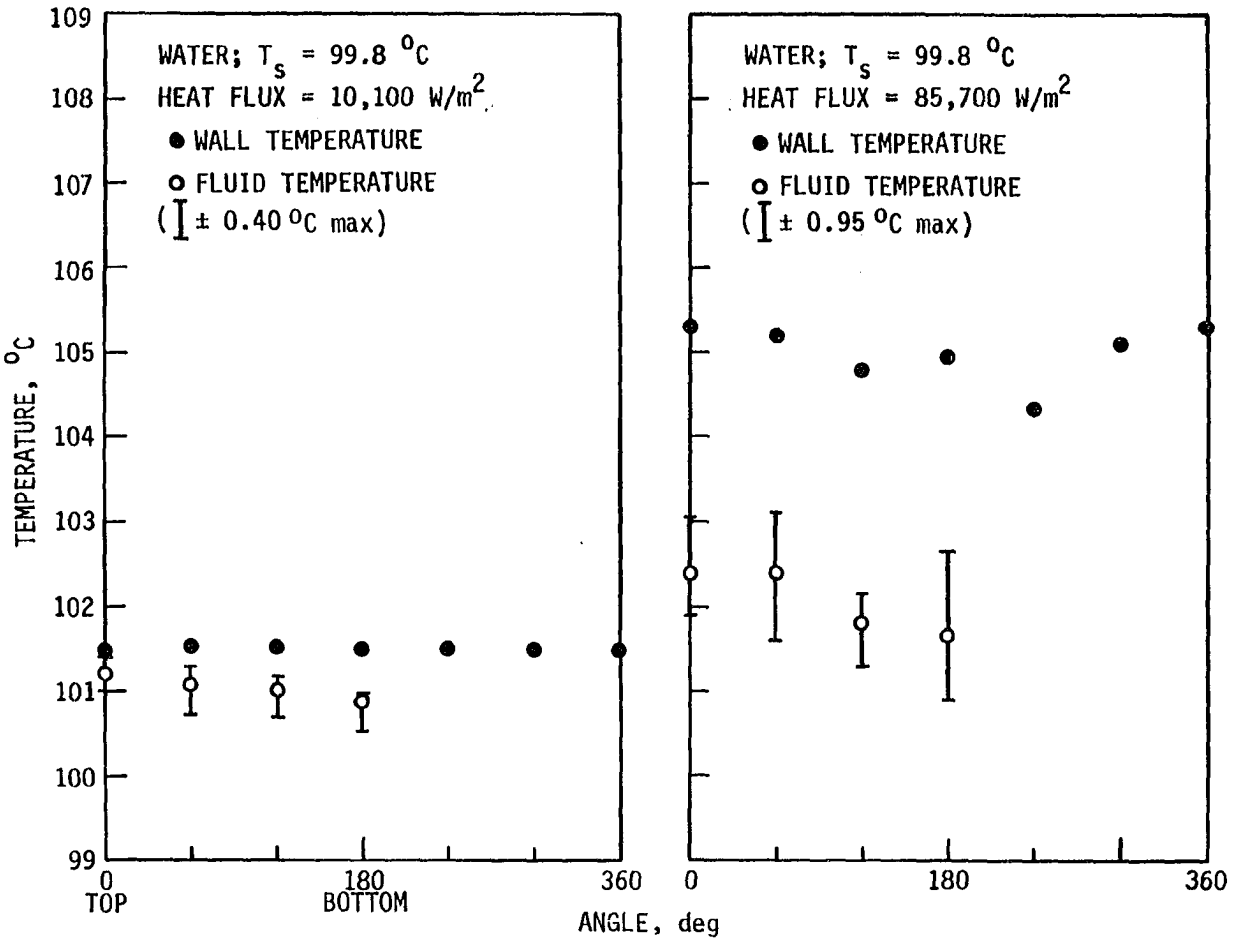

FIGURE 27. Temperature data for a single GEWA-T channel

easier to observe both the liquid inflow and the vapor ejection. The pulsating motion of the interface at the rim of the channel was confirmed by this test. The simulator was then oriented at different angles so as to simulate the different quadrants of the actual test section. The bubbles were detected at the channel rim for all orientations. The shape of these bubbles was predominantly spherical, except for the bubbles ejected while the test piece was upside down. In this position, the bubbles were of ellipsoidal shape, similar to those observed at the bottom of the actual test sections.

F. GEWA-T/R-113

Similar tests were performed on GEWA-T tubes in saturated R-113. The results obtained with each test section are described below in detail.

1. GEWA-T19B/F

The general bubbling activity was similar to the tests with water, except that at higher fluxes there were comparatively more sites per unit area and the departure diameters were smaller than with water. This was expected, in view of the properties of R-113, especially the small contact angle.

Though the degassing of the test section and the tank was performed for one hour, several bubbling sites were observed at a heat flux as low as 1,700 W/m^2. The bubbles were coming out of the top of the test section; however, they might have originated at spots other than the top

within the channels. This bubbling was due to some defects within the channels caused during manufacture. At these sites the gas was probably not completely expelled. Thus, these sites prevailed even during the decreasing heat flux mode, in spite of the fact that by that time the boiling process had continued for more than five hours. Figure 28 shows the boiling data for this run.

Up to a heat flux of 8,311 W/m^2, the mode of heat transport was natural convection, except for those isolated sites mentioned above. As the heat flux was increased from 8,311 W/m^2 (Point A) to 12,511 W/m^2 (Point B), nucleation started at one end of the test section. The effect was immediately reflected in the wall temperatures of this end of the test section, i.e., a slight drop in the temperature compared to the other end. Increasing the heat flux to 20,733 W/m^2 (Point C), a sudden burst of bubbles was observed. The entire test section had nucleated, triggering developed nucleate boiling.

The temperature overshoot (Points A - C) resulted in a boiling curve hysteresis as shown in Fig. 28. Due to partial nucleation of the test section, the temperature drop follows a step path between Points A and C. As noticed from the plot the magnitude of this overshoot is 3.5 K, which is comparatively lower than that with High Flux and Thermoexcel-E [43, 62]. The data of Marto and Lepere [28] for different surface aging techniques showed higher temperature overshoots for GEWA-T as compared to High Flux and Thermoexcel-E. But their data for GEWA-T, employing surface aging technique B are not available; therefore, their

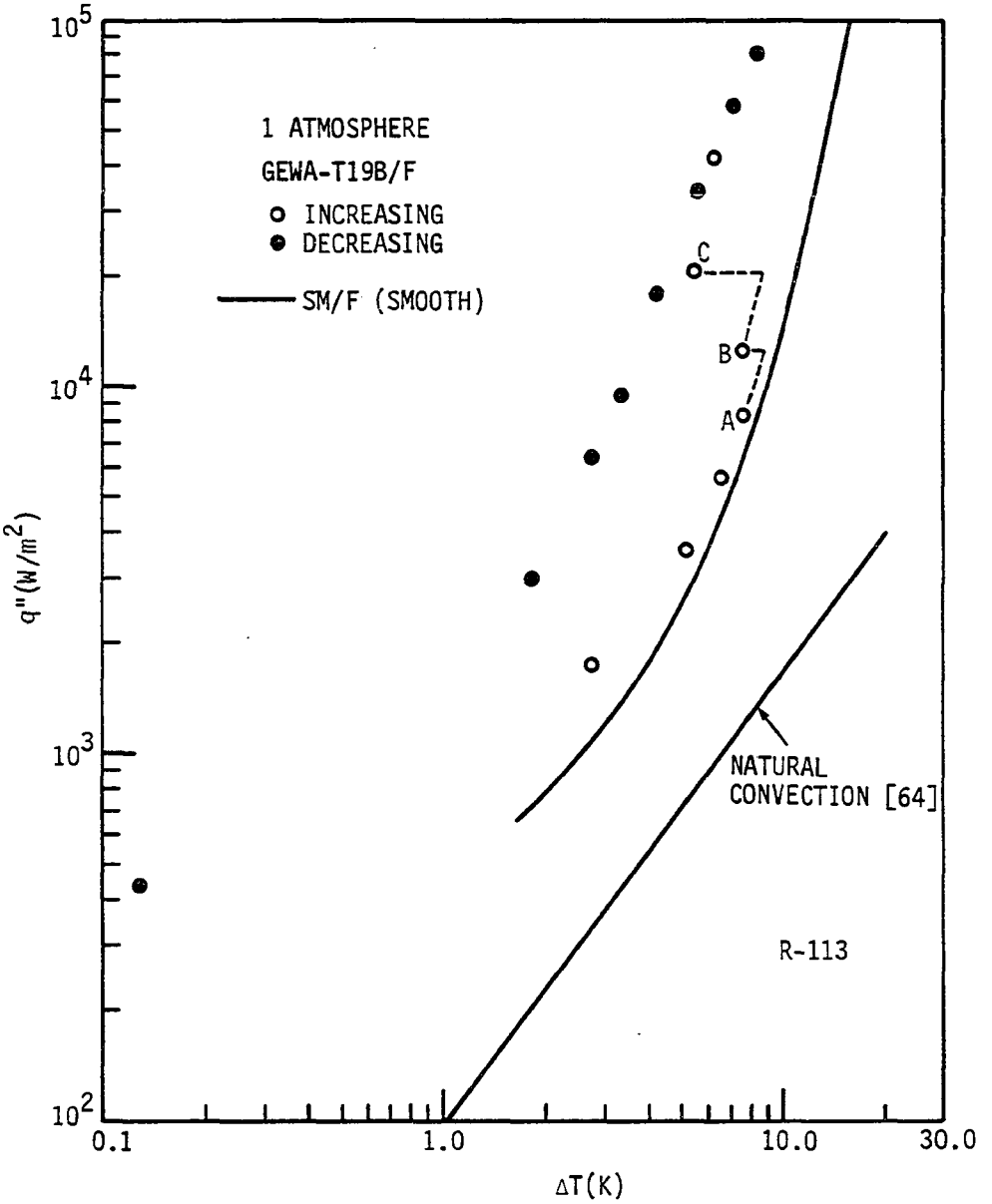

FIGURE 28. Boiling data for GEWA-T19B/F

statement that the superheat attained with technique B is the same as technique A cannot be confirmed. In technique A, the test section is permitted to cool down to a room temperature while immersed in the pool overnight, whereas in technique B, the test section is pre-boiled in a pool at 30,000 W/m^2 for one hour and then allowed to cool down for the next thirty minutes while the power to the test section and the pool is shut off. Marto and Hernandez [54], in fact, followed surface aging technique B in their experiment and observed a maximum temperature overshoot of 4.5 K. This behavior indicate that with GEWA-T surface the initial start-up problem should be less pronounced in industrial heat exchange units.

The site density increased with the increase in the heat flux. At a maximum heat flux of 80,429 W/m^2, the boiling was extremely vigorous. The test section was partially vapor blanketed. This is obvious by looking at the curve (Point C), where the slope tends to decrease. During the decreasing heat flux mode, the curve followed similar path up to a heat flux of 33,959 W/m^2. Below this point, the curve reflects the hysteresis. At 17,873 W/m^2, the vigorous activity died out, but there were still many distinctive sites all over the test section. One end had slightly more sites than the other end. Due to this behavior, the average ΔT value for the left end was less by 1 K than that for the right end. The sites observed during the initial non-boiling portion of the curve became visible again at low heat flux. This type of behavior is the reason for a leftward shift in the boiling curve at a heat flux less than 3,000 W/m^2, as shown in Fig. 28.

2. GEWA-T19C/F

Figure 29 shows the boiling curve for this particular run. During the increasing heat flux mode, no bubbles were observed up to a heat flux of 4,506 W/m^2. Beyond this point, partial nucleate boiling was observed. At a heat flux of 7,279 W/m^2 (Point A), five sites were observed at the left end, and two at the right end of the test section. This resulted in a difference of 1.31 K in ΔT between the two ends. Beyond Point A, the heat flux was carefully increased in small increments. Up to Point B, no change in the number of sites occurred, though the frequency of bubble generation at the existing sites increased. A sudden burst was observed when the heat flux was increased to 24,033 W/m^2 (Point C). Beyond this point, the curve followed the fully developed nucleate boiling path. The temperature overshoot observed was 2.4 K, lower than with GEWA-T19B/F. At the peak heat flux, the boiling was intense and the test section was partially blanketed by vapor as with GEWA-T19B. The decreasing heat flux mode showed a reduction in bubble activity with a drop in the heat flux. At a heat flux of 11,092 W/m^2 (Point D), a rather large number of sites were observed evenly distributed over the test section. At a heat flux lower than 1,473 W/m^2 (Point E), the heat transport mode changed to natural convection.

The GEWA-T test section used by Marto and Hernandez [54] was similar to GEWA-T19C of this study. Their data were converted to the same area base and compared to the present GEWA-T19C/F data. The results are quite similar, as shown in Fig. 30. This is most probably

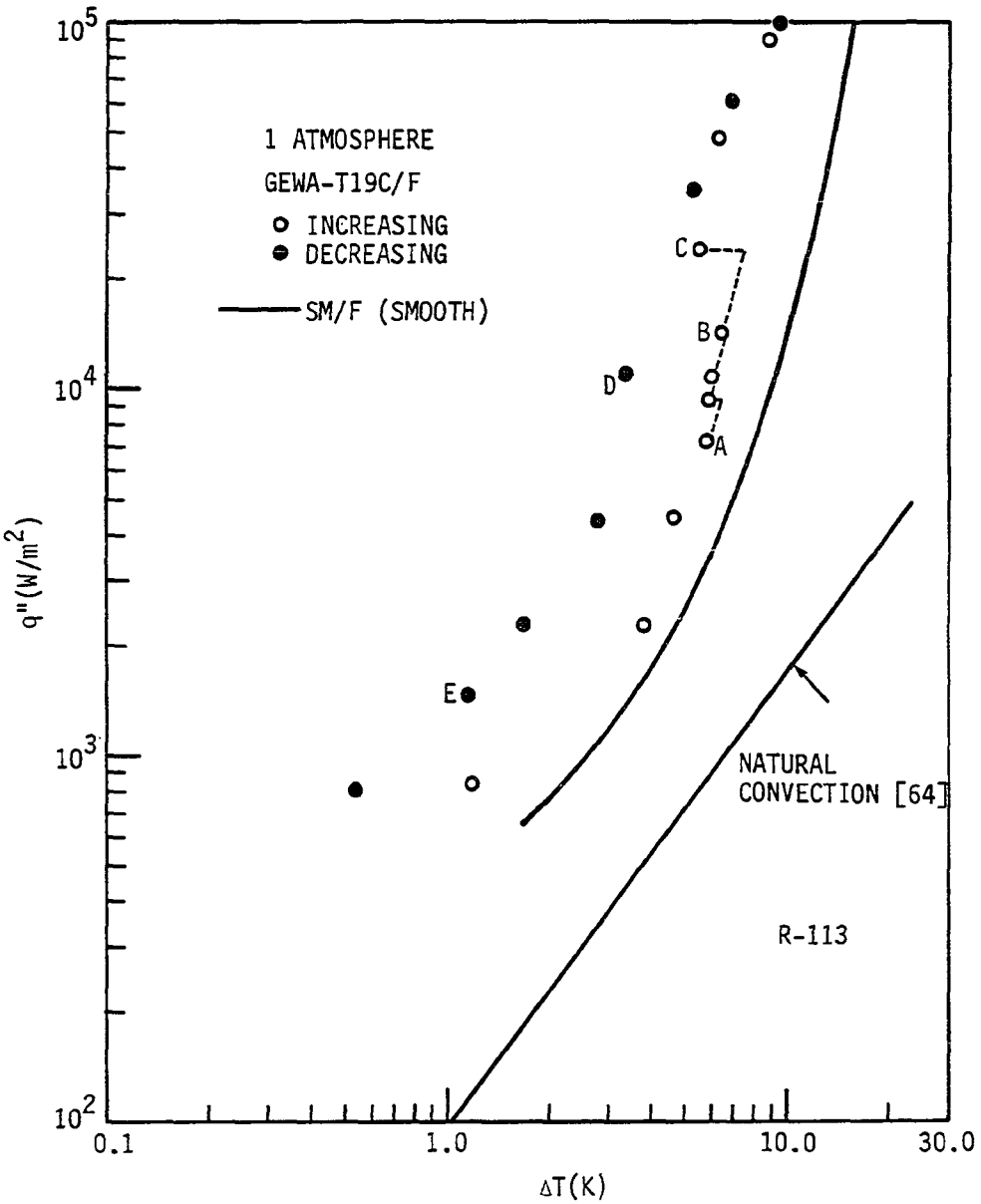

FIGURE 29. Boiling data for GEWA-T19C/F

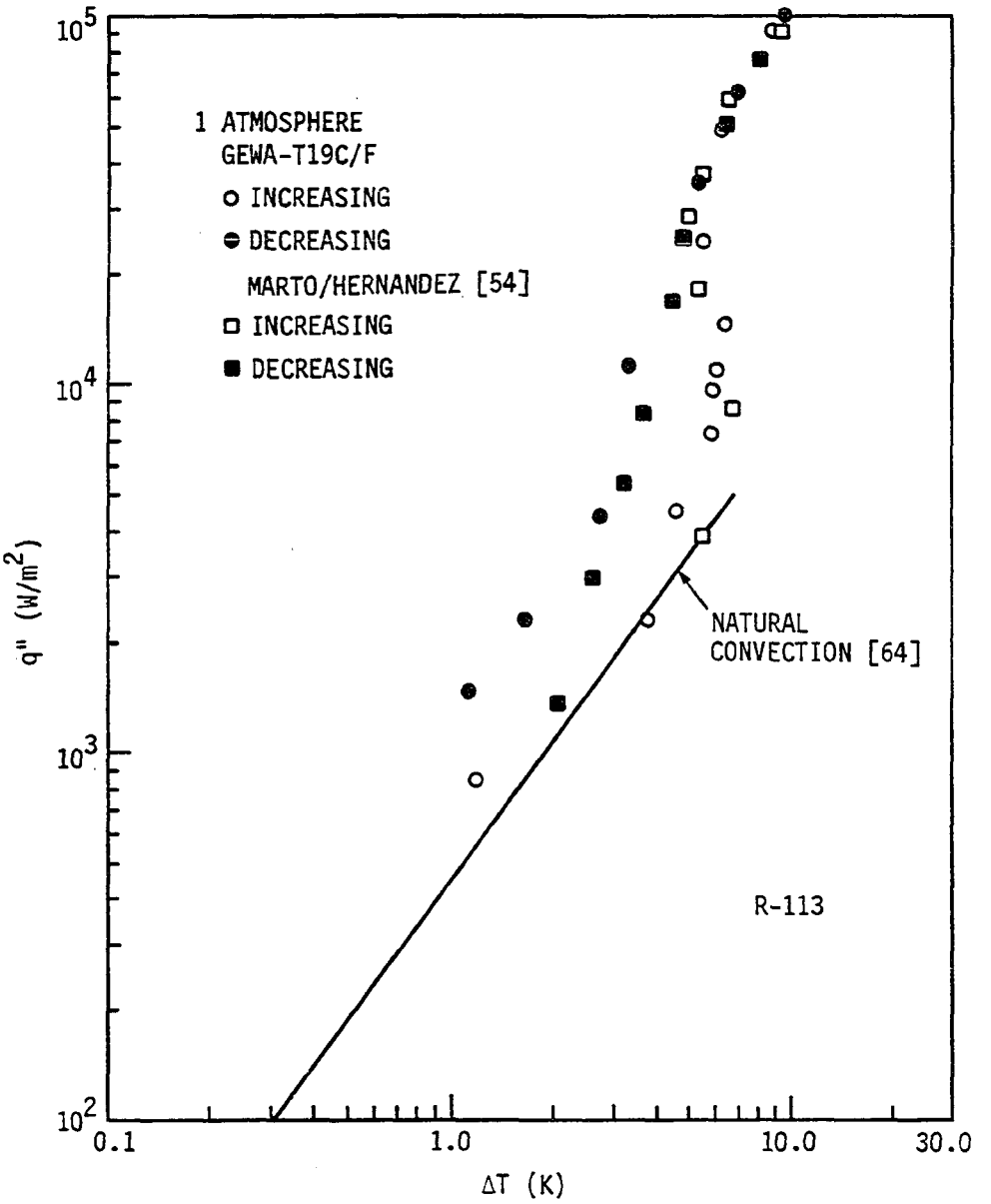

FIGURE 30. GEWA-T19C/F and Marto/Hernandez data with R-113

due to the fact that both studies employed surface aging techniques that were similar to some extent.

3. GEWA-T19D/F

The experimental results for this run are plotted in Fig. 31. Between a heat flux of 518 W/m^2 (Point A) and 4,572 W/m^2 (Point B), the heat transfer mechanism was natural convection, except at Point B where one site was active at the midsection of the test section. This "rogue site" is believed to be due to damage caused during the thermocouple hole drilling process. There was partial boiling beyond a heat flux of 4,572 W/m^2 (Point B) to 20,576 W/m^2 (Point C). A stepwise hysteresis similar to the above two runs was observed as shown in Fig. 31 with a maximum overshoot of 2.0 K. The temperature overshoot would have been slightly more if the power increase were more gradual.

The established nucleate boiling regime shows a similar trend as the other GEWA-T's. During the decreasing heat flux mode, the boiling prevailed until a heat flux of 2,813 W/m^2 (Point D). Below this point, the bubble activity died out and the mode of heat transport was once again entirely natural convection.

During this experiment, still pictures were also taken, as shown in Fig. 32. The pictures clearly indicate localized incipient boiling at the left midsection, a sudden burst, and then stabilized developed nucleate boiling during course of the run.

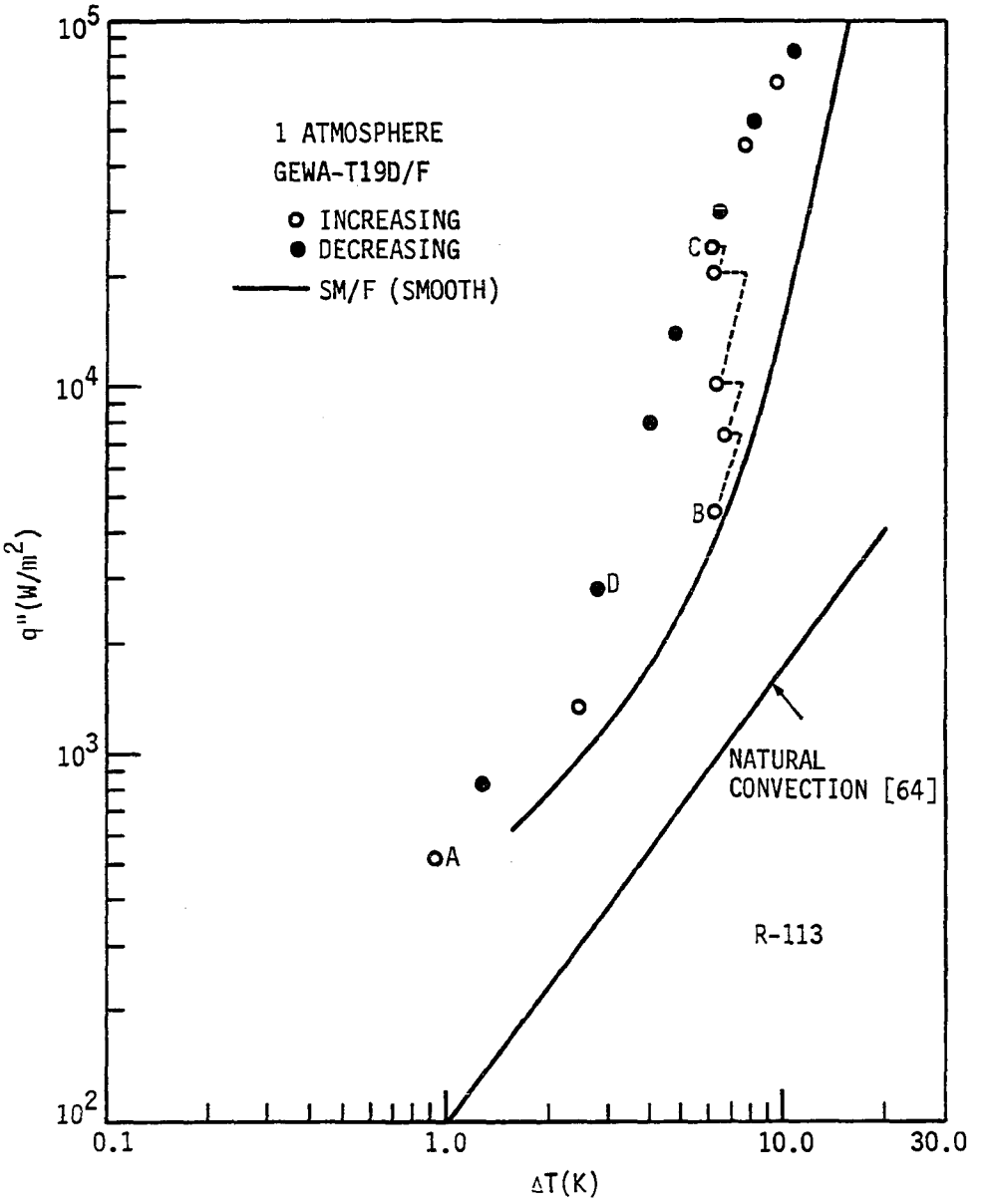

FIGURE 31. Boiling data for GEWA-T19D/F

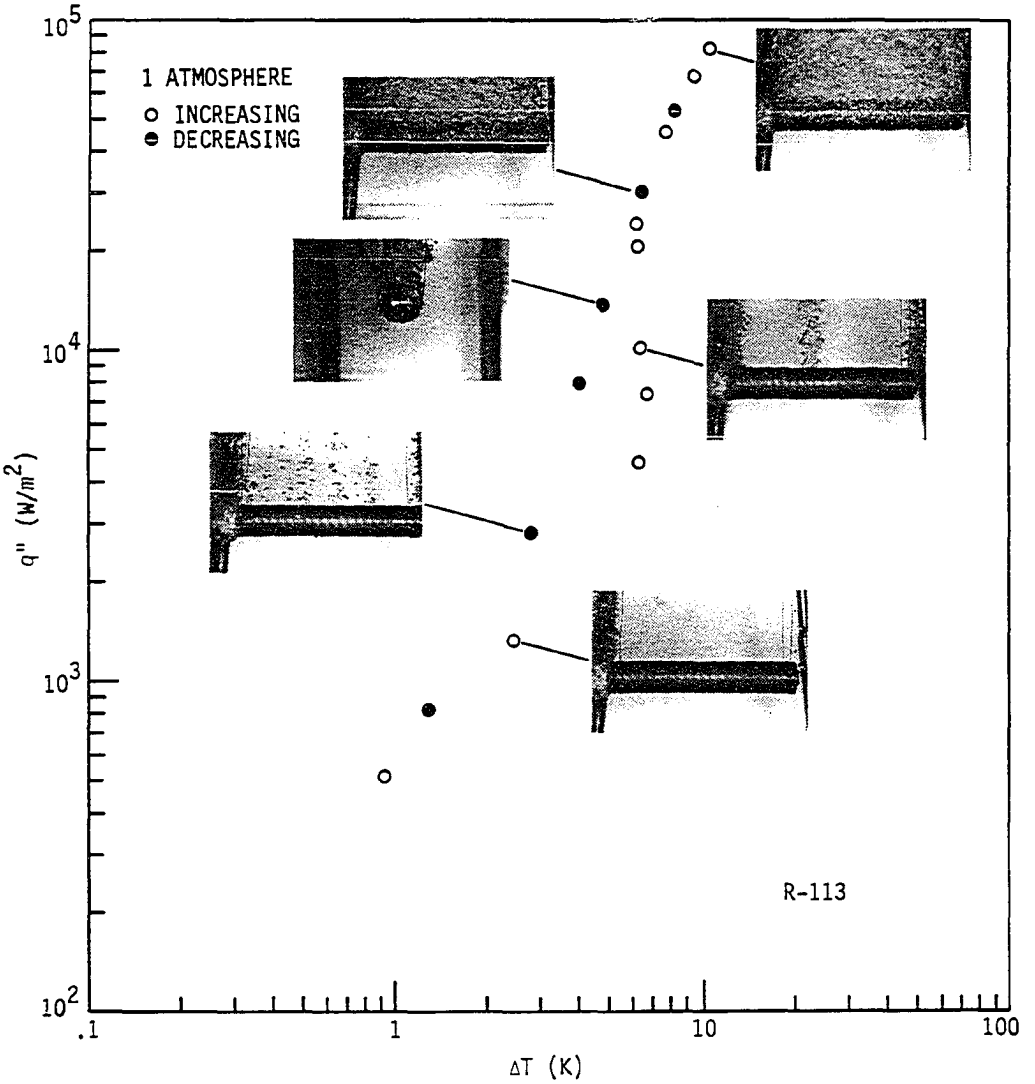

FIGURE 32. Bubble activity vs. heat flux for GEWA-T19D/F

4. GEWA-T19E/F

As mentioned earlier, the test section for this run was prepared locally. The degassing procedure was same as with the other test sections. During the increasing heat flux mode, natural convection prevailed up to a heat flux of 4,290 W/m^2 (Point A in Fig. 33), except for a single site at the bottom of the test section. Further increasing the heat flux to 6,091 W/m^2 only increased the frequency of ebullition at that site. At a heat flux of 9,265 W/m^2, three sites were active (Point B). As the heat flux was increased to 17,158 W/m^2 (Point C), the entire test section burst into nucleation. The temperature overshoot was 3.0 K.

A path similar to other GEWA-T's was traversed in the developed nucleate boiling zone up to the peak heat flux. The decreasing heat flux data followed the same path as the increasing heat flux data down to 28,130 W/m^2 (Point D). Site density and the bubble frequency dropped with further decrease in the heat flux below Point D; however, boiling prevailed until a heat flux of 2,917 W/m^2 (Point E) was reached. Below this point the mode of heat transfer was again pure natural convection.

G. Dependence of Enhancement on Gap Width in R-113

The overall enhancement obtained with these tubes was better than with water. The enhancement at 80,000 W/m^2 was 1.9, 2.0, 1.6, and 1.5 times that of smooth tube for GEWA-T19B, C, D, and E, respectively. Still the degree of enhancement was less than reported with other types

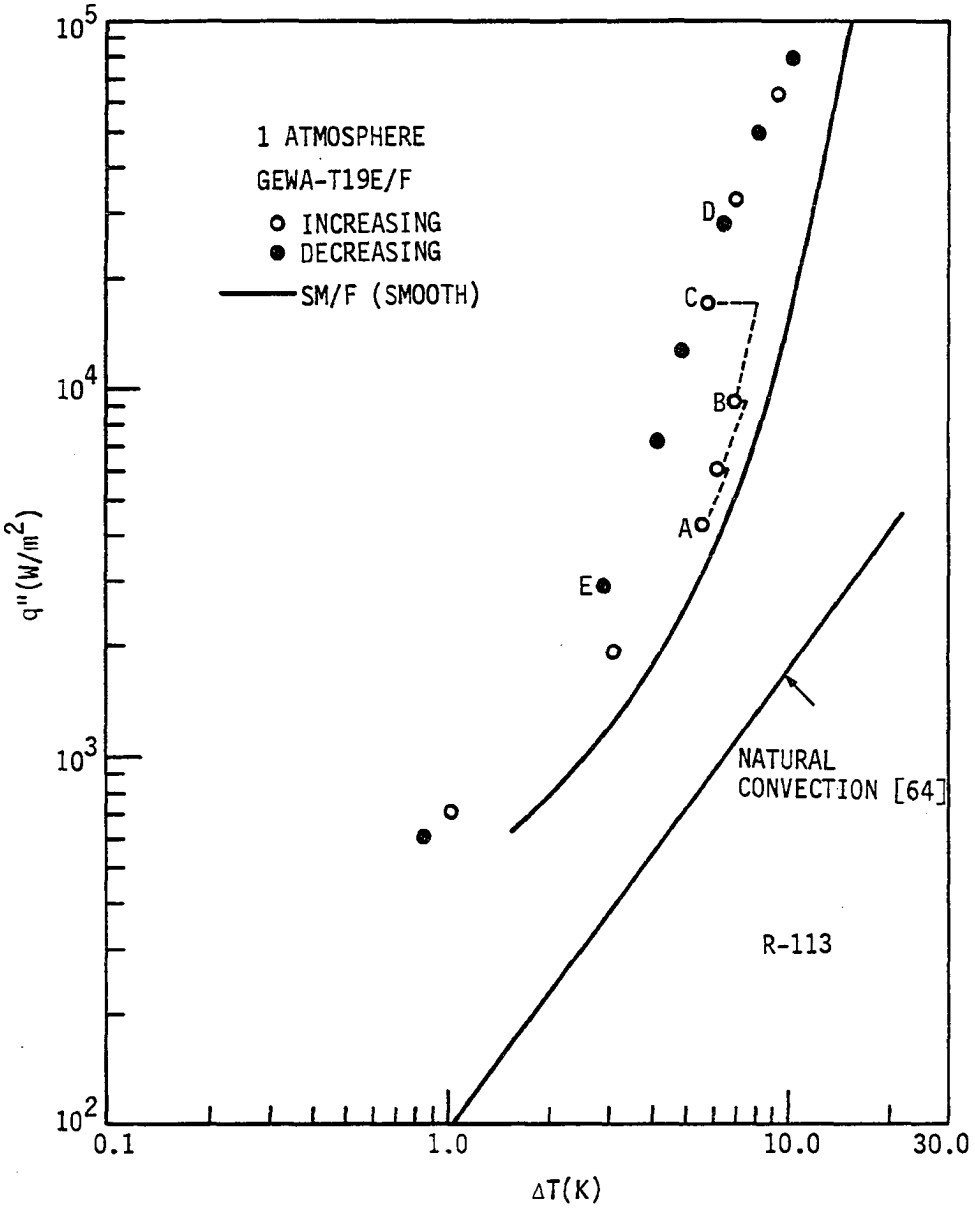

FIGURE 33. Boiling data for GEWA-T19E/F

of structured surfaces [28, 43]. Figure 34 shows a composite plot of the boiling curves for these tubes.

Unlike with water, a smooth functional relationship was observed between the heat transfer coefficient and the gap width. This is shown in Fig. 35 for different heat fluxes. The optimum gap width was established at S_T = 0.25 mm. Beyond this gap width there was a sharp drop in the performance, with an appreciable change in performance for gap sizes 0.55 mm and larger.

H. Visual Tests in R-113

Visual tests with the transparent single-channel simulator (Fig. 11) showed a peculiar liquid-vapor exchange occurring during boiling. Figure 36 shows the boiling process in detail. It was observed that at an initial stage when the heat flux is low several nucleation sites are activated. As the heat flux is slightly increased the liquid is sloshed out by the expanding vapor still residing in the channel. Ultimately, the vapor pressure within the elongated bubble gets larger than the retentive force and results in vapor escape. This causes a pumping action within the channel and allows the liquid to flow in. The fed liquid is vaporized and the process is repeated again. Increasing the heat flux merely increases the frequency.

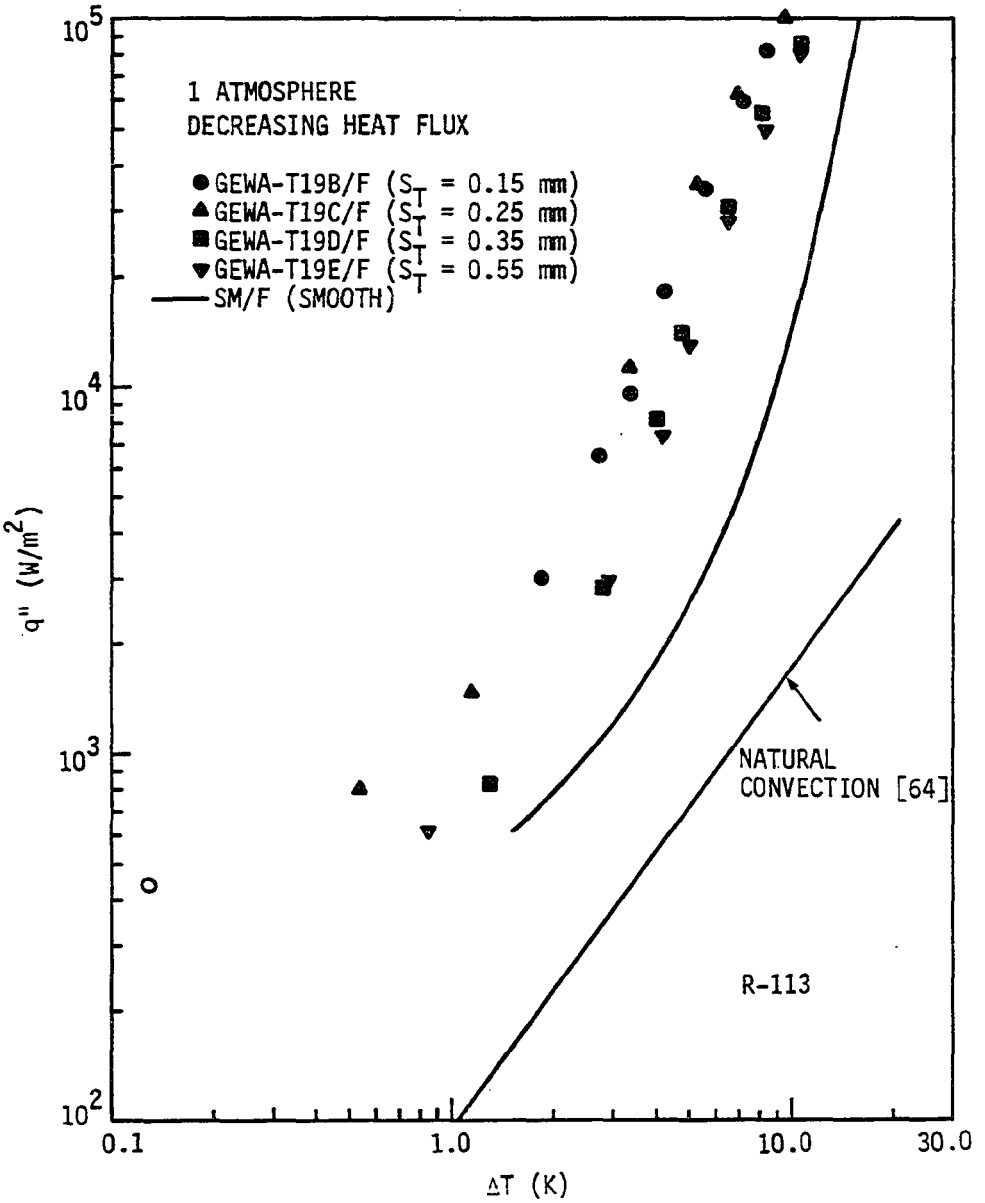

FIGURE 34. Composite plot for different GEWA-T surfaces in R-113

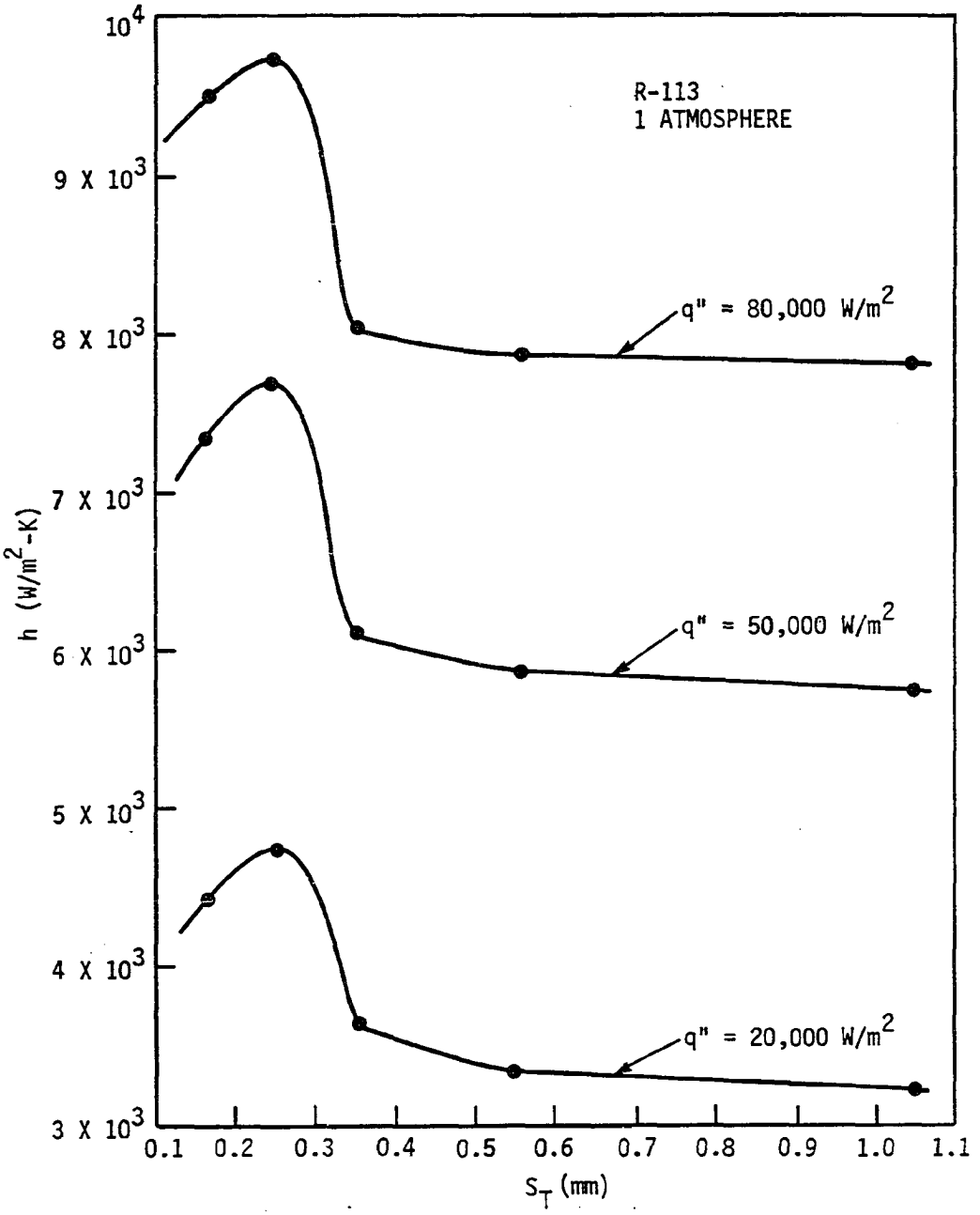

FIGURE 35. Heat transfer coefficient vs. gap width for R-113

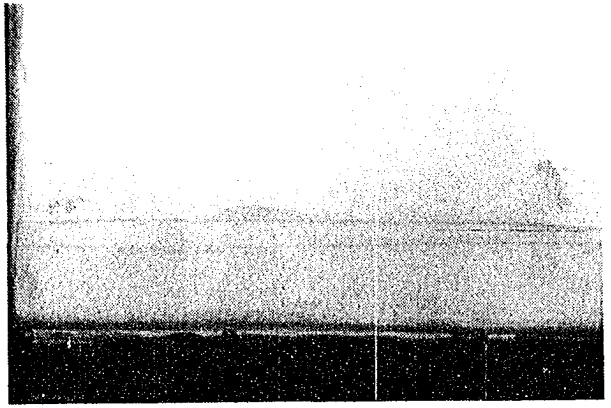

a. Nucleation at one or two spots.

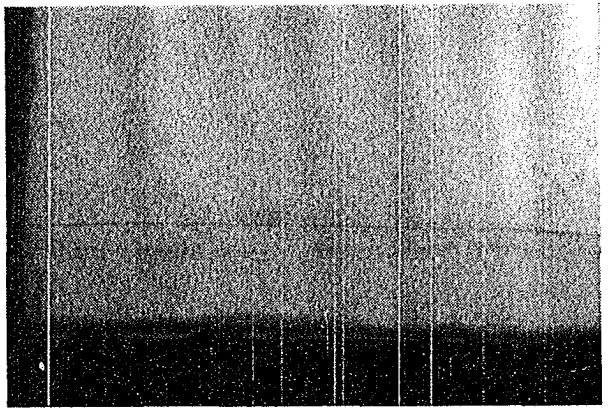

b. Growth of vapor within the channel and liquid sloshed out.

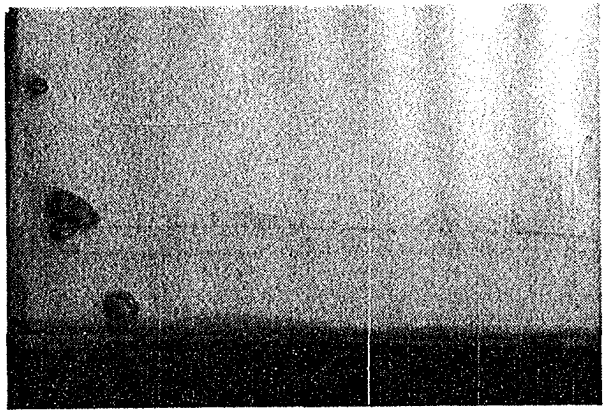

c. Vapor ejected and liquid fed in.

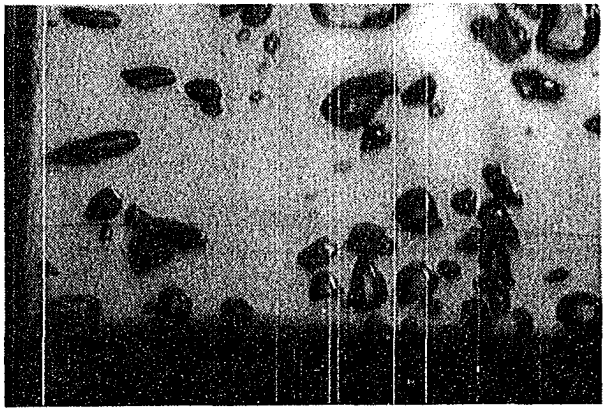

d. High heat flux; vigorous activity; channel core filled with vapor.

FIGURE 36. Boiling with GEWA-T19D simulator in R-113

I. Effect of Degassing

Degassing the test section was observed to be an important factor for each test run. It was noted that without degassing the increasing boiling curve was well to the left of the decreasing boiling curve. Some of the early tests in water with GEWA-T19D confirmed this fact. In one run, the pool was degassed by first bringing it to saturation and then cooling it down to 296 K. During this process, no power was supplied to the test section itself. The data are plotted in Fig. 37. Another run was performed with no degassing of the pool and the test section. As shown in Fig. 38, the boiling curve again showed a similar trend.

During one of these experiments, a camera was used to take still pictures of the test section as the experiment progressed. Figure 39 shows GEWA-T19C at the initial stages of power supply (30 W/m^2) to the test section. As can be seen, the density and the distribution of these gas sites are different than with a thoroughly degassed system. These observations suggest that the additional vapor produced by the outgassing enhances the heat transfer. But after a period of boiling (3 - 4 hours) associated with the increasing power, the gas is removed from the fluid as well as the surface, with the result that the decreasing power curve is displaced to a higher superheat. This is probably the reason for a rightward shift in the decreasing heat flux data of Arshad and Thome [57].

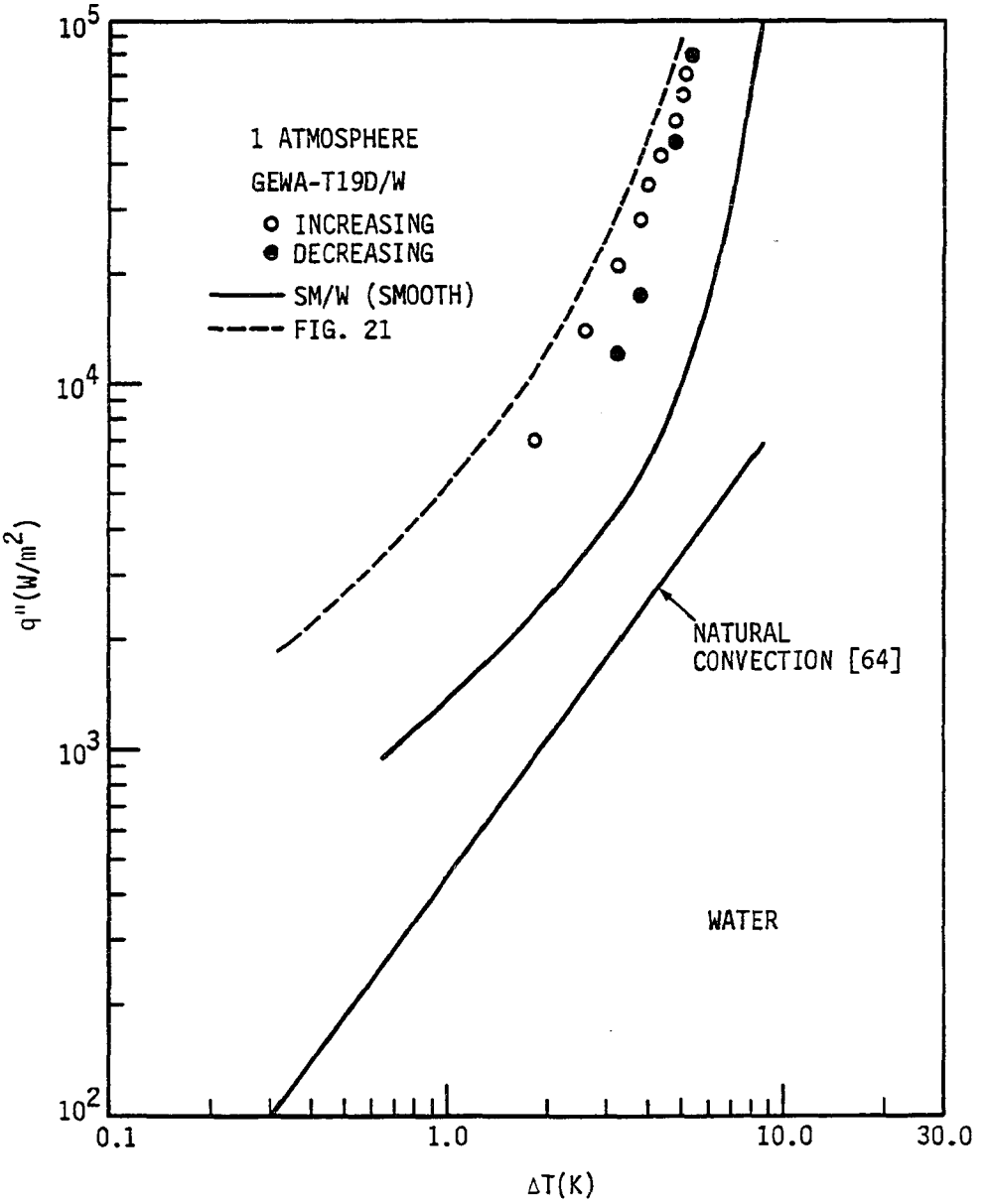

FIGURE 37. Boiling water data for a non-degassed GEWA-T19D

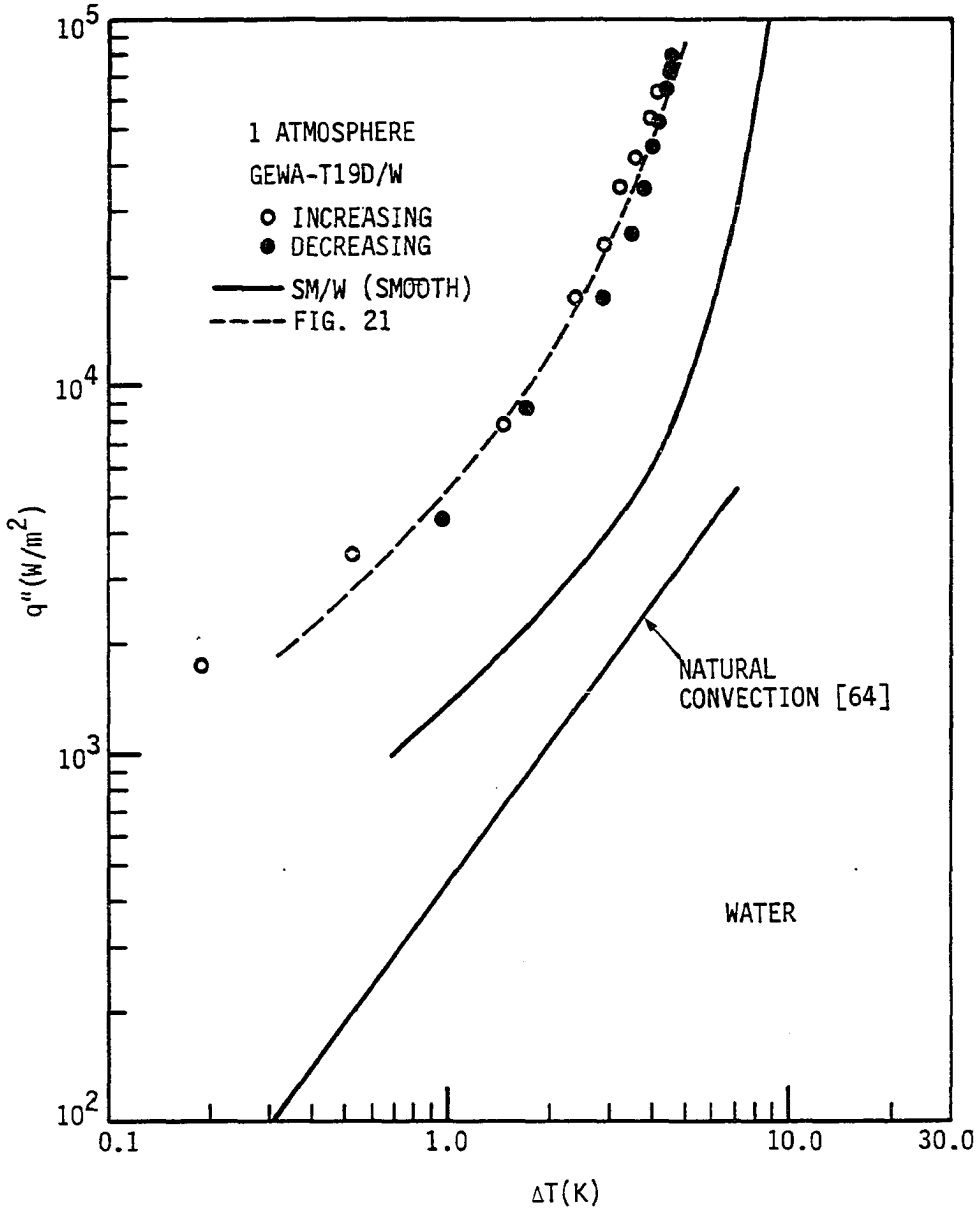

FIGURE 38. Boiling water data for a non-degassed pool and GEWA-T19D

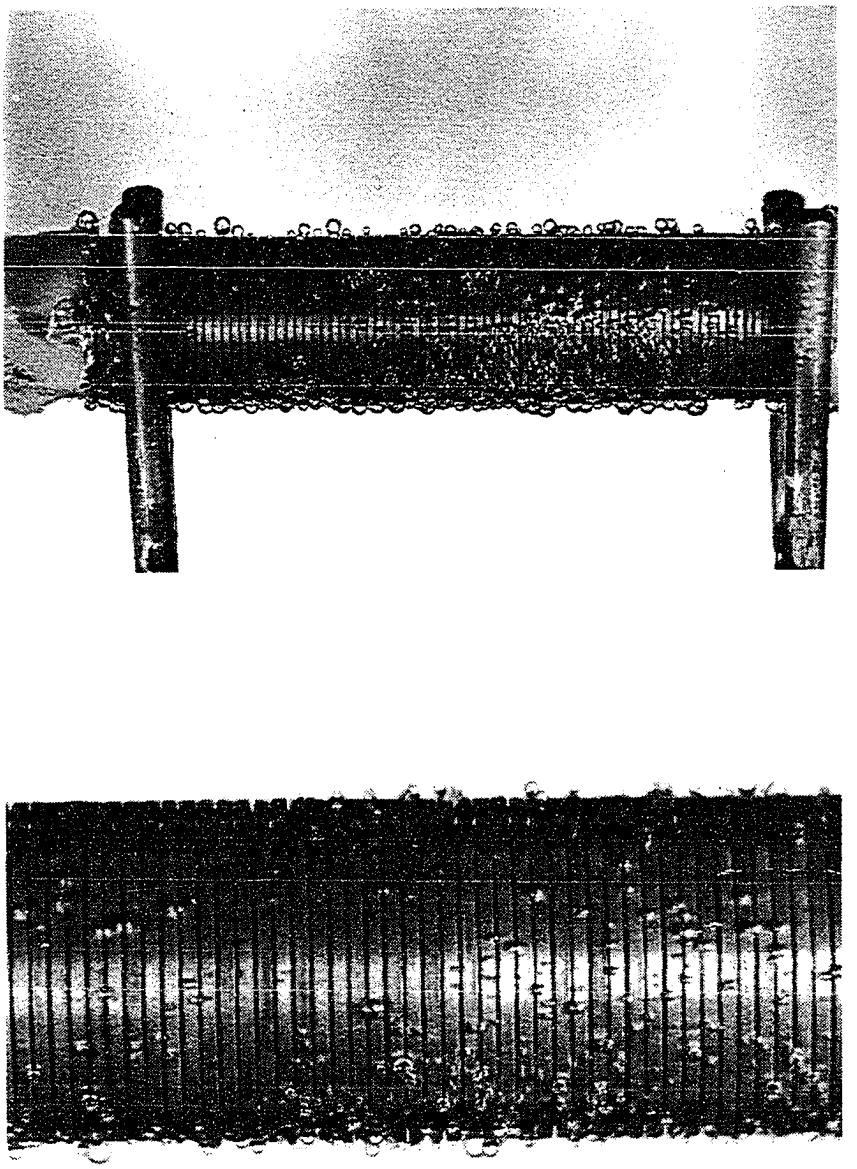

FIGURE 39. Non-degassed GEWA-T19C in water at start-up heat flux

J. Effect of a Channel Filler

It has been known for a long time that surfactants in the form of organic or inorganic additives can drastically change the boiling performance with water. Some investigators have also applied a second material over the actual boiling surface, e.g., wrapping a metal or nylon wire within the grooves of a plain fin tube [65, 66], whereas Shum applied a porous coating over a plain fin tube [67]. All techniques resulted in an enhancement of boiling heat transfer.

In an attempt to exploit this favorable experience a porous "wrap" was devised. The channels of a GEWA-T19D test section were filled with polystyrene di-vinyl benzene polymer (ordinary kitchen sponge with 99% porosity). The sponge was hand pressed in such a way that it covered the lower one-third of the entire test section, as shown in Fig. 40. Filling only part of the test section was purely a matter of choice.

The same cleaning and degassing procedure was employed as with the other test sections in water. The experimental procedure was also similar. It was observed that initially with no power (before degassing), there were already many bubbles covering the filled area of the test section. As the heat flux was increased, the overall activity of the bubbles increased. At a heat flux of 65,000 W/m^2, very vigorous boiling was observed. Large bubbles were observed at the bottom and the site density at the bottom was high as compared to other test runs. The data are shown in Fig. 41.

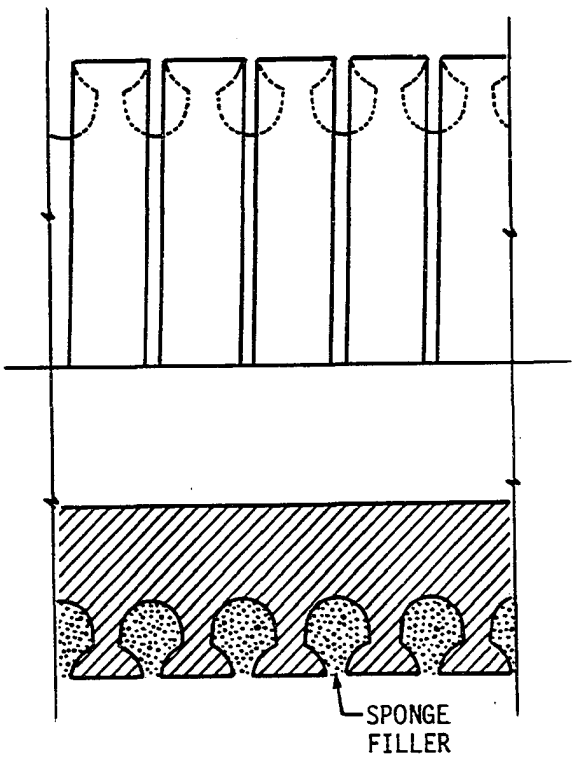

FIGURE 40. GEWA-T19D with filler

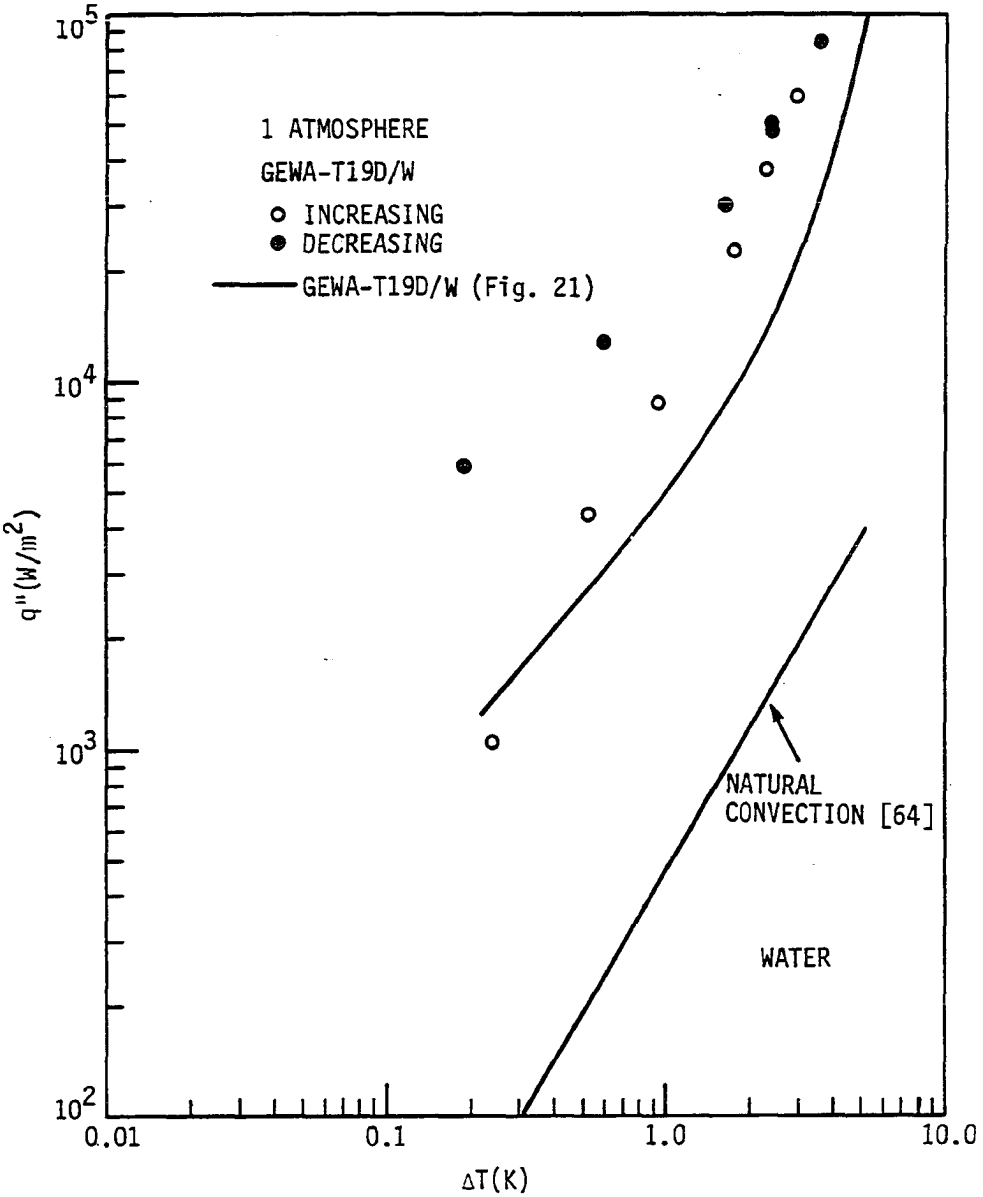

FIGURE 41. Enhancement of GEWA-T19D/W boiling due to filler

It was observed that the heat transfer enhancement was 1.43 times that of GEWA-T19D/W at a heat flux of 80,000 W/m^2. This is because of the fact that the sponged area of the test section was converted to a porous surface with hundreds of interconnected pores. The enhancement even further improved during the decreasing heat flux mode, a phenomenon similar to that observed with other porous surfaces [7, 8, 15, 28 - 30, 43], i.e., during this mode the majority of the sites had already been activated.

K. Effect of Fin Density

A GEWA-T26B/W with a gap width of S_T = 0.15 mm and fin density of 1020 fins/m was tested in water to check the effect of fin density on the thermal performance. The experiment was performed with similar working conditions as with GEWA-T19B/W. The results showed that the tube with a larger fin density had slightly better performance as shown in Fig. 42. This improvement could be attributed to the fact that the major heat transfer contribution with these surfaces is due to thin film evaporation. The larger density fins result in a greater film area per unit length of the tube.

L. Summary

The preceding experiments with actual GEWA surfaces and the simulators helped to understand the following:

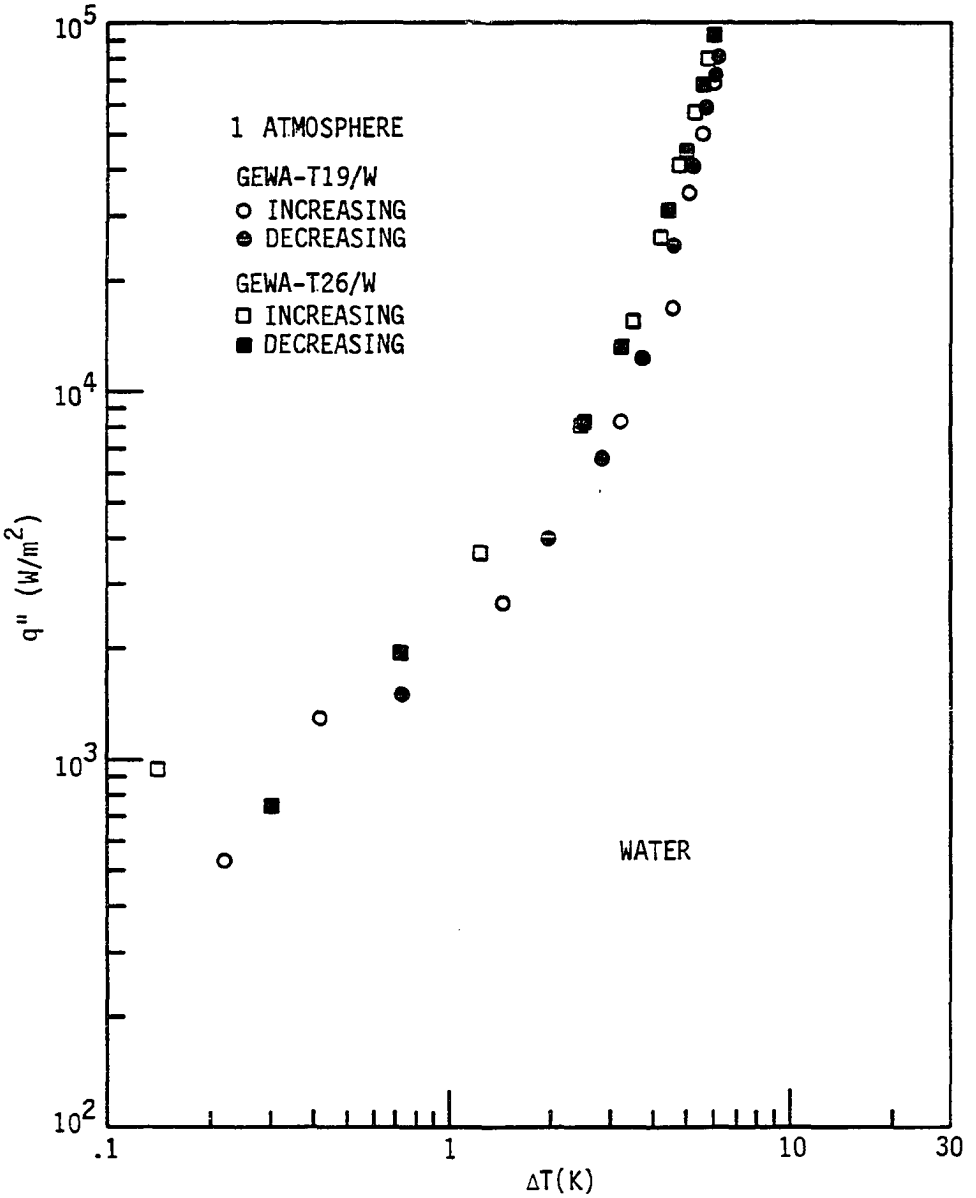

FIGURE 42. Boiling data for GEWA-T19B/W and GEWA-T26B/W

- The boiling performance of plain GEWA-K surface in water and R-113 as well as the fin density effect.
- Pool boiling enhancement of GEWA-T surfaces and the effect of fin gap on the heat transfer coefficient with these fluids.
- The effect of fin density of the GEWA-T surface on boiling performance with water.
- The effect of degassing on the boiling performance of these surfaces.
- The effect of a porous channel filler on the boiling enhancement of the GEWA-T surface in water.
- The basic mechanism of liquid-vapor exchange in the channel, as visually studied with the actual test section and single channel simulators.

V. QUANTITATIVE MODELS

In Chapter 2 it was noted that Nakayama et al. [20, 21] developed a semi-empirical model for boiling from the Thermoexcel-E surface. This is the most complex boiling model ever proposed and there is much confusion as to the assumed physics and degree of empiricism. Therefore, it was decided to perform an in depth analysis of this "dynamic" model and utilize parts of it for the development of a simple model for the GEWA-T surface.

A. Hitachi's "Dynamic Model"

A semi-empirical model was developed by Nakayama et al. [20, 21] for boiling from the Thermoexcel-E surface. The characteristics of this particular surface were described in Section C of Chapter 2. A brief description of the model was also mentioned in Section D of the same chapter. The model assumes that the pool is always at saturation corresponding to the system pressure and that the wall temperature is uniform, i.e., the temperature drop between the base and the surface is very small. The vapor is always at saturation.

The entire bubble cycle is divided into three phases, as shown in Fig. 43. For the mathematical formulation, Phases II and III are amalgamated because both represent dynamic phases. The analysis is thus applied to Phase I and Phase (II + III). The phases differ from one another by the different physics involved. These phases are defined as follows.

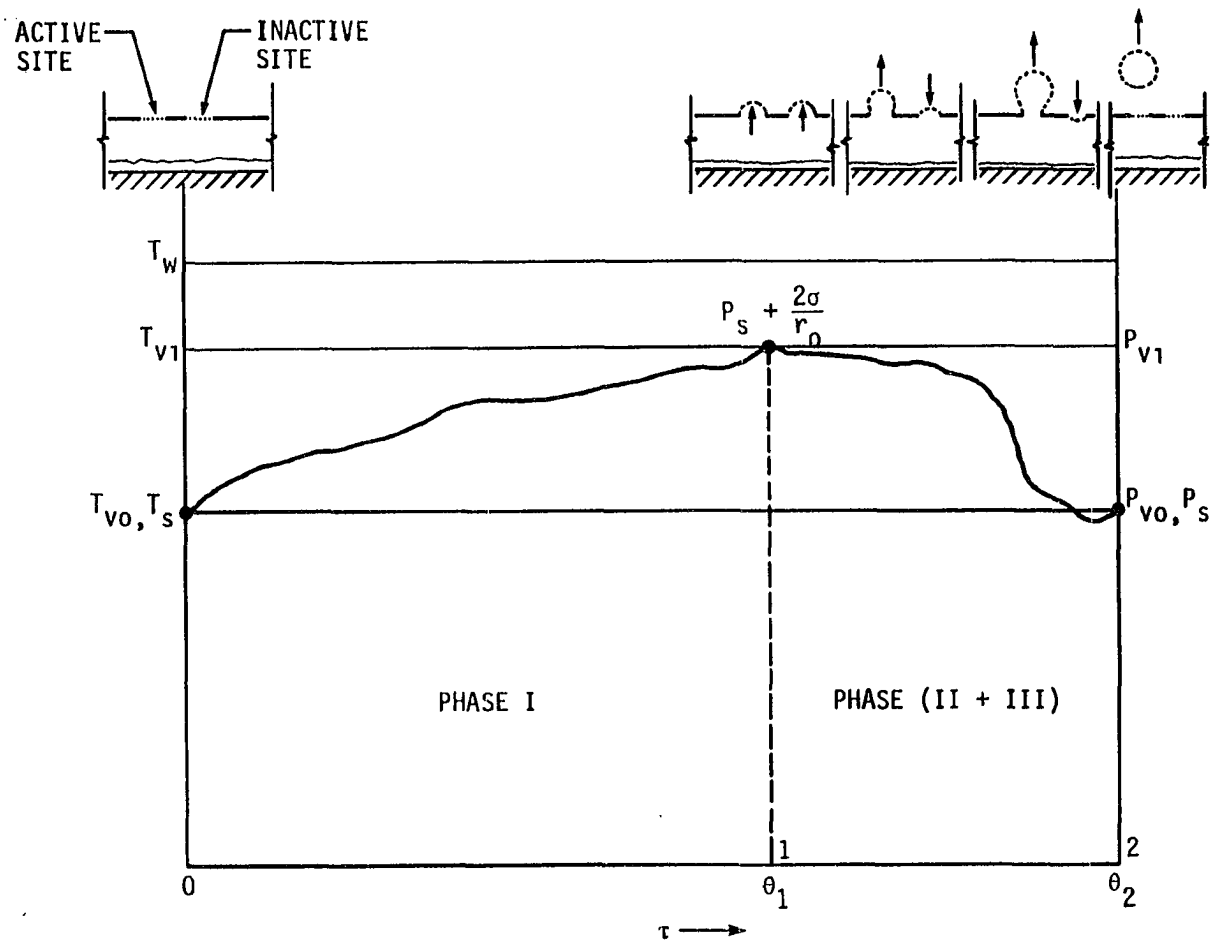

FIGURE 43. Different boiling stages for Thermoexcel-E

• Phase I (Pressure Build-Up Phase): In quasi-steady fashion the pressure is built up in the tunnel due to the evaporation of the contained liquid. This phase is terminated when the meniscus at the pores reaches hemispherical shape. At this point the pressure is maximum, as shown in Fig. 43 (Point 1).

• Phase II (Pressure Reduction Phase): Due to "natural perturbations" within the tunnel, some pores become active and experience rapid bubble growth. The vapor escapes into these bubbles and simultaneously renders some sites inactive (by causing interface recession) due to reduction in tunnel pressure. Initially the growth at an active site is due to pressure release, but later the growth is governed by the inertia of receding liquid around the bubble.

• Phase III (Liquid Intake Phase): The bubbles at the active sites expand to a point where the pressure in the bubble and the tunnel drops below the pool pressure resulting in a negative curvature at the inactive sites. It is during this short interval that the liquid flows into the tunnel via the inactive pores and spreads by capillary action to the corners. This phase is terminated by the departure of the bubbles. Both interfaces are flat at the beginning of the next cycle.

The core of the analysis is to find the amount of liquid evaporated and also the time required for the two phases. This establishes the latent heat flux, q''_l. But to find the total heat flux it is also necessary to estimate the enhanced free convection contribution, q''_{ex}, as shown in Fig. 44. All heat fluxes are based on the outside area as if the specimens were all solid.

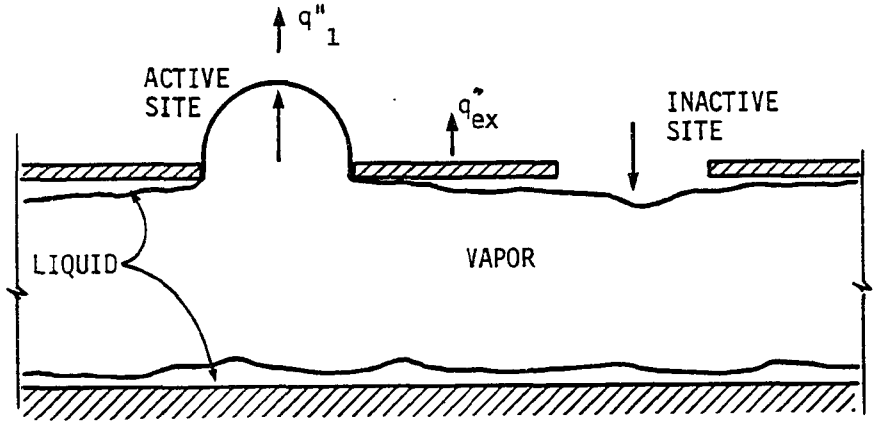

FIGURE 44. Boiling and natural convection contribution

It was assumed that q''_{ex} is controlled by the same mechanism as with a plain surface. Measurements were made with flat, face up, plain copper surfaces of different roughnesses in order to find a relation between q''_{ex}, ΔT, and N_A/A for R-11. The q''_{ex} values were obtained by subtracting q''_l from the total measured heat flux q":

$$q''_{ex} = q'' - q''_l \tag{5.1}$$

or,

$$q''_{ex} = q'' - \pi/12\ d_b^3\ f_b\ h_{fg}\ \rho_v\ (N_A/A) \tag{5.2}$$

The frequency, f_b, departure diameter, d_b, and number of active sites, N_A, were measured experimentally. The following equation for q''_{ex} was then postulated with the assumption that a negligible part of the surface area is taken up by the bubbling and essentially all of the area is exposed to natural convection:

$$q''_{ex} = (\Delta T/C_q)^{1/y}\ (N_A/A)^{-x/y} \tag{5.3}$$

where $x = -1/6$, $y = 2/3$, and $C_q = 18\ [K(cm^2/W)^{2/3}(1/cm^2)^{1/6}]$ were constants optimized from the data for variable-roughness plain surfaces. These values of x and y were similar to those of Nishikawa and Fujita [68]. But according to [68], these values are valid only for the laminar flow regime. For the turbulent flow regime, Nishikawa and Fujita [68] quoted $x = -1/5$ and $y = 3/5$. These values were given

earlier by Zuber [69] for a plain surface in water. Assuming that a similar relation is valid for q''_{ex} on Thermoexcel-E surfaces, and using $x = -1/5$ and $y = 3/5$, $C_q = 1.95$ $[K(cm^2/W)^{3/5}(1/cm^2)^{1/5}]$ was found for R-11. This value of C_q was based on only two Thermoexcel-E surfaces with pore sizes, d_o, equal to 0.1 and 0.04 mm; however, no significant effect of the pore size was observed. For water, it was found that $C_q = 3.93$ which was, coincidently, the same value obtained by Zuber [69] for water boiling on a plain surface.

1. Analysis of Phase I

Application of a heat balance at the tunnel wall resulted in

$$q_I = h_t A_t \Delta T = \dot{m}_v h_{fg} = k_l (A_\delta/\delta)\Delta T = k_l C_{tl}(T_w - T_v(t)) \qquad (5.4)$$

with C_{tl} being the ratio of liquid film area to the liquid film thickness. This was assumed to be constant and independent of time.

Using the Clapeyron relation, the perfect gas law, Laplace surface energy relation, and the continuity equation, and performing "some kind" of linearization between Point 0 (when the meniscus is flat) to Point 1 (when the meniscus is hemispherical), as shown in Fig. 43, an equation was obtained for the first period, θ_1:

$$\theta_1 = (V_{vm} h_{fg}/k_l C_{tl}) \left\{ A\ B + \rho_{vm1}/\Delta T_{t1}\ \ln\ (V_{v1}/V_t) \right\} \qquad (5.5)$$

where

$$A = \rho_{vm1}(h_{fg} - RT_{v0})/RT_{v0}^2$$

$$B = \ln((T_w - T_{v0})/(T_w - T_{v1}))$$

This elaborate form could have been avoided by simply utilizing the end point conditions; because, after all, a linearization was applied. The first term in the brackets in equation (5.5) is nearly zero, because $T_w - T_{vo} \simeq T_w - T_{v1}$ as $T_{v1} - T_{v0} = 0.1958$ K (T_{v1} is evaluated from the relation, $T_{v1} = T_{v0} + 2\sigma T_{v0}/r_0 \rho_{v0} h_{fg}$) for R-11 at saturation using a test section with pore radius $r_0 = 0.05$ mm. The expansion of $\ln(V_{v1}/V_t)$ in the second term results in

$$\ln ((V_t + V_{hem})/V_t) = \ln (1 + V_{hem}/V_t) = V_{hem}/V_t + (V_{hem}/V_t)^2/2 + (V_{hem}/V_t)^3/3 + ... \quad (5.6)$$

Here $V_{hem} = \frac{2}{3} \pi r_0^3 N$, the total bubble volume at the hemispherical condition, and $V_t = N\lambda_0 A_c$, the total tunnel volume, where N is the total number of pores, λ_0 is the pore pitch, and A_c is the tunnel cross-sectional area. Applying this to test section R(11)-1, which has $N = 2050$, $r_0 = 0.05$ mm, $\lambda_0 = 0.7$ mm, and $A_c = 0.4 \times 0.25$ mm^2, it is found that $V_{hem} = 0.00053669$ cm^3 and $V_t = 0.1434999$ cm^3. As $V_t >> V_{hem}$, the second and higher-order terms can be dropped. Thus, equation (5.5) reduces to

$$\theta_1 \simeq V_{vm} h_{fg}/k_l C_{tl} \left\{ (\rho_{vml}/\Delta T_{tl}) \left(V_{hem}/V_t \right) \right\}$$

$$= \rho_{vml} V_{hem} h_{fg}/k_l C_{tl} \Delta T_{tl} \quad (5.7)$$

where

$$V_{vm} = (V_t + V_{vl})/2$$

But,

$$V_{vl} = V_{hem} + V_t \simeq V_t$$

Therefore,

$$V_{vm} = V_t$$

and

$$\Delta T_{tl} = T_w - (T_{v0} + T_{vl})/2$$

which is a simple heat balance equation with ΔT_{tl} taken as the linear average temperature difference between Point 0 and Point 1 (Fig. 43). The equation for the amount of liquid evaporated is

$$m_{ll} = V_{vm}(\rho_{vl} - \rho_{v0}) + N\ (\pi d_0^3/12)\ (\rho_{v0} + \rho_{vl})/2 \qquad (5.8)$$

which is basically of the form $m_{ll} = N\ V_{hem}\ \rho_v$. The first term in equation (5.8) is almost negligible because the contribution from condensation due to pressurization is very small. This is just one place where the Nakayama et al. model is difficult to understand due to unnecessary mathematical complexity.

2. Analysis of Phase (II + III)

Both mass and momentum conservation principles were applied at the active as well as inactive sites in order to find the second period, θ_2. The heat balance equation at the tunnel wall is similar to that in Phase I, i.e.,

$$m_{l2}h_{fg}/\theta_2 = k_l C_{t2}\Delta T_{t2} \qquad (5.9)$$

where

$$\Delta T_{t2} = T_w - (T_{v1} + T_{v2})/2$$

a. Mass conservation Mass conservation in terms of interface movement was applied at active and inactive sites as shown in Fig. 45, with η defined as η'/r_0 and $\xi = \xi'/r_0$. η' and ξ' are the meniscus height at active and inactive pores, respectively. The instantaneous mass conservation at active and inactive pores is as follows:

$$\begin{aligned} \Phi/N &= ZN_A/N + Z_i N_i/N \\ \Phi^* &= \beta Z + (1 - \beta)Z_i \\ \Phi^* &\approx \beta Z + Z_i, \quad \text{since } \beta << 1 \end{aligned} \tag{5.10}$$

where, $\Phi^* = 6k_1 C_{t2} \Delta T_{t2}/\rho_{vm2} h_{fg} \sqrt{\sigma/r_0 \rho_1} N\pi r_0^2$, the ratio of total vapor generation rate to total number of pores,

$Z = \frac{d}{d\tau}\{\eta(\eta^2 + 3)\}$, non-dimensional mass flow rate at an active pore in terms of normalized interface bulge, η, with τ defined as $t/\sqrt{\rho_1 r_0^3/\sigma}$,

$Z_i = \frac{d}{d\tau}\{\xi(\xi^2 + 3)\}$, non-dimensional mass flow rate at an inactive pore in terms of normalized interface bulge, ξ,

β = ratio of active sites to total number of pores, N_A/N, also given as $(\Phi^* \theta_2^* - \xi_3(\xi_3^2 + 3) + 4)/(\eta_d(\eta_d^2 + 3) - 4)$. This was obtained by substituting Z and Z_i in equation (5.10) and performing an integration from $\tau = 0$ (initiation of Phase II) to θ_2^* (termination of Phase III); the non-

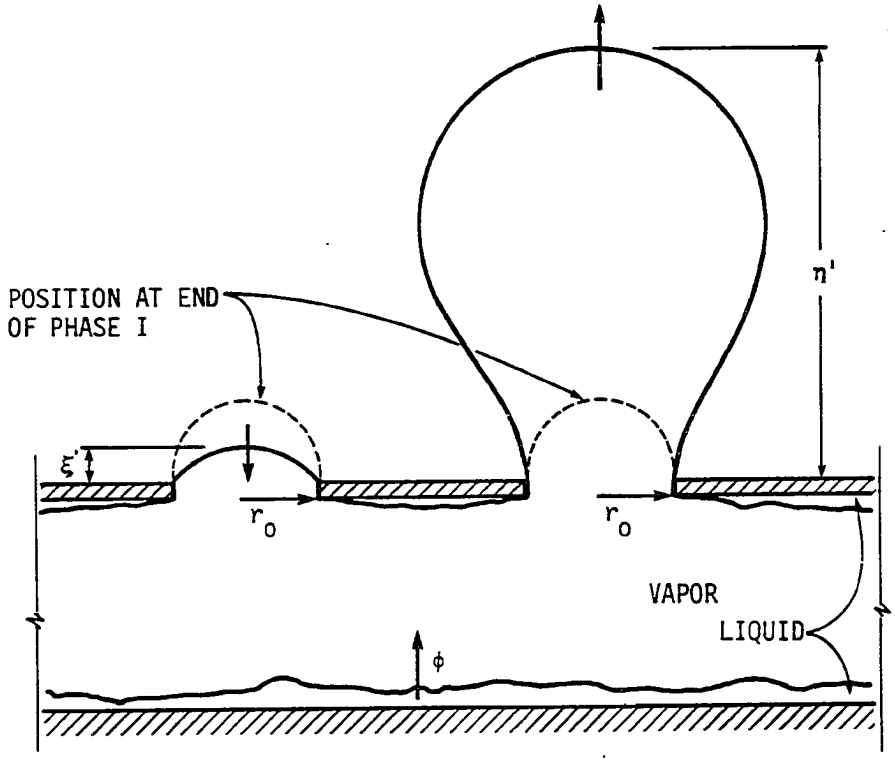

FIGURE 45. Interface movement at active and inactive sites

dimensional time $\theta_2^* = \theta_2/\sqrt{\rho_1 r_0^3/\sigma}$.

The term, η_d, defined as $d_b/2r_0 \left[1 + \sqrt{1 - (2r_0/d_b)^2}\right]$, is a non-dimensional height of the bubble at departure. The departure diameter, d_b, is equal to $C_b\sqrt{2\sigma/g(\rho_l - \rho_v)}$, where C_b is an empirical constant.

During the very short interval associated with Phase III, liquid is sucked into the tunnel at inactive sites due to pressure reduction in the tunnel which is caused by the vapor flow into the growing bubble. It was assumed that the recession is proportional to the cube root of the volume of liquid introduced during a complete cycle. No basis was provided for this assumption. The proportionality resulted in a constant C_3, i.e.,

$$\xi_3 = - C_3 \left[(m_{11} + m_{12})/\rho_l N_i \pi r_0^3\right]^{1/3}$$

Since $N_i = N(1 - \beta)$ and β is small relative to unity,

$$\xi_3 = - C_3 \left[(m_{11} + m_{12})/\rho_l N \pi r_0^3\right]^{1/3} \qquad (5.11)$$

b. Momentum conservation The basic assumptions for the bubble growth were

- No contribution from evaporation at the interface.
- No viscosity effects.

The momentum equation derived by L'Ecuyer and Murtby [70] for bubbling through an orifice was simplified using these assumptions. The growth equation in non-dimensional form is given as

$$P_{vb}^{*} - P_{s}^{*} = 4\lambda/\lambda^2+1 + (5\lambda^4 - 3\lambda^2 + 6)/16\lambda^4 \, (d\lambda/d\tau)^2 + (\lambda^2 + 1)(2\lambda^2 - 1)/8\lambda^3 \, d^2\lambda/d\tau^2 \qquad (5.12)$$

where

P_{vb}^{*} = non-dimensional pressure in the bubble,

P_{s}^{*} = non-dimensional ambient pressure, and

λ = non-dimensional distance between the test-section surface and the crown of the interface.

1) Active site In order to solve equation (5.12), a second-order, second-degree, non-linear differential equation, Nakayama et al. employed an approximate treatment by adopting an argument that the momentum balance at the time of maximum mass flow rate into the growing bubble at an active site was crucial for determining the period θ_2^{*}. Hence, if they could find this time in terms of θ_2^{*} and, consequently, the derivatives in equation (5.12), in terms of η_d and θ_2^{*}, they would end up with a simplified force balance equation.

In order to do this they introduced a dummy variable, $X = \sqrt{2/3}\ \eta^{3/2}$, resulting in

$$Z \simeq 3X \frac{dX}{d\tau} \qquad (5.13)$$

This holds good at a condition where the bubble has grown to a sufficient size that its dimensional height, η', is much larger than the pore radius, r_0, i.e., $\eta = \eta'/r_0 >> 1$. A quadratic equation satisfying $X = \sqrt{2/3}$ at $\tau = 0$, and $X = X_d = \sqrt{2/3}\ \eta_d^{3/2}$, $dX/d\tau = 0$ at $\tau = \theta_2^*$ was written as follows:

$$X = \sqrt{2/3} + 2(X_d - \sqrt{2/3})(\tau/\theta_2^*) - (X_d - \sqrt{2/3})(\tau/\theta_2^*)^2 \qquad (5.14)$$

Substituting equation (5.14) into equation (5.13), the maximum values of X and Z were evaluated as $X = (2/3)X_d$ and $Z = Z_{max} = 2.309X_d^2/\theta_2^*$ when $\tau = \tau_{zmax} = 0.423\theta_2^*$ (Appendix 4). Transforming X to η and evaluating the differentials $d\eta/d\tau$ and $d^2\eta/d\tau^2$ corresponding to Z_{max}, equation (5.12) was simplified to

$$P_{vb}^* - P_s^* = 5.242/\eta_d - 0.1457\eta_d^2/\theta_2^{*2} \qquad (5.15)$$

Application of a force balance between the bubble and the tunnel (Fig. 46) and utilizing the orifice equation required in an orifice constant, C_0, i.e.,

$$P_v^* - P_{vb}^* = 0.0329C_0(\rho_{vm2}/\rho_1)\eta_d^6/\theta_2^{*2} \qquad (5.16)$$

2) Inactive site As the interface movement at an inactive site was very small, $\xi = \xi'/r_0 << 1$, a static force balance was applied as follows:

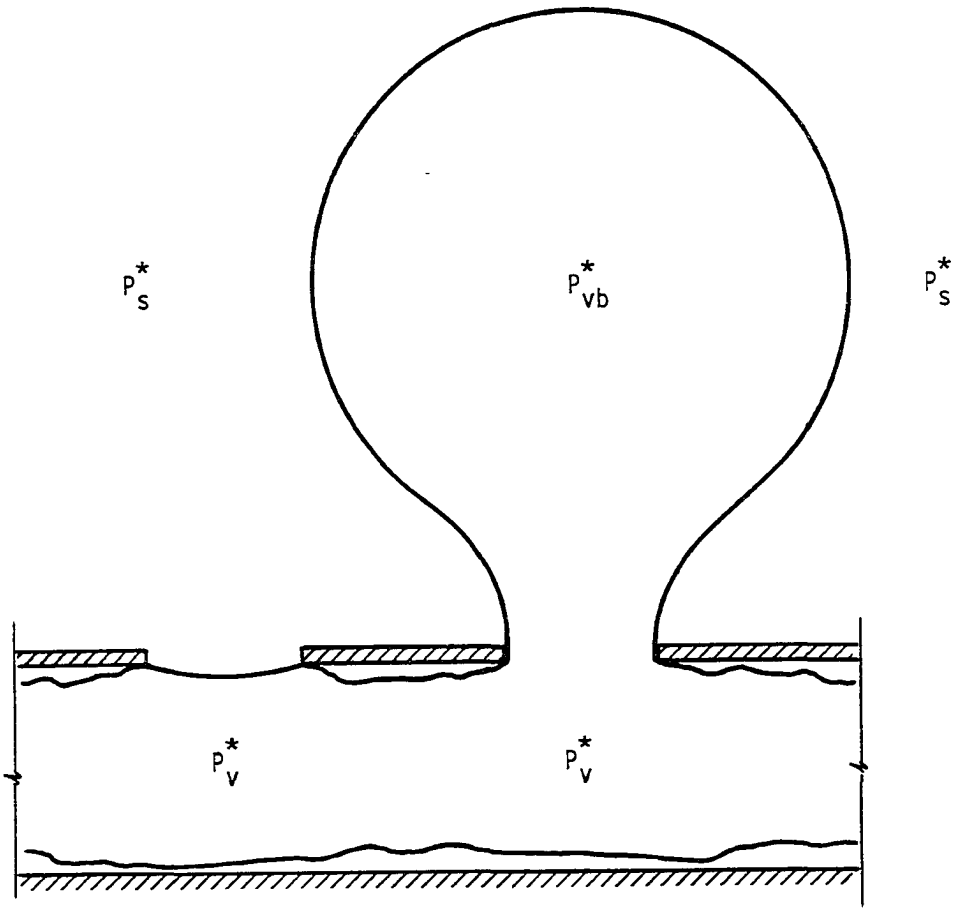

FIGURE 46. Pressure distribution in Phase II + III

$$P_v^* - P_s^* = 4\xi, \tag{5.17}$$

Integration of $\frac{d}{d\tau}\left\{\xi(\xi^2 + 3)\right\} = Z_i$ from $\tau = 0$ to τ_{zmax} and using equation (5.10) resulted in

$$\xi = 1/3 \left\{-\beta\int_0^{\tau_{zmax}} Z d\tau + \Phi^* \tau_{zmax} + 3\right\} \tag{5.18}$$

Substituting equations (5.13) and (5.14) into equation (5.18) and setting $\beta \simeq \Phi^* \theta_2 / \eta_d^{*3}$, the recession at the inactive pore at the time of maximum flow into the bubble at the active pore was evaluated as

$$\xi_{zmax} = 1 - 0.007\Phi^* \theta_2^* \tag{5.19}$$

It was computed that ξ_{zmax} was small, hence it was assumed equal to zero, for purposes of this part of calculation, thus transforming equation (5.17) to

$$P_v^* - P_s^* = 0 \tag{5.20}$$

Combining equations (5.15), (5.16), and (5.20) resulted in

$$\theta_2^* = \sqrt{(\eta_d^3/5.242)\left(0.1457 - 0.0329C_0(\rho_{vm2}/\rho_1)\eta_d^4\right)} \tag{5.21}$$

From equation (5.9) the mass of liquid evaporated during this period is

$$m_{12} = \theta_2 k_1 C_{t2} \Delta T_{t2} / h_{fg} \tag{5.22}$$

3. Evaluation of constants

Certain assumptions were made in order to find constants C_{t1} and C_{t2}. As pore sizes were not very small, it was assumed that the pressure drop between the bubble and the tunnel could be ignored, i.e., $C_0 \approx 0$. Substitution of the simplified equation (5.21) into equation (5.19) with $\xi_{zmax} \approx 0$, resulted in

$$\Phi^* = 1/0.007(0.1457\eta_d^3/5.242)^{1/2} \tag{5.23}$$

As defined earlier in Section 2, Φ^* is a non-dimensional parameter representing a ratio of vapor generation rate to the total number of pores available. Thus, substituting for Φ^* from Section 2 and equation (5.23), a numerical value for C_{t2} could be obtained as

$$C_{t2} = [\rho_{vm2} h_{fg} \sqrt{\sigma / r_0 \rho_l} N \pi r_0^2] / [0.042 k_l \Delta T_{t2} \sqrt{0.1457\eta_d^3/5.242}] \tag{5.24}$$

The only quantity to be measured in this expression is the departure diameter.

To find the value of C_{t1}, the period θ_1 was first obtained from the bubble frequency equation, i.e.,

$$f_b = 1/(\theta_1 + \theta_2) \tag{5.25}$$

The frequency was measured experimentally and θ_2 was evaluated from equation (5.21). Then C_{t1} could be evaluated from equation (5.5).

At an arbitrary reference state of $\Delta T = 1$ K or $q'' = 1.12$ W/cm^2 for the surface R(11)-1 (N = 2050), and using the measured values of $f_b = 130$ Hz, $d_b = 0.7$ mm, and $N_A/A = 13.5/\text{cm}^2$ the empirical constants were evaluated as follows:

$C_b = 0.442$,

$C_3 = 3.172$,

$C_{t1} = 313$ cm, and

$C_{t2} = 27{,}700$ cm.

Nakayama et al. [20, 21] were surprised at the tremendous difference between the constants C_{t1} and C_{t2}, but advanced the weak argument that C_{t2} should be larger than C_{t1} due to the dynamic behavior during the latter part of the cycle.

In order to construct a complete boiling curve, the following quantities are computed first:

1. θ_1 from equation (5.5)
2. m_{11} from equation (5.8)
3. θ_2 from equation (5.21)
4. m_{12} from equation (5.22)

5. ξ_3 from equation (5.11)

6. β from Section 2

Thus at a given ΔT, the total heat flux is calculated by the addition of $q''_l = (m_{11} + m_{12})h_{fg}/(\theta_1 + \theta_2)A$ and $q''_{ex} = (\Delta T/C_q)^{5/3} (N_A/A)^{1/3}$.

4. Summary

This detailed analysis can be summarized as follows:

- Add the latent and natural convection effects.
- Formulate latent heat component in terms of actual active and inactive pores; this requires four constants. These are determined by detailed observations of bubble frequency, f_b, bubble departure diameter, d_b, and the number of active sites, N_A, at a reference point.
- The natural convection term requires the same detailed data for a range of ΔT's. x, y, and C_q are the three constants in the correlation. This term is very important as natural convection makes a significant contribution to the total heat transfer.
- Once all seven constants are established, the "dynamic" model can be used to predict heat transfer characteristics beyond the reference point. It is noted that there are actually eight constants, since C_0 was arbitrarily set equal to zero. Furthermore, the C_t's each involve two constants, A_δ and δ, so that the total number of constants is actually ten.
- The model is complex, highly empirical, and the physics is obscure. Because of the large number of experimentally determined constants it is very difficult to tell whether the model is really validated.

5. Discussion

The detailed analysis of the Thermoexcel-E model presented above suggests that there are some fundamental flaws in the formulation of this model. Central to the critique is the concern as to whether Phase II and Phase III are actually treated by a dynamic analysis. The contention here is that the complex mathematics is unnecessary, because the end result is the solution to an analysis of a static system.

The areas that do not stand up to a rigorous examination are discussed below.

a. Pressure difference The rationalization for the formulation of $P_s^* > P_{vb}^*$ is poor. Looking at the two terms on the right hand side of equation (5.15) show that the second term, $0.1457\eta_d^2/\theta_2^{*2}$, is greater than the first term, $5.242/\eta_d$, by a very small amount. This had to be formulated in this fashion to comply with the assumption that the rapid bubble growth resulted in a minute positive pressure differential between the pool and the bubble at departure. The fact is that equation (5.15) can be presented with a number of different terms on the right hand side. It solely depends upon the assumptions made. Hence, this final form is believed to be a truncated form resulting from some radical assumptions, as indicated in Appendix 4. Depending upon the choice of assumptions, one could arrive at an absolutely different "equation (5.15)". So it is not necessary that the first term should be less than the second term.

b. The recession ξ To understand why ξ is equated to zero it is important to develop an equation with the term ξ, by combining equations (5.15), (5.16), and (5.17), i.e.:

$$4\xi = 0.0329C_0(\rho_{vm2}/\rho_1)\eta_d^6/\theta_2^{*2} - 0.1457\eta_d^2/\theta_2^{*2} + 5.242/\eta_d$$

and rearranging:

$$\theta_2^* = \sqrt{-(0.1457\eta_d^2 - 0.0329C_0(\rho_{vm2}/\rho_1)\eta_d^6)/(4\xi - 5.242/\eta_d)}$$

Numerical computation indicates that the ratio $5.242/\eta_d \approx 0.3776801$. Therefore according to their assumption that $C_0 = 0$, ξ had to be assumed negligible and equated to zero in order to have a positive θ_2^*.

c. Interface depression at inactive sites In equation (5.11) it was assumed that the recession at an inactive pore was proportional to the cube root of the liquid introduced during a complete cycle. According to Nakayama et al. [50] the maximum recession that an interface can attain is when $\xi' = -r_0$, or $\xi = \xi'/r_0 = -1$, that is, the fourth-order Runge-Kutta integration was stable until $\xi = -1$. A value larger than unity will in fact cause the liquid to flood in. But according to their model with $C_3 = 3.172$ for R(11)-1, the ξ values in Phase III, i.e., ξ_3, varied from -1.4565 to -3.1741 at $\Delta T = 1$ to 10, respectively, as shown in Appendix 5.

d. Prominent role of natural convection Heat flux values computed from the Nakayama et al. model showed disagreement with their statement that "...the latent heat component played a vital role in the heat transport". This was confirmed by evaluating q''_l and q''_{ex} for R(11)-1 using the model. The results, as indicated in Appendix 5 showed an opposite trend, with relatively higher values for q''_{ex} than q''_l at all ΔT's.

e. Physical nature of constants The constants C_{t1} and C_{t2} differed by nearly two orders of magnitude for R-11 and water. The reason put forward by Nakayama et al. is that during the dynamic phase relatively large heat transfer coefficients exist due to the dynamic behavior. But it seems strange to have a different heat transfer coefficient at a fixed heat flux. More importantly it is interesting to note that this statement is in contradiction to the mathematical nature of the so called "dynamic phase". If it had been a dynamic phase, then the time θ_2 should have varied with different ΔT's. But the fact of the matter is that this behavior is not observable. Equation (5.21) shows that θ_2 remains constant at any heat flux level.

It is important to note that the mathematical formulation dictates the numerical values of C_{t1} and C_{t2}. To show this, equations (5.23) and (5.24) are combined to give C_{t2} at a reference point of $\Delta T = 1$ K for saturated R-11:

$$C_{t2} = [\rho_{vm2} h_{fg} \sqrt{\sigma / r_0 \rho_l} N \pi r_0^2] / [(0.042 k_l \Delta T) \sqrt{0.1457 \eta_d^3 / 5.242}]$$

$$= 27{,}700 \text{ cm.}$$

Also to find C_{t1}, the time θ_1 is eliminated between equations (5.5) and (5.25), giving

$$C_{t1} = V_{vm} h_{fg} / k_l (1/f_b - \theta_2) \left\{ A\ B + \rho_{vml} / \Delta T_{t1}\ \ln(V_{vl}/V_t) \right\}$$
$$\simeq 313 \quad \text{cm.}$$

which shows that the numerical values of these constants depend on the physical properties of the fluid and the geometry of the surface. The only variable obtained from experiment is the frequency, f_b.

Thus, looking back at their analysis it is clear that the heat balance was applied only in Phase I. For Phase II + III a bubble growth analysis was applied; hence, avoiding the heat balance in the latter two phases, whereas fundamentally it is absolutely essential to satisfy the heat balance in every phase.

In the following section, a quantitative analysis will be applied to GEWA-T surface based on a simple heat balance.

B. Quantitative Model for GEWA-T Surface

A quantitative model was developed for the GEWA-T surface. There were two reasons for undertaking this analysis. First, there was sufficient information available from the visual studies with the simulators and the actual test sections as discussed in Chapter 4, and secondly, the lack of analytical work in the literature.

The dynamic model developed by Nakayama et al. [20, 21] could not be used to predict GEWA-T results. The basic reason is that these two surfaces are different from each other having different physical characteristics.

Xin and Chao [60] had performed analytical work but they did not predict the results for actual test sections. As discussed in Chapter 2, their work involved experimental and theoretical analysis of face-up, flat grooved surfaces believed to resemble the actual GEWA-T surface.

To arrive at predictive results for GEWA-T surface, it was decided to utilize some ideas provided by Nakayama et al. The model assumes that the mode of heat transport is basically due to agitated natural convection and thin liquid film evaporation, the same as in the Nakayama et al. model, except that the present model uses a heat balance principle. The entire bubble formation from a flat interface to the departure size occurs during a single phase, contrary to three phases in Nakayama et al. model.

At some spots along the groove the vapor pressure exceeds the pool pressure and the interface bulges out. The vapor bubbles are generated at these favored sites. Non-active regions are found adjacent to each active site. The flow of vapor shown in Fig. 47 results in a slight drop in the interface so that liquid can be sucked into the channel. The liquid thus introduced spreads at the channel wall (Fig. 48) and feeds the vapor generation. After bubble departure the entire interface returns to the initial stage. The cycle is repeated again.

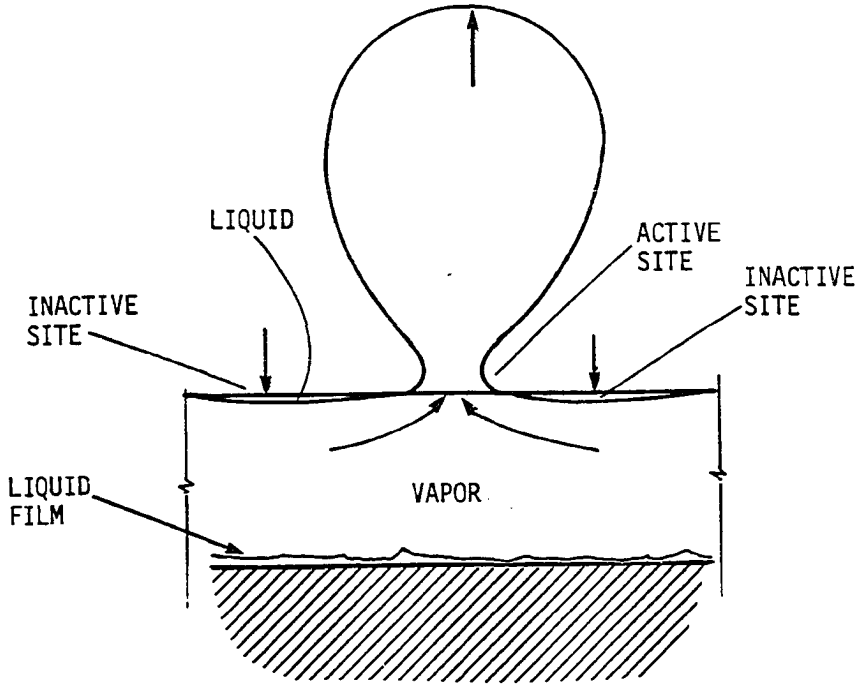

FIGURE 47. Model for boiling on a GEWA-T surface

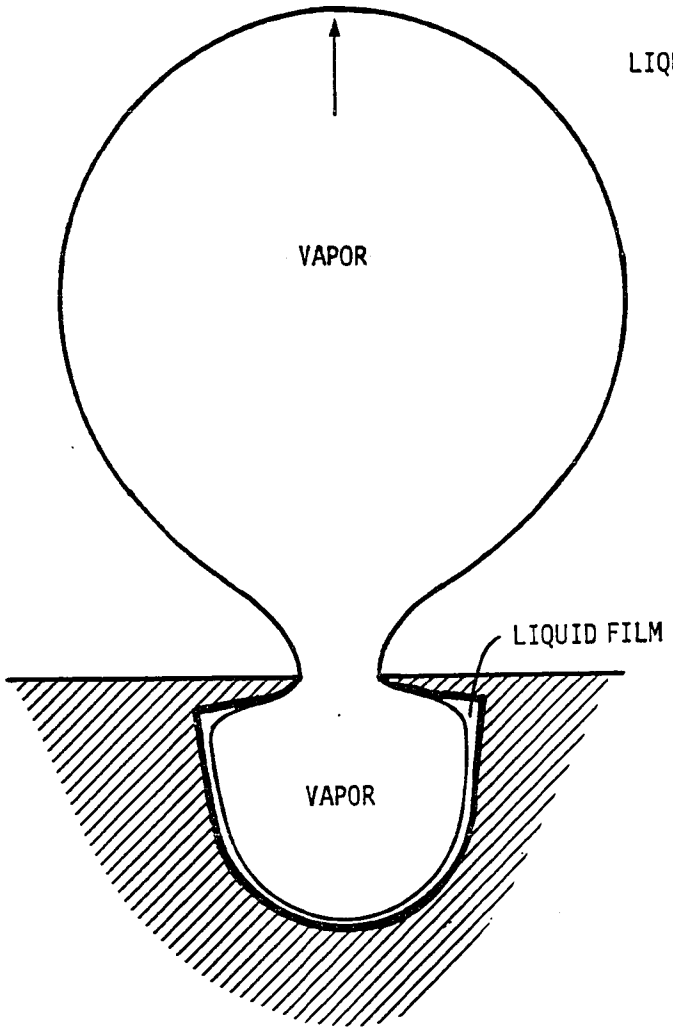

FIGURE 48. Cross section of a GEWA-T channel and an active site

1. Mathematical formulation

It is assumed that the pool and the vapor are always at the saturation temperature corresponding to the system pressure. The wall temperature is assumed to be uniform with negligible temperature drop between the base and the fin tip. The model is valid for the respective optimum gap widths with water and R-113 as described in Chapter 4. Beyond these gap sizes it is believed that the channels are partially flooded.

a. Latent heat component To find this component a heat balance is applied at the channel wall as follows:

$$q_l = h_t A_t (T_w - T_v) = \dot{m} h_{fg} = \frac{k_l A_\delta}{\delta} (T_w - T_v) \tag{5.26}$$

or,

$$q_l = k_l C_T \Delta T \tag{5.27}$$

Hence, the latent heat flux is given as

$$q''_l = k_l C_T \Delta T / A \tag{5.28}$$

where C_T is defined as the ratio of liquid film area to the liquid film thickness, A_δ/δ. C_T could be evaluated if A_δ and δ were known. But no measurements were performed to find these parameters. So, an empirical approach described below was applied to evaluate this constant for both water and R-113.

b. Agitated natural convection component It is assumed that the natural convection component is similar to the natural convection component when boiling from a plain surface. Thus the equation for this part is same as suggested by Zuber [69] and adopted by Nakayama et al. [20, 21], i.e.,

$$q''_{ex} = (\Delta T/C_q)^{1/y} (N_A/A)^{-x/y} \tag{5.4}$$

with $x = -1/5$ and $y = 3/5$. The C_q values used by Nakayama et al. were 1.95 $[K(cm^2/W)^{3/5}(1/cm^2)^{1/5}]$ for R-11 and 3.93 $[K(cm^2/W)^{3/5}(1/cm^2)^{1/5}]$ for water. As it was observed in GEWA-T experiments that the bubble population densities with both fluids were not drastically different, therefore, a single C_q value of 3 $[K(cm^2/W)^{3/5}(1/cm^2)^{1/5}]$, i.e., $((1.95 + 3.93)/2 \simeq 3)$ is used. This is taken as an approximate average of the above two C_q's. Thus, the total heat flux is given as

$$q'' = k_l C_T \Delta T/A + (\Delta T/C_q)^{1/y} (N_A/A)^{-x/y} \tag{5.29}$$

where N_A, the number of active sites was measured as a function of ΔT for water and R-113. A regression analysis of the data in Appendix 6 resulted in the following correlations for water and R-113, respectively:

For water, $N_A = -42.94 + 40.96\Delta T - 2.53\Delta T^2$ (ΔT in K) (5.30)

For R-113, $N_A = -32.13 + 20.25\Delta T + 0.85\Delta T^2$ (ΔT in K) (5.31)

The constant C_T is evaluated from equation (5.29) for GEWA-T19D/W at an arbitrary experimental condition of $\Delta T = 4$ K or $q'' = 45{,}000$ W/m^2. This point lies within the developed nucleate boiling portion of the experimental curve (Fig. 21). The value obtained for C_T is 12,779 (cm). It is obvious that C_T will be different for different fluids. Since it is a ratio of liquid film area to liquid film thickness, it should strongly depend upon the surface tension. Hence, C_T for R-113 is obtained by applying a multiplier, $\sigma_{R\text{-}113}/\sigma_{water}$, to C_T for water. This results in $C_T = 3214$ (cm) for R-113. With these constants equation (5.29) can be used for predictive results.

The maximum deviations of the data from the predicted values were 28% for water and 23% for R-113, as opposed to 30% for R-11 and 300% for water with the Hitachi model for the Thermoexcel-E surface. The contribution of q''_l and q''_{ex} is different for both fluids, indicating the effect of fluid property. In the case of water, q''_l dominates, whereas with R-113, the q''_{ex} contribution is dominant as shown in Table 2.

Basing the model on the fundamental heat balance avoids unnecessary mathematical tangles as compared to the Hitachi Dynamic Model. In fairness, one strong point about the Hitachi Dynamic Model is that it predicts the number of sites, thus bypassing the experimental measurements of N_A/A for a wide range of heat fluxes (or ΔT's).

TABLE 2. Heat flux contribution

	WATER		R-113	
ΔT K	q''_{ex} W/m^2	q''_{l} W/m^2	q''_{ex} W/m^2	q''_{l} W/m^2
1.5	1521	11479	351	306
2.0	3221	15305	2389	409
2.5	5363	19132	4382	511
3.0	7951	22958	6832	613
3.5	10968	26784	9776	715
4.0	14390	30610	13228	817
4.5	18191	34437	17200	919
5.0	22341	38263	21701	1022
5.5	26810	42089	26738	1124
6.0	31563	45916	32319	1226
6.5	36562	49742	38452	1328
7.0	41768	53568	45144	1430
7.5	47135	57395	52401	1532
8.0	52613	61221	60231	1634
8.5	58145	65047	68640	1737
9.0	63666	68873	77634	1839
9.5	69103	72700	87220	1941
10.0	74368	76526	97404	2043

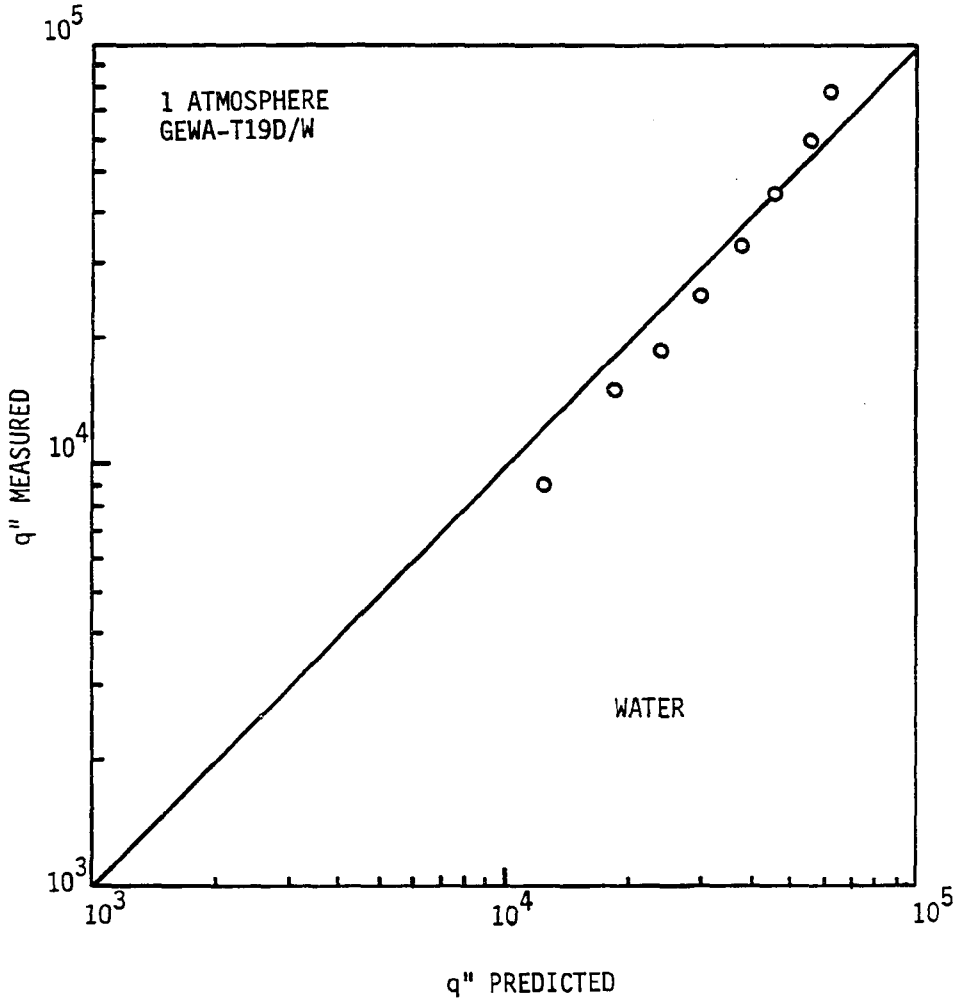

FIGURE 49. Predicted vs. experimental results for GEWA-T19D/W

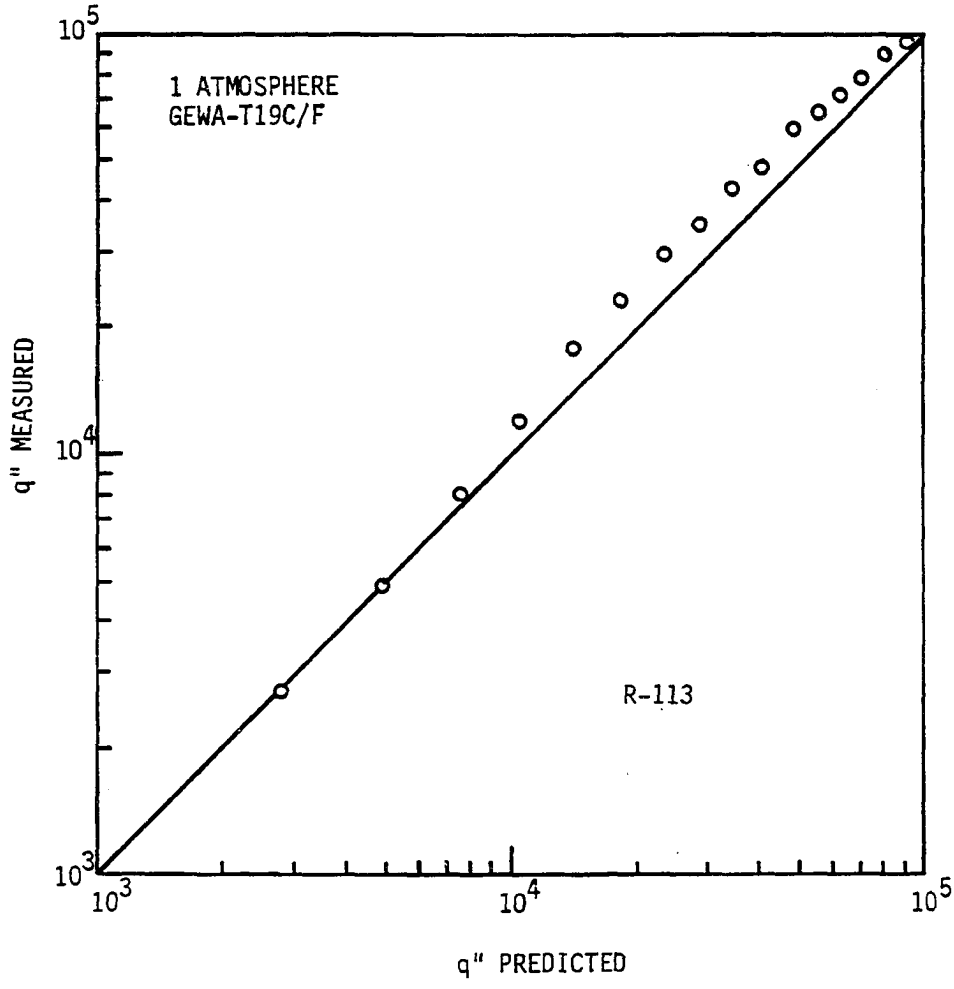

FIGURE 50. Predicted vs. experimental results for GEWA-T19C/F

VI. CONCLUSIONS AND RECOMMENDATIONS

Five GEWA-T surfaces (T-shaped fins), two GEWA-K surfaces (conventional low fins), and a smooth cylindrical surface were tested in pools of saturated distilled water and R-113 at atmospheric pressure. The enhanced surfaces showed better performance than the smooth tube. The degree of enhancement, defined as the ratio of wall superheat of a plain tube to the wall superheat of an enhanced tube at a fixed heat flux, was lower with water than with R-113. The maximum enhancement obtained with R-113 was two, whereas with water it was 1.6. A strong interdependence between thermal performance and gap width was detected with both fluids. For the GEWA-T surfaces, the best enhancement for water was obtained with a gap width of 0.35 mm and the best enhancement for R-113 was obtained with a gap width of 0.25 mm. These optimum sizes varied due to different liquid wetting characteristics, e.g., water has a much lower wetting ability as compared to R-113.

The fin density did not have a significant effect on the enhancement with the GEWA-K surface, whereas a slight enhancement was observed with the GEWA-T surface. This is probably due to the relatively larger channel area associated with a large fin density GEWA-T surface, which results in a larger liquid film area.

GEWA-T surface enhancement was improved by filling the channels or part of the channels with a porous material. At a heat flux of 80,000 $W/^2$, a partially filled GEWA-T tube showed an enhancement of 1.43 relative to an unfilled GEWA-T tube in water.

A liquid-vapor exchange, different from the one proposed and observed previously with the GEWA-T surface, was detected, with liquid entering and vapor being ejected at different locations around the circumference. This observation was further confirmed by a careful injection of blue dye at different locations around the circumference of a test section during an active experiment. Single GEWA-T channel simulators were fabricated for a detailed visual study. Also, special small gauge thermocouples were installed in a single channel of an actual GEWA-T test section. The response from these thermocouples during the actual test run revealed that there was some kind of liquid-vapor exchange within the channel. These observations proved useful in formulating a quantitative model of the boiling process on GEWA-T surfaces.

A critical study of the Hitachi Model for the somewhat similar Thermoexcel-E surface revealed that there are some basic flaws in the mathematical formulation. Too many assumptions and unnecessary mathematical complexity make it hard to follow and, hence, this model is not a good choice for design purposes. The analysis shows that the model is not a dynamic model. Using a basic heat balance, a simple model was developed that correlated the present experimental results for the GEWA-T surface.

It is recommended that these different gap size GEWA-T tubes be tested in other fluids, such as R-11, R-22, and Fluorinerts. The experiments should be carried to higher fluxes in order to understand

their peak nucleate heat flux or critical heat flux characteristics. Such high heat fluxes can occur in process heat exchangers.

Another important study could be carried out by studying the characteristics of these tubes in bundles. There are unresolved questions relating to the extent of the enhancement when strong convection currents, due to intense vapor generation from the lower tubes, are present.

It is also recommended to study the effect of roughening the walls of the channels, treating the walls with a second material, or filling the channels with a metallic or an organic porous material.

A study could be also conducted to understand the effect of tube diameter of the GEWA-T surfaces on the nucleate boiling performance, both as a single tube and as a bundle.

VII. REFERENCES

1. Joule, J. P. "On the Surface-Condensation of Steam." Philosophical Transactions of the Royal Society of London 151 (1861): 133-160.

2. Webb, R. L. and Bergles, A. E. "Heat Transfer Enhancement: Second Generation Technology." Mechanical Engineering 105, No. 6 (1983): 60-67.

3. Bergles, A. E., Nirmalan, V., Junkhan, G. H., and Webb, R. L. "Bibliography on Augmentation of Convective Heat and Mass Transfer-II." Heat Transfer Laboratory Report HTL-31, ISU-ERI-Ames-84221. Iowa State University, Ames, Iowa, 1983.

4. Webb, R. L., Bergles, A. E., and Junkhan, G. H. "Bibliography of U.S. Patents on Augmentation of Convective Heat and Mass Transfer II." Heat Transfer Laboratory Report HTL-32, ISU-ERI-Ames-84257. Iowa State University, Ames, Iowa, 1983.

5. Bergles, A. E., Nelson, R. M., Junkhan, G. H., and Webb, R. L. "Assessment, Development and Coordination of Technology Based Studies in Enhanced Heat Transfer." Heat Transfer Laboratory Report HTL-33, ISU-ERI-Ames-85024. Iowa State University, Ames, Iowa, 1984.

6. Webb, R. L. "The Evolution of Enhanced Surface Geometries for Nucleate Boiling." Heat Transfer Engineering 2, Nos. 3-4 (1981): 46-69.

7. Grant, A. C. "Porous Metallic Layer Formation." United States Patent No. 3,821,018, 1974.

8. Grant, A. C. "Porous Metallic Layer and Formation." United States Patent No. 4,064,914, 1977.

9. Fujikake, J. "Heat Transfer Tube for Use in Boiling Type Heat Exchangers and Method of Producing the Same." United States Patent No. 4,216,826, 1980.

10. Fujie, K., Nakayama, W., Kuwahara, H., and Kakizaki, K. "Heat Transfer Wall for Boiling Liquids." United States Patent No. 4,060,125, 1977.

11. Saier, M., Kastner, H. W., and Klockler, R. "Y and T-Finned Tubes and Methods and Apparatus for their Making." United States Patent No. 4,179,911, 1979.

12. Wieland-Produktinformation. "GEWA-T Tubes: High Performance Tubes for Flooded Evaporators." Wieland-Werke AG, Ulm, West Germany.

13. Czikk, A. M., Gottzmann, C. F., Ragi, E. G., Withers, J. G., and Habdas, E. P. "Performance of Advanced Heat Transfer Tubes in Refrigerant-Flooded Liquid Coolers." ASHRAE Transactions 76, Part I, No. 2123 (1970): 96-109.

14. Palen, J. W., Yarden, A., and Taborek, J. "Characteristics of Boiling Outside Large-Scale Horizontal Multitube Bundles." AIChE Symposium Series 68, No. 118, (1972): 50-61.

15. O'Neill, P. S., Gottzmann, C. F., and Terbot, J. W. "Novel Heat Exchanger Increases Cascade Cycle Efficiency for Natural Gas Liquefaction." Advances in Cryogenic Engineering 17 (1970): 420-437.

16. Gottzmann, C. F., O'Neill, P. S., and Minton, P. E. "High Efficiency Heat Exchangers." Chemical Engineering Progress 69, No. 7 (1973): 69-75.

17. Fricke, H. D. and Czikk, A. M. "Enhanced OTEC Sprayed Bundle Evaporator Performance Studies." In Advances in Enhanced Heat Transfer, pp. 23-29. New York: ASME, 1979.

18. Arai, N., Fukushima, T., Arai, A., Nakajima, T., Fujie, K., and Nakayama, Y. "Heat Transfer Tubes Enhancing Boiling and Condensation in Heat Exchangers of a Refrigerating Machine." ASHRAE Transactions 83, Part 2, (1977): 58-69.

19. Torii, T., Hirasawa, S., Kuwahara, H., Yanagida, T., and Fujie, K. "The Use of Heat Exchangers with Thermoexcel's Tubing in Ocean Thermal Energy Power Plants." ASME Paper No. 78-WA/HT-65, 1978.

20. Nakayama, W., Daikoku, T., Kuwahara, H., and Nakajima, T. "Dynamic Model of Enhanced Boiling Heat Transfer on Porous Surfaces. Part I: Experimental Investigation." Journal of Heat Transfer 102 (1980): 445-450.

21. Nakayama, W., Daikoku, T., Kuwahara, H., and Nakajima, T. "Dynamic Model of Enhanced Boiling Heat Transfer on Porous Surfaces. Part II: Analytical Modeling." Journal of Heat Transfer 102 (1980): 451-456.

22. Oktay, S. and Schmeckenbecher, A. F. "Preparation and Performance of Dendritic Heat Sinks." Solid State Science Technology 121, No. 7 (1974): 912-918.

23. Fujii, M., Nishiyama, E., and Yamanaka, G. "Nucleate Pool Boiling Heat Transfer from Micro-Porous Heating Surface." In Advances in Enhanced Heat Transfer, pp. 45-51. New York: ASME, 1979.

24. Bergles, A. E., Park, K. A., and Kim, C. "Cooling Enhancement for Chip/Module Testing." ISU-ERI-Ames-85431. Iowa State University, Ames, Iowa, 1984.

25. Nakayama, W., Nakajima, T., and Hirasawa, S. "Heat Sink Studs Having Enhanced Boiling Surfaces for Cooling of Microelectronic Components." ASME Paper No. 84-WA/HT-89, 1984.

26. Chu, R. C. and Moran, K. P. "Method for Customizing Nucleate Boiling Heat Transfer from Electronic Units Immersed in Dielectric Coolant." United States Patent No. 4,050,507, 1977.

27. Gouse, S. W., Jr. "An Index to the Two-Phase Gas-Liquid Flow Literature." M.I.T. Report No. 9. Cambridge, Massachusetts: The M.I.T. Press, 1966.

28. Marto, P. J. and Lepere, V. J. "Pool Boiling Heat Transfer from Enhanced Surfaces to Dielectric Fluids." Journal of Heat Transfer 104 (1982): 292-299.

29. Yilmaz, S., Hwalek, J. J., and Westwater, J. W. "Pool Boiling Heat Transfer Performance for Commercial Enhanced Tube Surfaces." ASME Paper No. 80-HT-41, 1980.

30. Yilmaz, S. and Westwater, J. W. "Effect of Commercial Enhanced Surfaces on the Boiling Heat Transfer Curve." In Advances in Enhanced Heat Transfer, HTD-Vol. 18, pp. 73-91. New York: ASME, 1981.

31. Bahhuth, A. and Genetti, W. E. "Nucleate Boiling Heat Transfer Enhancement with Heat Transfer Surface Cavities." AIChE Symposium Series 79, No. 225 (1983): 28-33.

32. Nakayama, W. "Boiling Heat Transfer on the Surface Having a Porous Structure Composed of Small Tunnels and Pores." Technical Report. Hitachi, Japan, Ltd., 1978.

33. Katz, D. L., Myers, J. E., Young, E. H., and Balekjian, G. "Boiling Outside Finned Tubes." Petroleum Refiner 34, No. 2 (1955): 113-116.

34. Zieman, W. E. and Katz, D. L. "Boiling Coefficients for Finned Tubes." Petroleum Refiner 26, No. 8 (1947): 620-624.

35. Myers, J. E. and Katz, D. L. "Boiling Coefficients Outside Horizontal Plain and Finned Tubes." Refrigerating Engineering 59 (1952): 56-59.

36. Bondurant, D. L. and Westwater, J. W. "Performance of Transverse Fins for Boiling Heat Transfer." Chemical Engineering Progress Symposium 67, No. 113 (1971): 30-37.

37. Hesse, G. "Heat Transfer in Nucleate Boiling, Maximum Heat Flux and Transition Boiling." International Journal of Heat and Mass Transfer 16 (1973): 1611-1627.

38. Gorenflo, D. "Zum Warmeübergang bei der Blasenverdampfung an Rippenrohren." Dissertation, Technische Hochschule Karlsruhe, 1966.

39. Zatell, V. A. "Method of Modifying a Finned Tube for Boiling Enhancement." United States Patent No. 3,768,290, 1973.

40. Gotoh, H., Kawai, S., and Machiyama, T. "Experimental Report on the Boiling Heat Transfer Characteristics of Steel Low-Finned Tubes." Bulletin of Science and Engineering Research Laboratory, No. 93 (1980): 88-92.

41. Danilova, G. N. and Dyundin, V. A. "Heat Transfer During Boiling of Freon 12 and 22 at Bundles of Finned Tubes." Heat Transfer-Soviet Research 4, No. 4 (1972): 48-54.

42. Mueller, J. and Hahne, E. "Boiling Heat Transfer in Finned Tube Bundles." Heat Transfer-Soviet Research 13, No. 6 (1981): 19-25.

43. Bergles, A. E., and Chyu, M.-C. "Characteristics of Nucleate Pool Boiling From Porous Metallic Coatings." Journal of Heat Transfer 104 (1982): 279-285.

44. Webb, R. L. "Nucleate Boiling on Porous Coated Surfaces." Heat Transfer Engineering 4 (1983): 71-82.

45. Webb, R. L. "Heat Transfer Surface having a High Boiling Heat Transfer Coefficient." United States Patent No. 3,696,861, 1972.

46. Nakayama, W., Daikoku, T., Kuwahara, H., and Kakizaki, K. "High-Flux Heat Transfer Surface Thermoexcel." Hitachi Review 24, No. 8 (1975): 329-334.

47. Chyu, M.-C. and Bergles, A. E. "Enhancement of Horizontal Tube Spray Film Evaporators by Structured Surfaces." In Enhanced Heat Transfer Equipment, HTD-Vol. 43, pp. 39-48. New York: ASME, 1985.

48. Yilmaz, S., Palen, J. W., and Taborek, J. "Enhanced Boiling Surfaces as Single Tubes and Tube Bundles." In Advances in Enhanced Heat Transfer, HTD-Vol. 18, pp. 123-129. New York: ASME, 1981.

49. Ogata, H. and Nakayama, W. "Heat Transfer to Boiling Helium from Machined and Chemically Treated Copper Surfaces." In Proceedings of the 1981 Cryogenic Engineering Conference, Vol. 27, pp. 309-317. San Diego, California: 1982.

50. Nakayama, W., Daikoku, T., and Nakajima, T. "Modeling of Liquid Suction Mechanism in Porous Surface Boiling." *ASME Paper No.* 80-HT-122, 1980.

51. Nakayama, W., Daikoku, T., Nakajima, T. "Effects of Pore Diameters and System Pressure on Saturated Pool Nucleate Boiling Heat Transfer from Porous Surfaces." Journal of Heat Transfer 104 (1982): 286-291.

52. Stephan, K. and Mitrovic, J. "Heat Transfer in Natural Convective Boiling of Refrigerant and Refrigerant-Oil Mixtures in Bundles of T-Shaped Finned Tubes." In Advances in Enhanced Heat Transfer, HTD-Vol. 18, pp. 131-146. New York: ASME, 1981.

53. Marvillet, C. "B E E F Loop." Technical Report, Groupement pour la Recherche sur les Echangeurs Thermiques, Centre d'Études Nucléaires de Grenoble, France, 1984.

54. Marto, P. J. and Hernandez, B. "Nucleate Pool Boiling Characteristics of a GEWA-T Surface in Freon-113." AIChE Symposium Series 79, No. 225 (1983): 1-10.

55. Macbeth, R. V. "Boiling on Surfaces Overlayed with a Porous Deposit: Heat Transfer Rates Obtainable by Capillary Action." Atomic Energy Establishment Winfrith Report, AEEW R-711, Winfrith, United Kingdom, 1971.

56. Smirnov, G. F. "Approximate Theory of Heat Transfer with Boiling on Surfaces Covered with Capillary-Porous Structures." Teploenergetika 24, No. 9 (1977): 77-80.

57. Arshad, J. and Thome, J. R. "Enhanced Boiling Surfaces: Heat Transfer Mechanism Mixture Boiling." In ASME-JSME Thermal Engineering Joint Conference Proceedings, Vol. 1, pp. 191-197. Honolulu, Hawaii: ASME, 1983.

58. Bingshen, C., Lixian, Z., Yingke, T., and Deng, S. J. "Investigation of Boiling Heat Transfer Mechanism and Performance of Mechanically Fabricated Porous Surface." In Proceedings of Joint Meeting of Chemical Engineering, Chemical Industry, and Engineering Society of China/AIChE, Vol II, pp. 664-672. Beijing, China: AIChE, 1982.

59. Liu, X. and Ma, T. Z. "Pool Boiling Heat Transfer from Sintered Screen Surfaces and from Surfaces with Re-entrant Grooves." Iowa State University, Ames, Iowa. Private communication, 1985.

60. Xin, M.-D. and Chao, Y.-D. "Analysis and Experiment of Boiling Heat Transfer on T-Shaped Finned Surfaces." In the 23rd National Heat Transfer Conference, August 4-7, 1985, Denver, Colorado.

61. Light, T. S. and Sawyer, P. B. "Resistivity of Very Pure Water and Its Maximum Value." In Power Plant Instrumentation for Measurement of High-Purity Water Quality, STP 742, pp. 175-184. Philadelphia: ASTM, 1980.

62. Chyu, M.-C. "Falling Film Evaporation on Horizontal Tubes with Smooth and Structured Surfaces." Ph.D. Dissertation. Iowa State University, Ames, Iowa, 1984.

63. Junkhan, G. H. and Bergles, A. E. "Heat Transfer Laboratory Data Acquisition System." Heat Transfer Laboratory Report HTL-12, ISU-ERI-Ames-77178. Iowa State University, Ames, Iowa, 1976.

64. Chapman, A. J. Heat Transfer. Third Edition. New York: Macmillan, 1974.

65. Webb, R. L. "Heat Transfer Surface Which Promotes Nucleate Ebullition." United States Patent No. 3,521,708, 1970.

66. Schmittle, K. V. and Starner, K. E. "Heat Transfer in Pool Boiling." United States Patent No. 4,074,753, 1978.

67. Shum, M. S. "Finned Heat Transfer Tube with Porous Boiling Surface and Method for Producing Same." United States Patent No. 4,182,412, 1980.

68. Nishikawa, K. and Fujita, Y. "Correlation of Nucleate Boiling Heat Transfer Based on Bubble Population Density." International Journal of Heat and Mass Transfer 6 (1963): 233-245.

69. Zuber, N. "Nucleate Boiling, The Region of Isolated Bubbles and the Similarity with Natural Convection." International Journal of Heat and Mass Transfer 6 (1963): 53-78.

70. L'Ecuyer, M. R. L. and Murtby, S. N. B. "Energy Transfer From a Liquid to Gas Bubbles Forming at a Submerged Orifice." NASA TN D-2547, 1965.

71. Morcos, S. M. and Bergles, A. E. "Combined Forced and Free Laminar Convection in Horizontal Tubes." ISU-ERI-Ames-74008. Iowa State University, Ames, Iowa, 1974.

72. ASHRAE. Thermodynamic Properties of Refrigerants. New York: American Society of Heating, Refrigerating, and Airconditioning Engineers, Inc., 1969.

73. ASHRAE. Thermophysical Properties of Refrigerants. New York: American Society of Heating, Refrigerating, and Airconditioning Engineers, Inc., 1973.

VIII. ACKNOWLEDGMENTS

The author gratefully extends his thanks and appreciation to his major professor Dr. Arthur E. Bergles for his guidance, assistance, and invaluable help through out the course of this study and to his committee members, Dr. George H. Junkhan, Dr. Donald M. Roberts, Dr. Bruce R. Munson, and Dr. Ron M. Nelson.

Thanks are due the U.S. Department of Energy for providing initial funds and to the Department of Mechanical Engineering and Engineering Research Institute at Iowa State University for additional support.

The author appreciates Dr. Ming-Chien Chyu's advice relating to technical problems.

The author is also grateful to Mr. Gaylord Scandrett, Mr. Hap Steed, and his colleague Mr. V. Nirmalan for their sincere help. Thanks are also due to Mr. Klaus Menze of Wieland-Werke AG, Federal Republic of Germany, for providing the test sections.

The author is indebted to his parents for their love, prayers, and blessings. Last, but not least, the author thanks his wife and children who had to go through thick and thin during their stay at Ames.

IX. APPENDIX 1: SATURATION TEMPERATURE CALCULATION

A. Water

$$F = 139.276781 + 6.4757873P - 0.1036991P^2$$

$$T_s = \frac{5}{9}(F - 32), \ ^\circ C$$

where,

$$P = 0.491154P_a + 0.036127H$$

P_a is atmospheric pressure, inches of mercury

H is liquid level above the midplane of a test section, cm

B. R-113

$$F = 37.21313 + 7.293994P - 0.125058P^2$$

$$T_s = \frac{5}{9}(F - 32), \ ^\circ C$$

where,

$$P = 0.49115P_a + 0.05464H$$

P_a is atmospheric pressure, inches of mercury

H is liquid level above the midplane of a test section, cm

X. APPENDIX 2: WORKING FLUID PROPERTIES

To plot a precise predicted natural convection curve, it is important to know the thermodynamic and thermophysical properties of the working fluids at different temperatures. The property relations for distilled water and R-113 were taken from [71 - 73].

A. Distilled Water

1. Density

$$\rho_l = (62.422 - 0.21862\theta - 0.21785\theta^2 + 0.01077\theta^3) \times 16.02, \text{ kg/m}^3$$

where,

$$\theta = (T - 50)/50$$

Temperature range: 50 - 200 °F

2. Isobaric thermal expansion coefficient

$$\beta = [(0.21862 + 0.4357\theta - 0.03231\theta^2)/(50\rho_l)] \times 1.81, \text{ 1/°C}$$

3. Viscosity

$$\mu = 0.0115826 \exp(5.6036 - 0.7609\theta + 0.1245\theta^2 - 0.01133\theta^3), \text{ N-s/m}^2$$

4. Thermal conductivity

$$k_l = (0.3392 + 0.0275\theta - 0.0034\theta^2) \times 1.72958, \text{ W/m-K}$$

5. Prandtl number

$$Pr = \exp(2.2279 - 0.8474\theta + 0.1401\theta^2 - 0.0120\theta^3)$$

B. R-113

1. Density

$$\rho_l = (103.55 - 0.0712T - 0.0000636T^2) \times 16.02, \text{ kg/m}^3$$

$$T = (T_w + T_s)/2.0, \ ^\circ\text{F}$$

2. Isobaric thermal expansion coefficient

$$\beta = -[(0.0712 + 0.0001272T)/\rho_l] \times 1.8, \ 1/^\circ\text{C}$$

3. Viscosity

For $T \leq 609.6$ R,

$$\mu = (10.48364 - 0.03139T + 0.00002443T^2) \times 10^{-3}, \text{ N-s/m}^3$$

4. Thermal conductivity

$$k_l = 0.0802 - 0.000205T, \text{ W/m-K}$$

T in °C

5. Specific heat

$$c_p = -2.68086 + 0.0321075T - 0.0000965643T^2 + 0.0000000999343T^3, \text{ kJ/kg-K}$$

T in K

XI. APPENDIX 3: PROGRAM FOR DATA ACQUISITION

```
0: fmt 1,"    POOL BOILING TEST ON GEWA-T19D IN WATER";wrt 6.1
1: fmt 2,"    ----------------------------------------",/,/;wrt 6.2
2: dim T[10,20],V[10,20],E[20],U[12],F[20],A$[100]
3: ent "Status",A$
4: wrt 6,A$
5: ent "WATTMETER READING",A
6: ent "INS OF Hg",H
7: ent "POOL LEVEL(cm)",D
8: fmt 2,"F1R1T1Z1M0P0"
9: fmt 3,"  ";wrt 6.3
10: 87.935*A→Q
11: fmt 5,f7.2,z
12: fmt 6,f7.2
13: wrt 6.3
14: for I=1 to 10;for J=1 to 16
15: wrt 709,"CLS",J-1;wrt 722.2;red 722,V[I,J]
16: 'TEMP'(1000V[I,J])→T[I,J]
17: 5/9*(T[I,J]-32)→T[I,J]
18: next J;next I
19: 16→X;for M=1 to 15
20: wrt 6.5,M;next M
21: wrt 6.6,X;fmt 2,"----",z
22: for K=1 to 29;wrt 6.2;next K;wrt 6.3
23: fmt 1,20x,"T/C WELL TEMP";wrt 6.3
24: for I=1 to 10;for J=1 to 15
25: wrt 6.5,T[I,J];next J
26: wrt 6.6,T[I,16];next I;wrt 6.3
27: for J=1 to 16
28: 0→Z
29: for I=1 to 10;Z+T[I,J]→Z;next I
30: Z/10→E[J];next J;wrt 6.3
31: fmt 2,20x,"AVG. POINT TEMP";wrt 6.2;wrt 6.3
32: for I=1 to 15;wrt 6.5,E[I];next I
33: wrt 6.6,E[16];wrt 6.3
34: Q/342*.0116→G
35: G*ln(.0116/.00994)→U[1]
36: G*ln(.0116/.00899)→U[2]
37: G*ln(.0116/.00908)→U[3]
38: G*ln(.0116/.00939)→U[4]
39: G*ln(.0116/.0095)→U[5]
40: G*ln(.0116/.01012)→U[6]
41: G*ln(.0116/.01044)→U[7]
42: G*ln(.0116/.00635)→U[8]
43: G*ln(.0116/.00925)→U[9]
44: G*ln(.0116/.00844)→U[10]
45: G*ln(.0116/.00939)→U[11]
46: G*ln(.0116/.01044)→U[12]
```

```
47: for J=1 to 12
48: E[J]-U[J]→F[J];next J
49: for I=13 to 16;E[I]→F[I];next I;wrt 6.3
50: fmt 7,20x,"CORRECTED TEMP";wrt 6.7;wrt 6.3
51: for J=1 to 15;wrt 6.5,F[J];next J
52: wrt 6.6,F[16];wrt 6.3
53: (F[13]+F[14]+F[15])/3→P
54: (F[1]+F[2]+F[3]+F[4]+F[5]+F[6])/6→L
55: (F[7]+F[8]+F[9]+F[10]+F[11]+F[12])/6→R
56: (L+R)/2→W;wrt 6.3
57: fmt 1,"  ",/;wrt 6.1
58: fmt 5,8x,"HEAT FLUX(W/m2)";wrt 6.5
59: fmt 4,f12.2;wrt 6.4,Q;wrt 6.3
60: fmt 5,8x,"POWER(W)";wrt 6.5
61: wrt 6.4,A;wrt 6.3
62: fmt 5,8x,"ATM PRESSURE(Ins Hg)";wrt 6.5
63: wrt 6.4,H;wrt 6.3
64: fmt 5,8x,"POOL LEVEL(cm)";wrt 6.5
65: wrt 6.4,D;wrt 6.3
66: fmt 5,8x,"POOL TEMP";wrt 6.5
67: wrt 6.4,P;wrt 6.3
68: fmt 5,8x,"LHS TEMP";wrt 6.5
69: wrt 6.4,L;wrt 6.3
70: fmt 5,8x,"RHS TEMP";wrt 6.5
71: wrt 6.4,R;wrt 6.3
72: fmt 5,8x,"WALL TEMP";wrt 6.5
73: wrt 6.4,W;wrt 6.3
74: .491154H+.036127D→B
75: 139.276781+6.4757873B-.1036991BB→Y
76: 5/9*(Y-32)→C
77: fmt 5,8x,"SATURATION TEMP";wrt 6.5
78: wrt 6.4,C;wrt 6.3
79: W-C→S
80: fmt 5,8x,"SUPERHEAT";wrt 6.5
81: wrt 6.4,S
82: end
83: "TEMP":
84: if p1<=1.494;ret
31.99925+46.80117p1-1.407396p1↑2+.07802p1↑3-.007394p1↑4
85: if p1<=3.941;ret
33.42956+44.48835p1-.07422p1↑2-.253895p1↑3+.02878p1↑4
86: if p1<=6.62;ret
33.82822+45.39092p1-1.015078p1↑2+.03592p1↑3-.000642p1↑4
*17292
```

XII. APPENDIX 4: TIME AT MAXIMUM VAPOR FLOW INTO A BUBBLE

In the Hitachi model a time term, τ_{zmax}, is defined as the time in Phase II + III when the flow of vapor into the bubble is maximum. But the detailed derivation is not given in [20, 21]. To find this time, equation (5.14) is substituted into equation (5.13). This gives the equation for "Z" in terms of time τ as follows:

$$Z = -4/3\theta_2^{*} + 4\tau/\theta_2^{*2} - 4\tau^2/\theta_2^{*3} + 4\tau^3/3\theta_2^{*4} + 2X_d^2\tau^3/\theta_2^{*4} - 4\sqrt{2/3}\,X_d\tau^3/\theta_2^{*4} + 2\sqrt{2/3}\,X_d/\theta_2^{*} + 4X_d^2\tau/\theta_2^{*2} - 10\sqrt{2/3}\,X_d\tau/\theta_2^{*2} - 6X_d^2\tau^2/\theta_2^{*3} + 12\sqrt{2/3}\,X_d\tau^2/\theta_2^{*3} \quad (12.1)$$

To find the maximum, differentiate equation (12.1) and equate it to zero

$$\frac{dZ}{d\tau} = 4/\theta_2^{*2} - 8\tau/\theta_2^{*3} + 4\tau^2/\theta_2^{*4} + 6X_d^2\tau^2/\theta_2^{*4} - 12\sqrt{2/3}\,X_d\tau^2/\theta_2^{*4} + 4X_d^2/\theta_2^{*2} - 10\sqrt{2/3}\,X_d/\theta_2^{*2} - 12X_d^2\tau/\theta_2^{*3} + 24\sqrt{2/3}\,X_d\tau/\theta_2^{*3} = 0 \quad (12.2)$$

Rearranging equation (12.2)

$$(4 + 6X_d^2 - 12\sqrt{2/3}\,X_d)\tau^2 - (12X_d^2\theta_2^{*} - 24\sqrt{2/3}\,X_d\theta_2^{*} + 8\theta_2^{*})\tau + (4X_d^2\theta_2^{*2} - 10\sqrt{2/3}\,X_d\theta_2^{*2} + 4\theta_2^{*2}) = 0 \quad (12.3)$$

Solving quadratic equation (12.3) results in

$$\tau = (\alpha \pm \sqrt{\psi})/\chi$$

where

$$\alpha = 12X_d^2\theta_2^* - 24\sqrt{2/3}\,X_d\theta_2^* + 8\theta_2^*$$

$$\psi = (12X_d^2\theta_2^* - 24\sqrt{2/3}\,X_d\theta_2^* + 8\theta_2^*)^2 - 4(4 + 6X_d^2 - 12\sqrt{2/3}\,X_d)\,(4X_d^2\theta_2^{*2} - 10\sqrt{2/3}\,X_d\theta_2^{*2} + 4\theta_2^{*2})$$

$$\chi = 2(4 + 6X_d^2 - 12\sqrt{2/3}\,X_d)$$

simplifying

$$\tau/\theta_2^* = 1 \pm \sqrt{(3X_d^4 - 9\sqrt{2/3}\,X_d^3 + 6X_d^2 - 2\sqrt{2/3}\,X_d)/(3X_d^2 - 6\sqrt{2/3}\,X_d + 2)} \qquad (12.4)$$

Now $X_d = 3/2\ X$, or $X_d = \sqrt{3/2}\,\eta^{3/2}$, therefore substituting for X_d in equation (12.4)

$$\tau/\theta_2^* = 1 \pm \sqrt{(3 - 6/\eta^{3/2} + 4/\eta^3 - 8/9\eta^{9/2})/(3 - 4/\eta^{3/2} + 4/3\eta^3)} \qquad (12.5)$$

For $\eta >> 1$, the inverse power terms of η could be neglected or,

$$\tau/\theta_2^* \equiv \tau_{zmax}/\theta_2^* = 1 \pm \sqrt{3}/3 = 1 - 0.57735 = 0.42265 \simeq 0.423$$

XIII. APPENDIX 5: PROGRAM AND RESULTS FOR HITACHI MODEL

```
1          REAL N,NA
     C
     C       THIS PROGRAM EVALUATES HEAT FLUX
     C       VERSUS WALL SUPERHEAT FOR THERMOEXCEL-E
     C       SURFACE R(11)-1 USING NAKAYAMA ET AL.
     C       "DYNAMIC" MODEL.
     C
2          CT1=313.0
3          CT2=27700.0
4          PRINT 100,CT1,CT2
5        100 FORMAT(////2X,4HCT1=,F6.2,5X,4HCT2=,F8.2)
6          PRINT 15
7         15 FORMAT(///3X,4HDELT,5X,4HQEX ,8X,2HQL,11X,1HQ,
          17X,4HBETA,7X,3HCY3)
8          TSAT=23.78
9          TABS=273.+TSAT
10         PS=1013320.
11         TW=24.78
12         TWW=24.78+273.
13         AKL=0.0008898
14         PHI=3.141592654
15         D0=0.01
16         N=2050.
17         PITCH=0.07
18         AC=0.04*0.025
19         VT=N*PITCH*AC
20         VCY=(N*PHI*D0*D0*D0)/12.
21         VV1=VT+VCY
22         VVM=(VT+VV1)/2.
23         R0=D0/2.
24         GC=0.0000001
25         TV0=TABS
26         R=0.0563
27         RR=R*10000000.
28         RHOV0=PS/(RR*TV0)
29         HFG=179.8
30         SIGMA=18.
31         TV1=TV0+(2.*SIGMA*TV0*GC)/(RHOV0*HFG*R0)
32         RHOV1=RHOV0+((1.-(R*TV0)/HFG)*(2.*GC*SIGMA/R0))
          2/(R*TV0)
33         RHOVM1=(RHOV0+RHOV1)/2.
     C
     C       PHASE I
     C
34         DO 40 K=1,12
35         TW=TW
36         TWW=TWW
```

```
      DTT1=TW-(TV0+TV1-546.)/2.
      AAN=(HFG*VVM)/(AKL*CT1)
      BAN=RHOVM1*(HFG-R*TV0)/(R*TV0*TV0)
      RATIO=(TWW-TV0)/(TWW-TV1)
      CAN=ALOG(RATIO)
      DAN=RHOVM1/DTT1
      EAN=ALOG(VV1/VT)
      T1=AAN*(BAN*CAN+DAN*EAN)
      AML1=VVM*(RHOV1-RHOV0)+VCY*RHOVM1
C
C       PHASE II+III
C
      AREA=8.048
      G=981.0
      CB=0.442
      C0=0.0
      C3=3.172
      CQ=1.95
      RHOL=1.4794
      RHOVM2=RHOVM1
      DO 10 J=1,1000
      OLD=RHOVM2
      DB=SQRT((2.*SIGMA)/(G*(RHOL-RHOVM2)))*CB
      RHOV2=RHOV0+((GC*4.*SIGMA/DB)
     3*(1.-R*TV0/HFG))/(R*TV0)
      RHOVM2=(RHOV1+RHOV2)/2.
      ANEW=RHOVM2
      TEST=ABS((ANEW-OLD)/ANEW)
      IF(TEST.LE.0.00000001)GO TO 20
   10 CONTINUE
   20 PAL=(2.0*R0)/DB
      QAL=PAL*PAL
      RAL=1.0-QAL
      SAL=SQRT(RAL)
      TAL=1.0+SAL
      UAL=1.0/PAL
      ETAD=UAL*TAL
      SAM=ETAD*ETAD*ETAD
      TAM=SAM*ETAD
      FF=SAM/5.242
      GG=0.1457-0.0329*C0*(RHOVM2/RHOL)*TAM
      WAM=FF*GG
      T2STAR=SQRT(WAM)
      RAD=(RHOL*R0*R0*R0)/SIGMA
      T2=T2STAR*SQRT(RAD)
      TV2=TV0+(GC*4.*SIGMA*TV0)/(DB*RHOVM2*HFG)
      DTT2=TW-(TV1+TV2-546.)/2.
      DELT=TW-TSAT
      AML2=T2*AKL*CT2*DTT2/HFG
      QL=((AML1+AML2)*HFG*10000.)/((T1+T2)*AREA)
```

```
83          RECE=(AML1+AML2)/(RHOL*N*PHI*R0*R0*R0)
84          CUBE=RECE**0.3333333333
85          CY3=-C3*CUBE
86          ADO=SQRT(SIGMA/(R0*RHOL))
87          PSTAR=(6.*AKL*CT2*DTT2)/(RHOVM2*HFG*N*PHI*R0*R0*ADO)
88          BETA=(PSTAR*T2STAR-CY3*(CY3*CY3+3.)+4.)/
           4(ETAD*(ETAD*ETAD+3.)-4.)
89          NA=BETA*N
90          FIRST=((TW-TSAT)/CQ)**1.6666666666667
91          SECOND=(NA/AREA)**0.33333333333333
92          PROD=FIRST*SECOND
93          QEX=PROD*10000.
94          Q=QL+QEX
95          PRINT 30,DELT,QEX,QL,Q,BETA,CY3
96       30 FORMAT(/2X,F5.2,2X,F8.0,3X,F8.0,4X,
           5F9.0,3X,F6.4,4X,F7.4)
97          TW=TW+1.0
98          TWW=TWW+1.0
99       40 CONTINUE
100         STOP
101         END
```

CT1=313.00 CT2=27700.00

DELT	QEX	QL	Q	BETA	CY3
1.00	7788.	3550.	11337.	0.0523	-1.4565
2.00	31488.	13483.	44970.	0.1080	-1.8469
3.00	71077.	27783.	98860.	0.1636	-2.1186
4.00	126551.	45199.	171750.	0.2191	-2.3343
5.00	197905.	64918.	262824.	0.2746	-2.5161
6.00	285140.	86385.	371524.	0.3300	-2.6749
7.00	388252.	109211.	497463.	0.3854	-2.8168

8.00	507240.	133116.	640356.	0.4409	-2.9456
9.00	642106.	157888.	799994.	0.4963	-3.0641
10.00	792846.	183370.	976216.	0.5517	-3.1741
11.00	959460.	209443.	1168903.	0.6071	-3.2769
12.00	1141950.	236006.	1377955.	0.6624	-3.3737

XIV. APPENDIX 6: ACTIVE SITES DATA FOR GEWA-T

The bubble sites were measured at different ΔT's for several test runs with water and R-113. These sites were observed around the circumference over random number of channels over the entire test section, as described in detail in Chapter 4. The results are:

Water		R-113	
ΔT (K)	N_A (sites)	ΔT (K)	N_A (sites)
1.5	13	2.0	11
2.0	29	2.81	32
3.0	56	4.05	65
4.0	82	4.81	83
5.0	98	5.3	101
		6.48	132
		7.6	172

XV. APPENDIX 7: ERROR ANALYSIS

It is true that there is no exact measured value for a particular quantity. All measurements are generally inaccurate in some degree. The aim should be to make the error as small as possible.

The difference between the observed value of a physical quantity and the "accurate" value is called the error of observation. This type of error which usually occurs in physical science is further grouped as accidental and systematic. Accidental errors could be revealed by repeated observations. The systematic error could be handled by the application of error analysis. The error analysis of physical quantities in this study, e.g., the heat flux and wall superheat, are presented below.

As the measurement techniques and test heaters were similar to [62], the error analysis was adopted from [62]. The main source of uncertainty in the heat flux was linked to the electric power measurement. The wattmeter was calibrated with an uncertainty of $\pm$ 0.005 W at 10 W and $\pm$ 1 W at 1000 W. Thus the uncertainty in the heat flux was evaluated to be $\pm$ 0.44 W/m^2 at the lower end of the heat flux and $\pm$ 89 W/m^2 at 80,000 W/m^2.

The uncertainty in the wall superheat was due to uncertainty in the wall temperature and saturation temperature. The uncertainty in the wall temperature after calibration was $\pm$ 0.06 K. The temperature at the fin root diameter, D_b, was calculated by employing the conduction equation. A technique developed by Chyu [62] was used to measure the

distance between the thermocouple bead location and the fin base, with a probable measurement error of ± 0.04 mm, resulting in an uncertainty of ± 0.04 K in the temperature difference between these two locations.

The saturation temperature was calculated by an expression fitting the data from steam and R-113 tables (see Appendix 1). The atmospheric pressure used for saturation temperature calculation was the main source of uncertainty. However, the total uncertainty in the saturation temperature was negligible. Thus the total uncertainty in the wall superheat was ± 0.1 K.